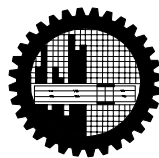


Preparation of Fe–Si mixed oxide surface and its application in the removal of toxics from water

By
SAMIRA SAIMOMA

SUBMITTED IN PARTIAL FULFILMENT OF THE REQUIREMENT FOR
THE DEGREE OF MASTER OF PHILOSOPHY
(M. PHIL.) IN CHEMISTRY



DEPARTMENT OF CHEMISTRY
BANGLADESH UNIVERSITY OF ENGINEERING AND TECHNOLOGY (BUET)
Dhaka-1000, Bangladesh
MAY, 2011

Declaration

This thesis work has been done by the candidate himself and does not contain any material extracted from elsewhere or from a work published by anybody else. The work for this thesis has not been presented elsewhere by the author for any degree or diploma.



Signature of the candidate

Samira Saimoma

Name of the candidate

Dedicated to

My
Ammu (Ms. Hasina Shahadat Khan)
Husband (Mr. S. R. Khan)
&
daughter
Rayedah Khan (Soshmeto)

Department of Chemistry
Bangladesh University of Engineering and Technology (BUET)
Dhaka, Bangladesh.



Certification of Thesis

A thesis on

**"Preparation of Fe-Si mixed oxide surface and its
application in the removal of toxics from water"**

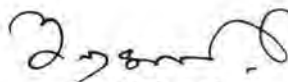
Submitted by

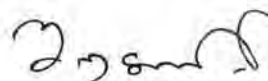
Samira Saimoma

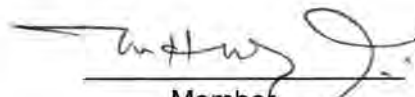
Roll No: 100703206F, Session: October, 2007 has been accepted as satisfactory in partial fulfilment of the requirements for the degree of Master of Philosophy (M. Phil) in Chemistry on May 15, 2011.

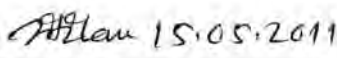
Board of Examiners


1. **Dr. Al-Nakib Chowdhury**
Professor
Department of Chemistry
BUET, Dhaka.
2. **Head**
Professor
Department of Chemistry
BUET, Dhaka
3. **Dr. Md. Monimul Haque**
Professor
Department of Chemistry
BUET, Dhaka
4. **Dr. Md. Nazrul Islam**
Associate Professor
Department of Chemistry
BUET, Dhaka
5. **Dr. Abu Jafar Mahmood**
Supernumerary Professor
Department of Chemistry
University of Dhaka, Dhaka.


15.05.11
Supervisor & Chairman


15.05.11
Member (Ex-officio)


15.5.11
Member


15.05.2011
Member


Member (External)

Acknowledgement

My profound gratitude to my adorable research supervisor, Professor Dr. Al-Nakib Chowdhury, Head of the Department of Chemistry, University of Engineering and Technology (BUET), Dhaka, Bangladesh for his stimulating inspiration, positive criticism and sagacious advices. His intense interest and valuable suggestions in this research work inspired me to face problems with confidence.

I would like to thank Professor Dr. Md. Monimul Huque, Professor Dr. Md. Manwarul Islam, Professor Dr. Md. Rafique Ullah, Professor Dr. Md. Wahab Khan, Professor Dr. Shakila Rahman, Dr. Md. Nazrul Islam, Dr. Md. Mominul Islam and Mrs. Danisha Tabassum. I am also highly thankful to other teachers of Department of Chemistry, BUET.

I am indebted to the authority of BUET for providing me financial support for this research work.

I would like to express my deep gratitude to all of my beloved family members, specially my mom, dad, mother in law, father in law, brother in law, sister in law, sister (Semme), husband (Mr. Khan) and daughter (Soshmeto) for their great sacrifice during my entire research activity.

I would also like to thank my friends S. M. Aktaruzzaman, Biplob Kumer Deb, Tonima Tanim, Abdur Rahim, Kamrun Nahar, Hoore Jannat, Yousuf Jamal, Jahirul Islam, Sayed Abdul Monim, Sayed Shahed, Arup Roy, Bin Yeamin and Shahinur Rahman for their generous support, constant inspiration and encouragement during my whole research period.

I would also like to thank all staffs of Chemistry Department in BUET for their enormous support. Special thanks to Mr. Mamun Or Rashid, Department of Chemistry, BUET, Dhaka for composing the thesis; Mr. Kabir Hossain, Department of Chemistry, BUET, Dhaka, for his cooperation in taking IR spectra and Mr. Md. Yousuf Khan, Instrument Engineer, Department of MME, BUET for his cooperation in taking SEM and EDX of my research work samples.

Finally, I express my highest gratitude from the core of my heart to the most beneficent, merciful and almighty Allah.

SAMIRA SAIMOMA

Author

Contents

Abstract

Chapter 1

Introduction		Page No.
1.1	Materials	12
1.2	Distinct types of materials	12
	1.2.1 Metals	12
	1.2.2 Semiconductors	13
1.3	Nanomaterials	14
1.4	Oxide materials	15
1.5	Types of oxide materials	17
1.6	Iron(III) oxide	18
1.7	Silicon oxide	19
1.8	Synthesis techniques of metal oxide and mixed metal oxides	19
	1.8.1 Precipitation method	19
	1.8.2 Co-precipitation method	20
	1.8.3 Sol-gel method	21
1.9	Applications of mixed metal oxides	23
1.10	Characterization of metal oxide and mixed oxide material	23
1.11	Surface morphology	24
1.12	Importance of dye removing	24
1.13	Dye	26
1.14	Classification of dyes	26
1.15	Color in compounds and its sensation	28
1.16	Harmful impact of dye pollutants	32
1.17	Dye treatment techniques	33
1.18	Adsorption phenomena: Surface process	33
1.19	Types of adsorption	34
	1.19.1 Physisorption	34
	1.19.2 Chemisorption	34
1.20	Purpose of the adsorption study	35
1.21	Adsorption isotherms	35
1.22	Model of adsorption isotherms	37
1.23	Photochemistry	41
1.24	Theoretical aspects of the experimental techniques	44
	1.24.1 SEM Technique	44
	1.24.2 Elemental analysis: Energy dispersive X-ray micro analysis(EDX)	46

1.24.3	X-Ray diffraction	47
1.24.4	Infra-red (IR) spectroscopy	48
1.24.5	Principle of absorption spectroscopy	49
1.25	Characterization of surface properties by adsorption methods	50
1.26	Determination of specific surface area by adsorption Measurements	52
1.26.1	Gas adsorption measurements	52
1.26.2	Dye adsorption measurements	52
1.27	Point of zero charge	53
1.28	Methods for the determination of point of zero charge (PZC)	55
1.28.1	Mass titration	55
1.29	Literature survey and aim of the present work	56

Chapter 2

Experimental

2.1	Materials and Probes	
2.1.1	Chemicals	63
2.1.2	Instruments	63
2.2	Preparation of metal oxide and mixed oxide material	64
2.3	Characterization of synthesized materials	64
2.3.1	IR spectra	64
2.3.2	X-ray Diffraction	65
2.3.3	Surface Morphology	65
2.3.4	Electron Diffraction X-ray (EDX) Spectra	65
2.4	Removal of MB and OG dye using the (Fe-Si) mixed oxide	66
2.4.1	Preparation of dye solution	66
2.4.2	Determination of the concentration of dye solutions	66
2.4.3	Adsorption (batch) process	67
2.4.4	Spectrum of MB	67
2.4.5	Spectrum of OG	68
2.4.6	Determination of molar absorption co-efficient (ϵ) of MB	69
2.4.7	Determination of molar absorption co-efficient (ϵ) of OG	70
2.4.8	Effect of pH on the spectral behavior of MB	71
2.4.9	Effect of pH on the spectral behavior of OG	72
2.5	Determination of specific surface area of synthesized material	73
2.6	Determination of (pH_{PZC}) of iron-silicon mixed oxide	75

Chapter 3

Result and Discussion

3.1	Characterization of synthesized oxide materials	77
3.1.1	EDX spectral analysis	77
3.1.2	X-ray diffraction	82
3.1.3	IR spectral analysis	85
3.1.4	Scanning electron microscopy	88
3.1.5	Determination of specific surface area of the mixed (Fe-Si) oxide by the (MB) dye adsorption method	91
3.1.6	Determination of point of zero charge (pH_{PZC}) of the mixed (Fe-Si) oxide	94
3.2	Removal of organic dyes (MB and OG) using batch experiment	103
3.2.1	Comparative study of the removal of dyes between the multi-component (Fe-Si) and single oxide surface	103
3.2.2	Effect of variation of Na_2CO_3 concentration on adsorbent Preparation	106
3.2.3	Effect of Si/Fe molar ratio on adsorbent strength	108
3.2.4	Effect of pH on MB uptake	109
3.2.5	Effect of contact time and kinetic study	111
3.2.6	Effect of concentration of dye and isotherm study	117
3.2.7	Effect of adsorption dose	121
4.0	Conclusion	125
	References	128

Abstract

Mixed oxide of iron-silicon adsorbent was synthesized chemically by a sol-gel method. Fe-Si binary oxide adsorbents were prepared by varying the concentration of Fe(III) while the concentration of Na_2CO_3 and Na_2SiO_3 were kept constant and also by varying the concentration of Na_2CO_3 while the concentration of Fe(III) and Na_2SiO_3 was chosen to be constant. In this study Fe/Si molar ratio and Na_2CO_3 concentration were selected to be 3:1 and 0.5 M respectively.

The mixed oxide thus obtained and characterized by a wide range of EDX, XRD, SEM, UV-Visible and IR spectroscopy techniques. Elemental analysis exhibited the presence of iron, silicon and oxygen elements in the mixed oxide with a composition of $\text{Fe}_{1.47} \text{Si}_{0.53} \text{O}_3$. The results showed that the iron-silicon mixed oxide were successfully synthesized. The IR spectra yielded the characteristics signals of silicon oxide ($470, 1099 \text{ cm}^{-1}$), iron oxide ($457, 545, 569 \text{ cm}^{-1}$) and iron-silicon mixed oxide (962 cm^{-1}) and confirmed the presence of the components in each substrate. The average crystallite size was calculated from the XRD data to be approximately 18 nm. The specific surface area of this binary oxide was found to be $46.79 \text{ m}^2\text{g}^{-1}$. The point zero charge of this surface was observed to be at pH 8.8.

Surface capacity of the mixed metal oxide (MMO) were studied and thus it was used as an adsorbent for the removal of organic dyestuff from water. In that case, organic cationic (methylene blue abbreviated as MB) and anionic (orange green abbreviated as OG) dyes were attempted to be adsorbed on the MMO surface.

The adsorption data showed that both the MB and OG dyes can be adsorbed on the mixed oxide surface. But the extent of MB adsorption is much more higher than OG, suggesting the present MMO an attractive adsorbent for the removal of the cationic dye MB.

The adsorption property of mixed oxide for removal of organic cationic MB dye was investigated with various parameters including effect of pH, contact time, initial dye concentration, temperature and dose of mixed oxide. The adsorbent was tested for removal of dyes from their aqueous solution. The maximum adsorption capacity of binary mixed (Fe-Si) oxide for MB dye was found at pH 7. Kinetic study showed that MB followed pseudo-second-order kinetics equation for MB. Adsorption isotherm was interpreted by Langmuir equation from the obtained

data. This study clearly demonstrated that dye can be removed efficiently by the Fe-Si mixed oxide surface.

Chapter - 1

INTRODUCTION

1.1 Materials

Materials have been vital to human civilization and Materials science is one of the oldest forms of engineering and applied science. The field has now broadened to include every class of material and now in the twentieth century materials not just one, but many have become the most important single factor on which the advance of technology and industry depends. Despite the amazing variety of modern day of materials, the search still goes on for materials to meet new and critical service requirements not only in an advance technology area such as aerospace, but in the manufacture of industrial and consumer products as well. Also, superior materials are needed to meet higher quality and reliability standard, epitomizes by long term product warranties and the demand for safe products. Finally, the search goes on constantly for new and superior materials at lower costs.

Moreover, now-a-days, the wide variety of choice of combination of properties are used; because it is expected to have more excellent results than a single component. For an example the mixed-oxide gels may appear to have more excellent absorptive abilities than the gels of a single component [1].

Metal oxides study is a significant part of materials science with their diverse application including adsorptive abilities. They even also have so many other potential applications like as catalyst, semiconductor, alternative cathode materials, pH sensing materials, capacitors, coating materials, pigments and so on. Among these so many function its adsorption behaviors have been particularly established here in this paper; where metal mixed oxide surface can be a vital adsorbent for removing textile organic dyes (cationic and anionic), toxic elements like arsenic, waste materials and so on [2].

1.2 Distinct types of materials

Materials science encompasses various classes of materials, each of which may constitute a separate field. Here some varieties have been discussed.

1.2.1 Metals

Metals are crystalline solid materials consist of metal atoms distributed in a definite pattern resulting from their close packing. The types of close packing arrangement depend upon the size and electronic configuration of the atoms involved in the formation of crystal lattice. Since the metal atoms are all in direct contact with one another in the lattice and their valence electrons are in identical energy states, it is believed that the electrons are free to migrate between atoms. Metal atoms have an excess of low energy orbital vacancies. These vacancies enable valence electrons to move from near a certain nucleus to near any other nucleus where their position remains indistinguishable from the first. Thus, metals may be pictured as a collection of positive atomic cores embedded in a fluid or sea of electrons. For this fluid of electrons, metals are good conductors of electricity and heat. Metals have metallic luster; they are malleable, ductile and high melting points. Metals have simple crystal lattices since metallic bonding envisages closest packing of atoms-one layer above another. Metals may have any system of seven common crystal systems. Fe, Cu, Al, Ag, Au etc are the most common metals which are very useful to us.

1.2.2 Semiconductors

Semiconductors are special kind of materials which have the properties of semi conductivity is an electrical property of materials. A relatively small group of elements and compounds have an important electrical property, semi conduction in which they are neither good electrical conductors nor good electrical insulators. Instead, their ability to conduct electricity is intermediate. Si, Ge, impure ZnO, impure NiO are some examples of semiconductors.

In a semiconductor element, the energies of the valence electrons, which bind the crystal together, lie in the highest filled energy band, called the valence band. The empty band above called the conduction band and is separated from the valence band by an energy gap. The magnitude of the energy gap or the width of the forbidden energy zone is characteristic of the lattice alone and varies widely for different crystals.

Semiconductors are of two kinds such as

- (i) Intrinsic semiconductor
- (ii) Extrinsic semiconductor

(i) Intrinsic semiconductors: If a pure, elemental substance shows the semiconducting properties, it is called intrinsic semiconductor. Pure Si, Ge shows these semiconducting properties. For this semiconduction results from the thermal promotion of electrons from a filled valence band to an empty conduction band. There, the electrons are negative charge carriers. The removal of electrons from the valence band produces electron holes which are positive charge carrier and identical to the conduction electrons

(ii) Extrinsic semiconductors: Extrinsic semiconductor result from impurity additions known as dopants, and the process of adding these components is called doping. These types of semiconductors are extrinsic semiconductors. At room temperature the conductivity of semiconductors results from electrons and holes introduced by impurities in the crystal. The presence of an impurity lowers considerably the energy gap necessary to transfer an electron from the valence band to the conduction band. This indicates that the ground state energies of such easily excited electrons must lie in the forbidden energy region. Two such discrete energy levels, known as donor levels and acceptor levels, may be introduced into the forbidden energy zone at a small interval of energy below the conduction band or above the valence band. Donor levels give rise to electrons in the conduction band, whereas acceptor levels lead to the formation of holes in the valence band. Impurity of Si, with B, P, NiO, ZnO are the examples of extrinsic semiconductors. Extrinsic semiconductors are of two kinds such as p-type extrinsic semiconductor and n-type extrinsic semiconductor.

1.3 Nanomaterials

Nowadays nano metal oxide is one of the promising materials for scientists. The applications of nano oxide particles are increasing day by day. The most commonly used transition metal oxides are titania, manganese oxide, zinc oxide, cobalt oxide, nickel oxide, iron oxide etc.

Nanotechnology is expected to be the basis of many of the main technological innovations of the 21st century. Research and development in this field is growing rapidly throughout the world. A major output of this activity is the development of new materials in the nanometer scale, including nanoparticles. A unique aspect of

nanotechnology is the vastly increased ratio of the surface area to volume present in many nanoscale materials which opens new possibilities in surface-based science, such as catalysis. A number of physical phenomena become noticeably pronounced as the size of the system decreases. These include statistical mechanical effects, as well as quantum mechanical effects, for example the “the quantum size effect” where the electronic properties of solids are altered with great reductions in particle size. This effect does not come into play by going from macro dimension. However, it becomes dominant when the nanometer size range is reached.

Materials reduced to the nanoscale can suddenly show very different properties compared to what they exhibit on a macroscale, enabling unique applications. For instance, opaque substances become transparent (copper); inert materials become catalyst (platinum); stable materials turn combustible (aluminum); solids turn into liquids at room temperature (gold); insulators become conductors (silicon). Materials such as gold, which is chemically inert at normal scales, can serve as a potent chemical catalyst at nanoscales. Much of the fascination with nanotechnology exhibits at the nanoscale.

A nanoparticle (which historically has included nanopowder, nanocluster and nanocrystal) is a small particle with at least one dimension less than 100 nm. This definition can be fleshed out further in order to remove ambiguity from future nano nomenclature. A nanoparticle is an amorphous or semicrystalline zero dimensional (0D) nano structure with at least one dimension between 10 and 100 nm and a relatively large ($\geq 15\%$) size dispersion [3].

1.4 Oxide materials

There are various types of oxides in nature. Oxides of more electropositive elements tend to be basic. They are called basic anhydrides; adding water, they may form basic hydroxides. For example, sodium oxide is basic; when hydrated, it forms sodium hydroxide. Oxides of more electronegative elements tend to be acidic. They are called acid anhydrides; adding water, they form oxoacids. For example, anhydride; perchloric acid is a more hydrated form. Some oxides can act as both acid and base at different times. They are amphoteric. An example is aluminium oxide. Some oxides do not show behavior as either acid or base

An oxide is a chemical compound containing at least one oxygen atom as well as at least one other element. Most of the Earth's crust consists of oxides. Oxides result when elements are oxidized by oxygen in air. Virtually, all elements burn into atmospheric oxygen. In the presence of water and oxygen (or simply air), some elements - lithium, sodium, potassium, rubidium, cesium, strontium and barium - react rapidly, even dangerously to give the hydroxides. In part for this reason, alkali and alkaline earth metals are not found in nature in their metallic, i.e., native, form. The surface of most metals consists of oxides and hydroxides in the presence of air. A well known example is aluminum foil, which is coated with a thin film of aluminum oxide that passivate the metal, slowing further corrosion. Due to its electro negativity, oxygen forms chemical bonds with almost all elements to give the corresponding oxides. So-called noble metals (common examples: gold, platinum) resist direct chemical combination with oxygen, and substances like gold (III) oxide must be generated by indirect routes.

Many oxides are black but others can be very colorful. The large diversity of oxides can be partially attributed to the extreme abundance of oxygen in the Earth's crust. Oxygen comprises over 45% of the Earth's crust by weight. Most of this is locked up in more complex minerals based on chemical complex anions such as CO_3^{2-} , BO_3^{3-} , SO_4^{2-} , NO_3^- , SiO_4^{4-} , PO_4^{3-} and others. But great opportunities exist for single oxygen ions to combine with various elements in many different ways. In a strict sense, minerals that belong to the more complex mineral classes such as the silicates are really oxides. But this would be cumbersome for mineralogists to be able to deal with only the four different classes of the elements class, the halides class, the sulfides class and finally the extremely large oxides class with all of its many subclasses and over 90% of all known minerals. By convention therefore, the oxides are limited to non complex minerals containing oxygen or hydroxide. Oxides also contain mostly ionic bonds and this helps distinguish members from the more complex mineral classes whose bonds are typically more covalent in nature. Quartz, SiO_2 , would be considered an oxide, and still is in some mineral guides and texts, except for its

covalent silicon oxygen bonds and its structural similarity to the other Tectosilicates.

Inorganic oxides are one of the most important materials for science and technology. Especially transition metal oxides have characteristics surface. It has drawn great attention to researchers. Metal oxide has been used as catalyst, sensor, and adsorbent for removal of toxic chemical, electrode material as well as used in electro chromic device and solar cell etc. Nowadays nano metal oxide is one of the promising materials for scientists. The applications of nano oxide particles are increasing day by day. The most commonly used transition metal oxides are titania, manganese oxide, zinc oxide, cobalt oxide, nickel oxide, iron oxide etc [4].

1.5 Types of oxide materials

The oxide catalysts are mainly classified into three groups:

(a) Semiconductor oxides

These are the oxides of transition metal, for example, NiO, ZnO, MnO₂, TiO₂, Cr₂O₃ etc. The catalytic activity is mainly due to lattice defect and oxidation state of the metal ion. The important reactions that are catalyzed by semiconductor oxides include oxidation (both complete and partial), dehydrogenation, desulphurization of hydrocarbon etc.

(b) Insulator oxides

This group includes Al₂O₃, SiO₂ and MgO etc. The catalytic activity is mainly due to acid-base properties of these oxides. The important reactions that are catalyzed by insulator oxides are alkylation of aromatic hydrocarbons, dehydration of alcohol etc.

(c) Mixed metal oxide (MMO)

Mixed metal oxide formed from two or more types of oxides phases. It is a new type of material. These oxides could be used as surface material. Mixed systems have the potential for exhibiting chemical properties that differ notably from those of the corresponding single component oxides. The incorporation of one metal

oxide are to other oxide may change the band gap energy of host metal oxide. Mixed metal oxides widely used as catalyst, adsorbent, sensors, oxidant, and electrode material. It is also used for the removal of toxic chemicals from the environment.

Better catalytic activity is observed with the mixed oxide catalysts according to the following mechanisms: stabilization, control of redox properties, creation of acidity and basicity, combination of more than two functions to evolve acid oxidation and acid-base bi-functional catalysts. For examples,

- V-P oxides for selective oxidation of butane to malefic anhydride.
- Bi-Mo oxides for selective oxidation of propene to acrolene.
- Perovskite oxides (LnCoO_3 , LaCoO_3 , LnMnO_3 etc.) for hydrogenation of alkenes.

1.6 Iron(III) oxide

Iron(III) oxide is the inorganic compound with the formula Fe_2O_3 . It is of one of the three main oxides of iron, the other two being iron(II) oxide (FeO), which is rare, and iron(II,III) oxide (Fe_3O_4), which also occurs naturally as the mineral magnetite. As the mineral known as hematite, Fe_2O_3 is the main source of the iron for the steel industry. Fe_2O_3 is paramagnetic, reddish brown, and readily attacked by acids. Rust is often called iron(III) oxide, and to some extent, this label is useful, because rust shares several properties and has a similar composition. To a chemist, rust is considered an ill-defined material, described as hydrated ferric oxide [5].

Alpha phase

$\alpha\text{-Fe}_2\text{O}_3$ has the rhombohedral, corundum ($\alpha\text{-Al}_2\text{O}_3$) structure and is the most common form. It occurs naturally as the mineral hematite which is mined as the main ore of iron. It is antiferromagnetic below ~ 260 K (Morin transition temperature), and weak ferromagnetic between 260 K and 950 K Neel temperature.

Beta phase

Cubic face centered, metastable, at temperatures above 500 °C converts to alpha phase. It can be prepared by reduction of hematite by carbon, pyrolysis of iron(III) chloride solution, or thermal decomposition of iron(III) sulfate.

Gamma phase

Cubic, metastable, converts to the alpha phase at high temperatures. Occurs naturally as the mineral magnemite and Ferromagnetic. Ultra fine particles, smaller than 10 nanometers, are superparamagnetic. Can be prepared by thermal dehydration of gamma iron(III) oxide-hydroxide, careful oxidation of iron(II,III) oxide. The ultrafine particles can be prepared by thermal decomposition of iron(III) oxalate [6].

1.7 Silicon oxide

The chemical compound silicon dioxide, also known as silica (from the Latin *silix*), is an oxide of silicon with a chemical formula of SiO_2 and has been known for its hardness since antiquity. Silica is most commonly found in nature as sand or quartz, as well as in the cell walls of diatoms. Silica is the most abundant mineral in the Earth's crust. Silica is manufactured in several forms including fused quartz, crystal, fumed silica (or pyrogenic silica, trademarked Aerosil or Cab-O-Sil), colloidal silica, silica gel, and aero gel. In addition, silica nanosprings are produced by the vapor-liquid-solid method at temperatures as low as room temperature [7].

1.8 Synthesis techniques of metal oxide and mixed metal oxides

Supported metal oxide and mixed metal oxide are usually prepared by the following methods:

- (i) Precipitation.
- (ii) Co-precipitation.
- (iii) Incipient wet impregnation.
- (iv) Deposition.
- (v) Grafting.
- (vi) Sol-gel method.
- (vii) Precipitation-deposition.

(viii) Selective removal.

1.8.1 Precipitation method

Hydroxide or carbonate of the desired metal is precipitated out from solution by using a precipitating agent [8]. The hydroxides or carbonates are decomposed by heating to the oxides, which are, reduced to the metal when required on to a suspension of the support. In all precipitations it is essential to carefully control all the details of the process including.

- i) The order and rate of addition of one solution into the other.
- (ii) The mixing procedure.
- (iii) The pH and variation of pH during the process.
- (iv) The maturation process.

Precipitation involves two distinct processes, namely nucleation and growth. Nucleation requires that the system is far from equilibrium. Growth of the new phase takes place in conditions which gradually approach the equilibrium state.

Many procedures are used for precipitation. One simple method is to add drop-wise the solution containing the active component to the precipitating solution, or vice versa. There is little difference between those inverse procedures. In both cases high super saturation can be produced locally, leading, if the solubility constant is low, to fine precipitates. If not, redissolution takes place at the beginning of the process, when agitation disperses the precipitate in the liquid. In both cases, concentrations change continuously throughout the precipitation process resulting in an inhomogeneous product being formed, at least with respect to texture. Any precipitation process is situated somewhere between two extremes. Either the solutions are contacted instantaneously (only an ideal situation as, in all cases, diffusion has to take place), the super saturation decreasing continuously, or the super saturation is maintained constant during the whole precipitation process.

Instantaneous precipitation is achieved by two methods. The first consists in pouring continuously, in constant proportion, both solutions into a vessel under constant and vigorous stirring. The second consists in mixing the solutions

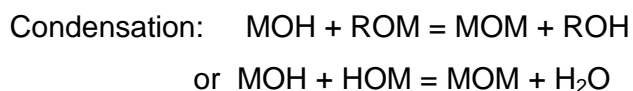
through specially designed mixing nozzles. The latter method ensures a better uniformity in composition and texture of the Precipitate.

1.8.2 Co-precipitation method

This method involves the addition of a precipitation agent leading to the formation of a mixture of metal compound and the support, both previously in solution. This method is traditionally associated with nickel alumina catalyst used mostly in the hydrogenation of unsaturated fatty oils [9]. At a defined temperature the precipitating agent is OH⁻ ions that convert the active metal salts to a mixture of metal hydroxide. After drying, the decomposed and reduced to get a co-precipitated supported catalyst. This method offers a better surface in terms of homogeneity, though some of the active component may be embedded within the carrier and hence not available. This method is especially employed for the preparation of mixed oxide catalyst.

1.8.3 Sol-gel method

Sol-gel preparation, which involves the formation of a sol followed by formation of a gel, typically uses either colloidal dispersions or inorganic precursors as the starting material. However, it is important to realize that sol-gel preparation can be done with a wide variety of precursors. With an alkoxide (M(OR),) as a precursor, sol-gel chemistry can be described in terms of two classes of reactions:



Despite its oversimplification, this description of sol-gel chemistry identifies two key ideas. First, a gel forms because of the condensation of partially hydrolyzed species into a three-dimensional polymeric network. Second, any factors that affect either or both of these reactions are likely to impact on the properties of the gel. In fact, it is the control of many of these factors, generally referred to as sol-gel parameters that separate sol-gel preparation from other methods. A representative but not exhaustive list of these parameters includes type of precursor, type of solvent, water content, acid or base content, precursor concentration, and temperature. These parameters affect the structure of the

initial gel and, in turn, the properties of the material at all subsequent processing steps [10].

A gel, a solid matrix encapsulating a solvent, needs to be dried to remove the solvent. The time between the formation of a gel and its drying, known as aging, is also an important parameter. As Scherer pointed out, a gel is not static during aging but can continue to undergo hydrolysis and condensation. Furthermore, syneresis, which is the expulsion of solvent due to gel shrinkage, and coarsening, which is the dissolution and reprecipitation of particles, can occur. These phenomena can affect both the chemical and structural properties of the gel after its initial formation. One other parameter that affects a sol-gel product is the drying condition. Conventional evaporative drying, such as heating a gel in an oven, induces capillary pressure associated with the liquid-vapor interface within a pore. In a sample with a distribution of pore sizes, the resultant differential capillary pressure often collapses the porous network during drying. The dried sample, known as a xerogel, thus often has a surface area and pore volume that is too low to be of catalytic interest. There are several ways to minimize the deleterious effect of conventional drying, and xerogels with high surface areas and pore volumes can be prepared with care. One other approach is that of Kistler, who used supercritical drying to bypass the problem of differential capillary pressure. The resultant materials, known as aerogels, have high surface area, porous structure, and low density. In a way drying can be viewed as part of the overall aging process because the material can, and often does, undergo physical and chemical changes during this stage [11].

Let us return to the issue of control and see how it is relevant to the preparation of catalytic materials. In the preparation of single-component materials, sol-gel preparation can achieve very high purity because of the quality of available precursors. Furthermore, the textural properties of the product, most notably surface area and pore size distribution, can be tailored. However, we believe the area in which sol-gel preparation is going to make the biggest impact is multi-component systems. We see the following specific advantages: (i) the ability to control structure and composition at a molecular level, (ii) the ability to introduce

several components in a single step, (iii) the ability to impose kinetic constraints on a system and thereby stabilize metastable phases, and (iv) the ability to fine tune the activation behavior of a sample and thereby trace the genesis of active species [10]. Finally, with either single-component or multi-component systems, sol-gel preparation allows different product forms to be made. As we shall see, one particular interesting class of materials is inorganic membranes that can perform both catalytic and separation function.

1.9 Applications of mixed metal oxides

From the past and even recently MMO materials preparation have received great interest because of the large variety of their potential applications such as in catalysis [12, 13] adsorption [14-15], as anode [16] and alternative cathode material [17].

In Chem. Commun., Taylor et al [18] also reported the use of a mixed oxide of copper and zinc as catalysts.

MMO can also be used as material as capacitor [19], its films as pH sensing materials [20], as pigments [21] and also found as coating materials [22].

Metal oxides with wide or moderate band gap, such as TiO_2 , CeO_2 , ZrO_2 , and HfO_2 , have been widely used for various applications like semiconductor materials in dye-sensitized solar cell, catalysts, fuel cells, resistors, gas sensors, transparent optical device, and optical coatings [23-24]. Oxide materials, which have very important optical properties, can also be used in the fields such as short wavelength lasers, blue light emitting diodes, UV detectors, gas sensors, etc. [25]. The American Nuclear Society (ANS) also endorses the rapid application of mixed oxide (MOX) fuel technology to accomplish the timely disposition of surplus weapons-grade plutonium in the United States and in the Russian Federation (November 2002).

1.10 Characterization of metal oxide and mixed oxide material

Metal and mixed metal oxide characterization is necessary to establish understanding and control of metal and mixed metal oxides synthesis and application. Characterization is done by using a variety of different techniques, mainly drawn from metal oxide materials. Common techniques are Electron Microscopy [TEM, SEM], Atomic Force Microscopy [AFM], Dynamic Light Scattering [DLS], X-ray Photoelectron Spectroscopy [XPS], powder X-ray Diffractometry [XRD], Energy Dispersion X-ray (EDX) spectroscopy and Fourier Transform Infrared Spectroscopy. Whilst the theory has been known for over a century, the technology for Nanoparticle Tracking Analysis (NTA) allow a direct tracking of the Brownian motion and this method therefore allow the sizing of individual nanoparticles of metal oxide in solution [26].

1.11 Surface morphology

Scientists have taken to naming their particles after the real world shapes that they might represent. Nanospheres [27], Nanoreefs [28], nanoboxs [29], microsphere [27] and more have appeared in the literature. These morphologies sometimes arise spontaneously as an effect of a templating or directing agent present in the synthesis such as micellular emulsions or anodized alumina pores, or form the innate crysllographic growth patterns of the materials themselves. Some of these morphologies may serve a purpose, such as long carbon nanotubes being used to bridge an electrical junction, or just a scientific curiosity like the stars shown at left.

1.12 Importance of dye removing

Water is absolutely essential to animals and plants in order for their survival. Human beings use water for drinking, bathing, washing, culinary purpose, transportation, industrial and agricultural activities etc [30]. The day to day human activities and industrial revolution have influenced the flow and storage of water and the quality of available fresh water. Many industries like textile, refineries, chemical, plastic and food processing plants produce wastewater characterized by a perceptible content of organics [31]. Significant amounts of chemically different dyes are used in various industries such as textile, pesticide, paint, solvent, pharmaceuticals, paper, pulp and petroleum etc [32-33].

Textile and other industrial dyes have become major environmental contaminants in many countries including Bangladesh owing to their nonbiodegradability and toxicity [34-36]. Several of these dyes are stable and resist photodegradation by sunlight, oxidation by molecular oxygen O₂, and decomposition by common acids and bases.

The textile industry plays a part in the economy of several countries around the world. A typical textile dyeing process consists of resizing, scouring, bleaching, dyeing, finishing and drying operations. Dyeing is a fundamental operation during textile fiber processing. The dyeing process consumes large quantities of water for dyeing, fixing and washing and produce large volume of wastewater [37]. Over the last decades, the increasing demand for dyes by the textile industries has shown a high pollutant potential. It is estimated that around 10-15% of the dyes are lost in the effluent during the dyeing processes [38].

The effluent generated from the textile processing industries are considered to be a very complex and inconsistent mixture of many pollutants, such as, mixture of heavy metal ions (e.g., Cr, Al, Cu etc.), suspended solids, dissolved solids, inorganic salts, dispersing agents, dyestuffs, and other toxic organic pollutants including poly vinyl alcohol, starches, various surfactants, organic-chlorine based pesticides, biocides as well as acidic and alkaline contaminants.

Effluents discharged from textile and dyeing industries are characterized by low BOD, high COD and variation of pH in the range of 2-12 [38-40]. Color is usually the first contaminant to be recognized in wastewater; a very small amount of dye in water (10-20mg/L) is also highly visible and affects water transparency and the gas solubility of water bodies. The discharge of these colored dye effluent as wastewater in the ecosystem is a damaging source of esthetic pollution, eutrophication, and interruption in many natural processes (e.g., photosynthesis, respiration) and perturbations in aquatic life. These dyes in the strongly absorb sunlight, which decreases the intensity of light absorbed by water plants and phytoplankton, reducing photosynthesis and the oxygenation of water reservoirs [41]. Dyes often contain elements such as nitrogen, Chlorine or sulfur. The

oxidation product of these molecules may be more toxic than the parent molecule. Because of these unbearable problems created by the discharge of dyes as effluent, it requires clear concepts about dye and its undesirable impact and a quick search for the remedy of these problems.

1.13 Dye

A dye can generally be described as a organic colorants that has an affinity to the substrate which it is being applied and consists of a color producing structure.

Dyes can be firmly fixed to the fabrics and other supporting materials used in textile, food and other industries for imparting different shades of colors [40]. All colored compounds are not dyes. A substance is referred to as a dye when it bears the following criteria

1. It must have a desired color to match the object to be dyed.
2. It must be capable of being fixed to the fabrics or supports directly or indirectly with the help of certain reagents called mordant.
3. When fixed to the supports, the color must be fast to light and resistant to soap and water and to a certain extent to dilute acids and alkalis.

Both dyes and pigments appear to be colored because they absorb some wavelengths of light preferentially. In contrast with a dye, a pigment generally is insoluble, and has no affinity for the substrate. Some dyes can be precipitated with an inert salt to produce a lake pigment.

1.14 Classification of dyes

The dyes were obtained from animal, vegetable or mineral origin, with no or very little processing. By far the greatest source of dyes has been from the plant kingdom, notably roots, berries, bark leaves and wood, but only a few have ever synthetic been used on a commercial scale.

Dyes can be classified as anionic, cationic and nonionic according to their dissociation in an aqueous solution. According to the application they can be classified as bellow

- 1. Reactive dyes:** Dyes with reactive groups that form covalent bonds with OH⁻, NH⁻ or HS⁻ groups in fibers are known as reactive dyes. The reactive group is often a heterocyclic aromatic ring substituted with chloride or fluoride (e.g., dichlorotriazine).
- 2. Metal complex dyes:** These are strong complexes of one metal atom (usually Cr, Cu, Co or Ni) and one or two dye molecules, respectively 1:1 and 1:2 metal complex dyes.
- 3. Acid dyes:** Acid dyes are anionic compounds that are mainly used for dyeing nitrogen containing fabrics like wool, polyamide, and silk and modified acryl. Most acid dyes are azo, anthraquinone or triarylmethane.
- 4. Basic dyes:** Basic dyes are cationic compounds that are used for dyeing acid group containing fibers, usually synthetic fibers like modified polyacryl.
- 5. Pigment dyes:** These insoluble, nonionic compounds or insoluble salts retain their crystalline or particulate structure throughout their application.
- 6. Sulfur dyes:** Sulfur dyes are complex polymeric aromatics with heterocyclic S-containing rings.
- 7. Solvent dyes:** Solvent dyes are nonionic dyes that are used for dyeing substrates in which they dissolve (e.g., plastics, varnish, ink, waxes and fats).
- 8. Food dyes:** Food dyes are usually used in foods, soft drinks, medicines etc. These dyes should be used in such quantity that would not cause any health hazard to human being. These dyes are prepared from coal tar such as tartrazine, sunset yellow, carmoisine, green-S, allura red, caramel aqua marine etc.
- 9. Organic ionic dyes:** Methylene blue (MB) and orange green (OG) Procion red (PR) are the typical organic ionic dyes. MB is cationic in nature while OG and PR is an anionic one. Molecular weight of MB and OG are 355.89 and 452.38. λ_{\max} of MB and OG are 664 nm and 477 nm respectively. Their chemical structures are shown in Fig. 1.1.

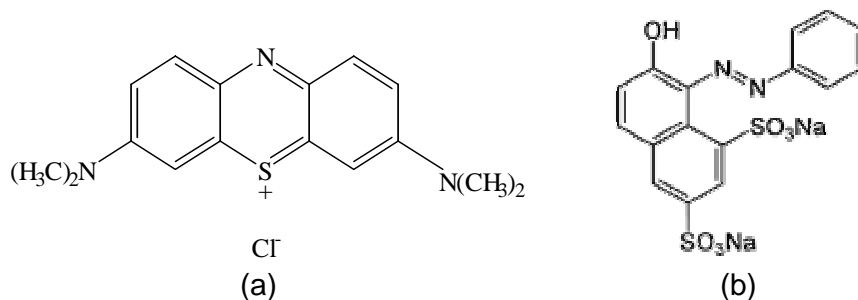


Fig. 1.1: Chemical structure of (a) MB and (b) OG.

1.15 Color in compounds and its sensation

If a substance absorbs visible light, it appears to have a color [42]. So in order for a compound to be colored light absorbing system (chromophore) must be present in it. Various theories have been put forward to establish a relationship between color and constitution. Some important theories are Witt's theory, quinoid theory, resonance theory, molecular orbital theory.

Witt's theory:

According to Otto N. Witt (1876) all colored compounds contain unsaturated groups, which are responsible for exhibiting color and he called these groups as chromophores. A compound containing a chromophore is called chromogen. The most effective are shown in Fig. 1.2:

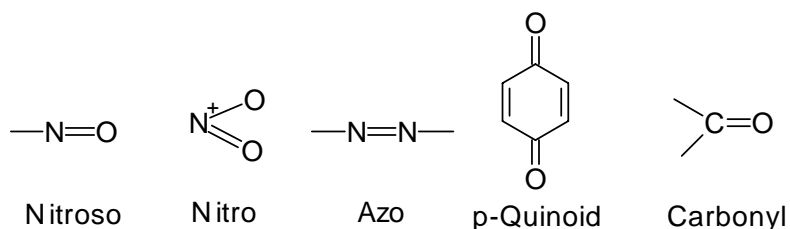


Fig. 1.2: Structures of some effective chromophores.

On the other hand, there are some groups whose presence in a chromogen, modify the color of chromogen but it cannot impart color to it, are called auxochromes. Auxochromes are either acidic or basic and usually salt forming groups, such on $-\text{NH}_2$, $-\text{OH}$ etc. or solubilizing radicals $-\text{COOH}$, SO_2H . Since,

auxochromic groups are capable of forming salts with acidic or basic groups of the fiber; they help the chromogen to fix permanently to the fiber. Therefore if a chromogen has one or more auxochromes, the resulting substance is called a dye i.e.



There are two types of chromophores -

1. Independent chromophores: when a single chromophore is sufficient to impart color to the compound. For example, azo groups (-N=N-), nitroso group (-NO) etc.

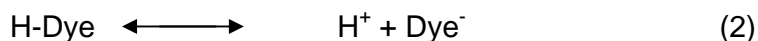
2. Dependent chromophores: when more than one chromophore is required to produce color in the chromogen. For example, >C=C< group etc.

A bathochromic effect (red shift) and a hypsochromic effect (blue shift) are the shifting of the absorption band to the longer and shorter wavelengths, respectively. A hyperchromic effect and hypochromic effect are those which respectively increases and decreases the intensity of absorption.

Quinonoid theory:

The notable points on this theory are –

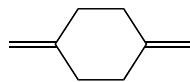
1. Dyes are either weak acid or base.
2. While in solution it (Dye) undergoes ionization as



3. The unionized H-Dye molecule and the anion dye are tautomeric forms of the dye.

4. One tautomeric form possesses the quinonoid structural unit and is called the

quinonoid form.



It has a deep color. The other form has a less intense coloring group, say, $-N=N-$ and or simply benzene ring and is called the benzenoid form. This form has light color or no color.

5. The change of the dye is accompanied by a change in the pH of the solution. To illustrate the Quinonoid theory, Methyl orange, an acidic azo dye, has been taken as an example in Fig. 1.3:

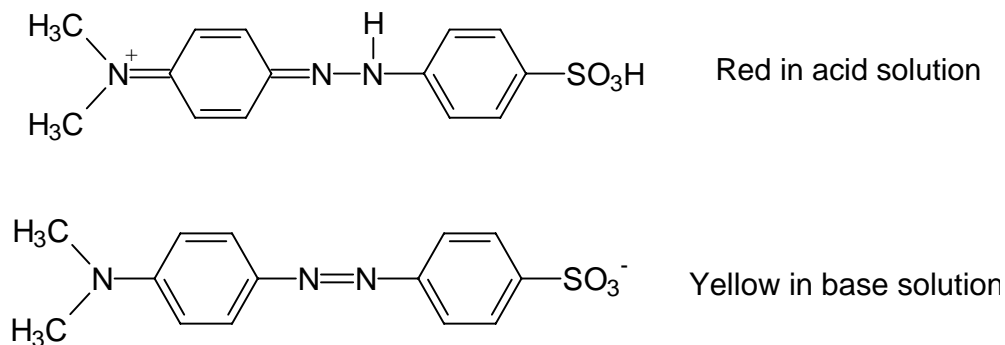


Fig. 1.3: Illustration of Quinonoid theory.

Molecular orbital approach to color

In molecular orbital (MO) theory, an atom or molecule is excited when one electron is transferred from a bonding to an anti-bonding orbital. Electronic transitions, however, can occur in different ways. A transition in which a bonding σ -electron is excited to an anti-bonding σ -orbital is referred to as a σ to σ^* transition. In the same way, Π to Π^* represents the transition of a bonding Π -

electron to an antibonding Π -orbital. An n to Π^* transition represents the transition of one electron of a lone pair, i.e., a non-bonding pair electron of electrons, to an anti-bonding Π -orbital (Fig.1.4).

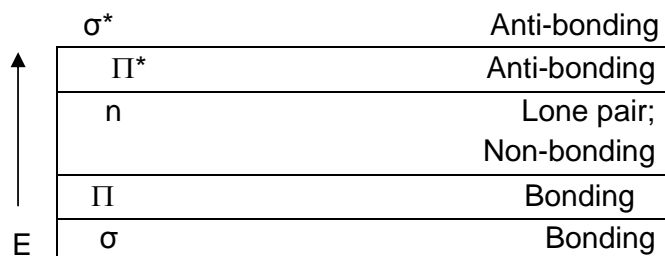
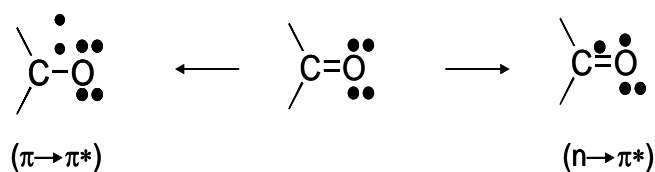
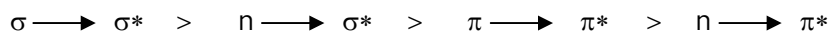


Fig. 1.4: Schematic representation of different transitions.

This type of transition occurs with compounds containing double bonds involving hetero-atoms, e.g., $>C=O$, $>C=N-$, $>C=S$, etc., and may be represented as follows:



The transitions are brought about by the absorption of different amounts of energy. Of the large number of possibilities, only the following transitions are allowed, and their general order of energy difference is:



Since the energy difference between the highest occupied Π -orbital level and lowest unoccupied level is smaller than any other electronic transition, the longest wavelength in the absorption spectrum corresponds to this transition, and the shorter wavelengths correspond to the other transitions. Calculation and

experimental work has shown that as conjugation increases, the energy difference between the highest occupied and lowest unoccupied π -orbital decreases (V.B. theory). Thus, as conjugation increases, the maximum in the absorption band shifts to the longer wavelength, and when it reaches the visible region, complementary color will appear in the compound. We see the color complementary to that which is absorbed

Table 1.1: Clarification of absorbed color and its complementary color.

Light absorbed		Color observed
Wavelength (nm)	Color of absorbed light	
400	Violet	Greenish Yellow
425	Indigo blue	Yellow
450	Blue	Orange
490	Blue-green	Red
510	Green	Purple
530	Yellow-Green	Violet
550	Yellow	Indigo-blue
590	Orange	Blue
640	Red	Bluish-Green
730	Purple	Green

Whereas, benzene is a symmetrical molecule and consequently has no associated transition dipole, some of its bending vibrational modes distort its shape to affect absorption. Introduction of substituents into the benzene ring destroys its symmetry and thereby gives rise to increased intensity of absorption, and by extending of conjugation, increases the wavelengths of the absorption band.

1.16 Harmful impact of dye pollutants

The color produced by minute amount of organic dyes in water is considered to be very important, because, the color in water is aesthetically unpleasant. Disposal of this colored water into receiving water can be toxic to aquatic life. They upset the biological activity in water bodies. They also pose a problem because they may be

mutagenic, carcinogenic and can cause severe damage to human beings, such as, dysfunction of kidney, reproductive system, liver, brain and central nervous system. The most acutely toxic dyes for algae are cationic, basic dyes. The most acutely toxic dyes for fish are basic dyes, especially those with a triphenylmethane structure. Fish also seem to be relatively sensitive to many acid dyes. The chance of human mortality due to acute dyestuff toxicity is probably very low. However, acute sensitization reactions by humans to dyestuffs often occur. Especially some disperse dyestuffs have been found to cause allergic reactions, i.e. eczema or contact dermatitis. Reduction of azo dyes, i.e. cleavage of the dyes azo linkage(s), leads to formation of aromatic amines. The acute toxic hazard of aromatic amines is carcinogenesis, especially bladder cancer.

1.17 Dye treatment techniques

Various physical, chemical and biological treatment techniques can be employed to remove color from dye containing wastewaters [31-33, 36, 39, 40, 41]. Physico-chemical techniques include membrane filtration, coagulation/flocculation, precipitation, flotation, adsorption, ion exchange, ion pair extraction, ultrasonic mineralization, electrolysis, advanced oxidation (chlorination, bleaching, ozonation, Fenton oxidation and photocatalytic oxidation) and chemical reduction. Biological techniques include bacterial and fungal biosorption and biodegradation in aerobic, anaerobic, anoxic or combined anaerobic/aerobic treatment processes.

1.18 Adsorption phenomena: Surface process

Adsorption is operative in most natural physical, biological, and chemical systems, and is widely used in industrial applications such as activated charcoal, synthetic resins and water purification. Although there is no chemical distinction between the molecules or atoms on the surface and the molecules or atoms in the bulk, energy considerations lead to quite dissimilar properties.

Adsorption is a process that occurs when a gas or liquid solute accumulates on the surface of a solid or a liquid (adsorbent), forming a molecular or atomic film (the adsorbate).

Adsorption is a surface phenomenon. Formally adsorption may be defined as a process in which the concentration of a chemical species is greater in the surface than in the bulk resulting from inelastic collision suffered by molecules on the surface. The species that is adsorbed is called adsorbate and the material of the surface on which adsorption takes place is called adsorbent. Adsorption strictly refers to accumulation of adsorbate on the surface only due to residual field of forces. It is different from absorption, in which a substance diffuses into a liquid or solid to form a solution. The term sorption encompasses both processes, while desorption is the reverse process.

1.19 Types of adsorption

Adsorption is a consequence of surface energy. In a bulk material, all the bonding requirements (be they ionic, covalent or metallic) of the constituent atoms of the material are filled. But atoms on the (clean) surface experience a bond deficiency, because they are not wholly surrounded by other atoms. The adsorbed material is generally classified as exhibiting two categories:

- (a) Physisorption.
- (b) Chemisorption.

1.19.1 Physisorption

Physisorption occurs when non-balanced physical forces appear at the boundary of the phases and adsorbed species is attached to the surface by weakly Van der Waals force. Physisorption is characterized by,

- (i) Low heat of adsorption (10-40 KJ/mol).
- (ii) Non specific.
- (iii) Mono or multi-layer.
- (iv) Rapid, non activated and reversible.
- (v) Significant at low temperature.
- (vi) No electron transfer.

1.19.2 Chemisorption

Adsorption, which results from chemical bond formation (strong interaction) between the adsorbent and the adsorbate in a monolayer on the surface, is called chemisorption.

Chemisorption is characterized by,

- (i) More heat of adsorption (80-400 KJ/mol, sometimes endothermic).
- (ii) Very specific for active site of heterogeneous catalyst.
- (iii) Mono-layer only.
- (iv) Effective over a wide range of temperature.
- (v) Slow, activated and irreversible.
- (vi) Electron transfer between adsorbate and surface.

1.20 Purpose of the adsorption study

Numerous investigations have focused on surface adsorption as a means of removing textile dyes from water. Beside, the following information can be obtained in an adsorption experiment:

- (i) Nature of adsorption, that is whether it is adsorbed physically or chemically and the conditions (temperature, pressure, state or adsorbent etc.) under which the adsorption takes place.
- (ii) Thermodynamic data regarding the adsorption process. This include the amount of the adsorbent adsorbed under various equilibrium concentrations at definite temperature.
- (iii) Specific surface area-surface area of one gram of the substance by the adsorption process can also be measured.

1.21 Adsorption isotherms

Adsorption is usually described through isotherms. Many different types of isotherms have been observed in the literature [43,44] These isotherms can have very different shapes depending on the type of adsorbent, the type of adsorbate, and intermolecular interactions between the solute and the surface.

The variation of surface coverage (Θ) with equilibrium pressure (or concentration in the case of solution) at a given temperature is called adsorption isotherm. According to IUPAC classification [45], there are six different types of adsorption isotherm as shown in the Fig. 1.5:

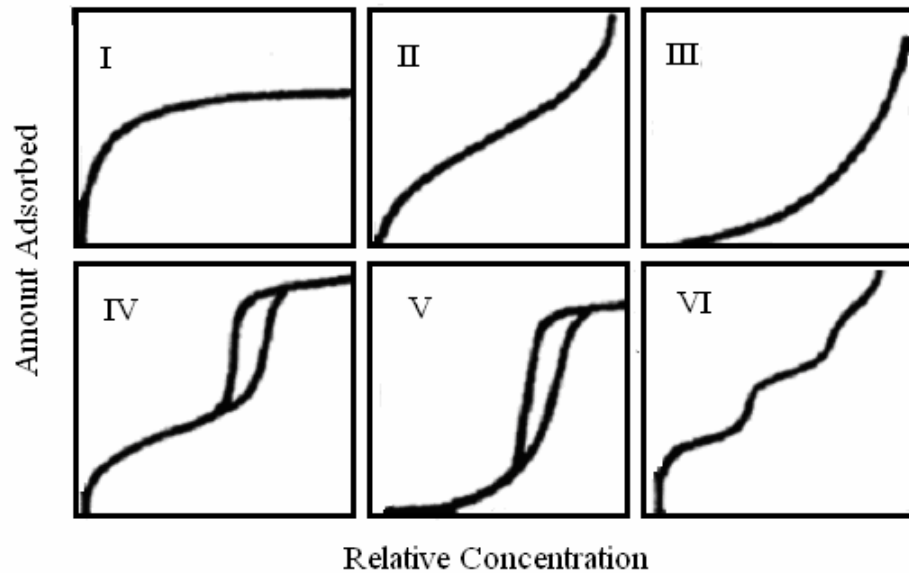


Fig. 1.5: IUPAC Classification of adsorption isotherms.

(a) Type 1: This shape of the isotherm is characterized by the asymptotic approach of monolayer of adsorbate on the surface.

(b) Type 2: This is the most common type of isotherm corresponding to multi-layer formation on a surface of high adsorption potential.

(c) Type 3: This pattern of isotherm is comparatively uncommon, corresponding to multi-layer formation on the solid.

(d) Type 4 & 5: These are analogous to type 2 & 3 on porous adsorbents where the adsorption is limited by the volume of mesopores, causing the adsorption to

level off at a pressure less than saturation pressure of adsorbate (P_0). They reflect capillary condensation and may show hysteresis effect.

IUPAC classification considers adsorption at sub critical temperature, but adsorption at near critical and super critical temperature was not considered. Hence this classification is incomplete. Considering the adsorption at near or super critical temperature a new classification is proposed as shown in the Fig. 1.6.

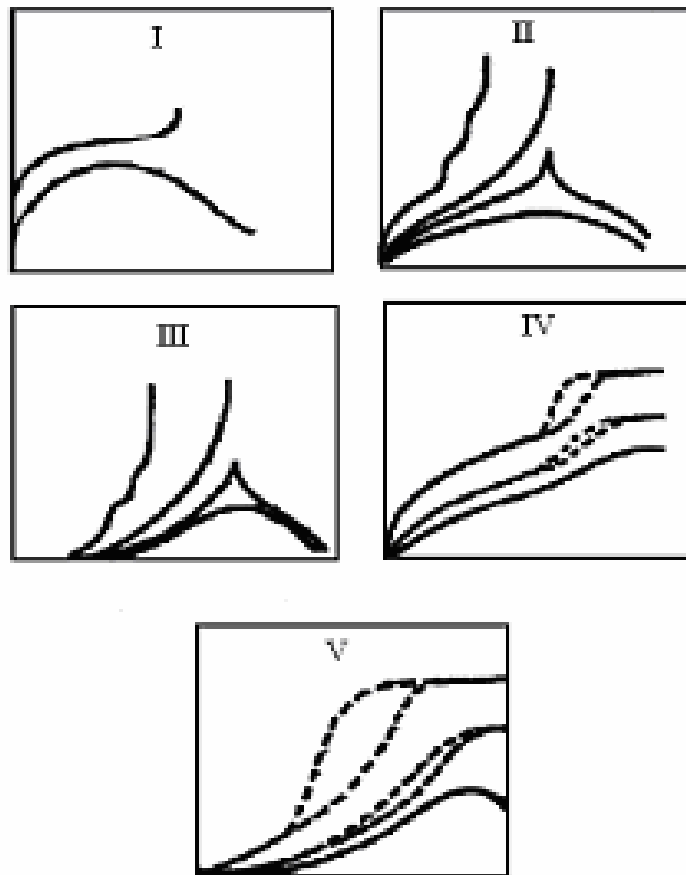


Fig. 1.6: A new classification for adsorption isotherms.

1.22 Model of adsorption isotherms

Several theoretical models were proposed in order to explain the experimental adsorption isotherms:

- (a) Langmuir isotherm.
- (b) Freundlich isotherm.
- (c) BET isotherm.
- (d) Temkin isotherms etc.

A (i) Langmuir isotherm:

Characteristics feature of Langmuir isotherm equation:

- (i) Adsorption is limited to monolayer formation.
- (ii) In the case of physisorption, this equation satisfactorily explains adsorption behavior only at low surface coverage and at low adsorbate pressure.
- (iii) In the case of chemisorption which is associated with monolayer coverage Langmuir equation is quite consistent.

Langmuir derived the following equation (a) to explain the experimental adsorption isotherm,

$$\Theta = aC_e / (1 + aC_e) \dots\dots\dots (1)$$

The fraction of the surface of the surface covered by the adsorbate can be expressed as,

$$\Theta = q/q_m \dots\dots\dots (2)$$

From eqn. (1) and (2)

$$q/q_m = aC_e / (1 + aC_e) \dots\dots\dots (3)$$

Where, $x/m = q$ = the amount of adsorbate adsorbed at eqm. Concentration, (C_e) in mol g^{-1}

$K' = q_m$ = monolayer capacity in mol g^{-1}

$a = K$ = adsorption constant (eqm. constant for adsorption process) in L mol^{-1}

From eqn. (3), we have,

$$C_e / (x/m) = C_e / K' + 1 / KK' \dots\dots\dots (4)$$

From plot of $C_e / (x/m)$ vs C_e ,

Slope = $1/K'$

$K' = 1/\text{slope} = \text{monolayer capacity},$

And, intercept = $1/KK$

$K = 1/(\text{intercept} * K') = \text{equilibrium constant} = a$

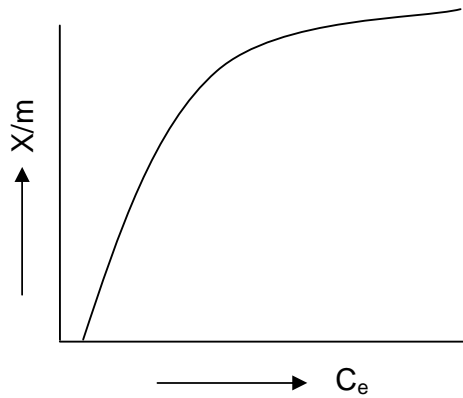


Fig. 1.7a: Langmuir plot of X/m vs concentration (C_e).

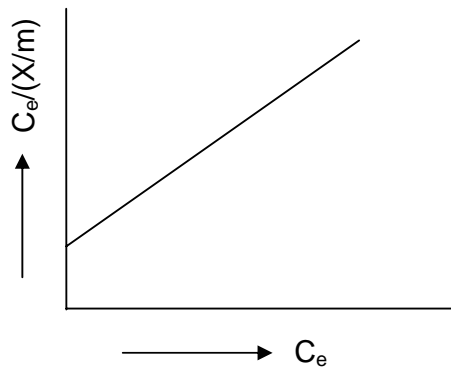


Fig. 1.7b: Langmuir-Hinshelwood plot of $C_e/(X/m)$ vs C_e .

- ii) **Freundlich adsorption isotherm:** The variation of adsorption with concentration of the substance in solution is usually represented by Freundlich isotherm as follows:

$$y = kC^{\frac{1}{n}} \quad (1.4.11)$$

$$\text{or, } \log y = \log k + \frac{1}{n} \log C \quad (1.4.12)$$

- iii) **BET adsorption isotherm:** The theory of Brunauer, Emmett and Teller (BET) is an extension of the Langmuir treatment to allow for multilayer adsorption on non-porous solid surface. The BET equation is usually written as:

$$\frac{P}{X(P_o - P)} = \frac{1}{X_m C} + \frac{C - 1}{X_m C} \cdot \frac{P}{P_o} \quad (1.4.13)$$

where, P_o = saturation vapor pressure, X_m = the monolayer capacity and

$$C = \exp [(\Delta H_L - \Delta H_1) / RT].$$

B. Factors affecting adsorption

i) **Temperature:** The level of adsorption at any particular concentration decreases with the increase in temperature; that is the overall process is exothermic. At higher temperature the adsorbed molecules have greater vibrational energies and therefore, more likely to desorb from the surface.

ii) **Nature of the solvent:** The solvent has an important effect, since it competes with the surface of the adsorbent in attracting the solute. There are three different ways to describe the influence of solvent on adsorption behavior of the solvent (a) its interaction with the solute in solution, (b) its interaction with the adsorbed layer, and (c) its interaction with the solute in the adsorbed layer. However, when the solvent is water, it is worthless to consider the solvent effect.

iii) **Particle and pore size:** The adsorption efficiency increases as mean diameter of the particle decreases. Large surface area is available for adsorption with the

small particles. Another reason is the reduced diffusive path length of the interior of small adsorbent particles and the adsorbate particles require less energy of jump from one active site to another, resulting in higher uptake by the adsorbent.

iv) pH of the solution: The effect of pH is extremely important when the adsorbing species is capable of ionizing in response to prevailing pH. It is well known that substances adsorb poorly when they are ionized. When the pH is such that an adsorbable compound exists in ionic form, adjacent molecules of the adsorbed species on the adsorbent surface will repel each other to a significant degree, because they carry the same electrical charges. Thus the adsorbing species cannot be packed together very densely on the surface. This is the common observation that non-ionized forms of acidic and basic compounds adsorb much better than their ionized counterparts. The acidic species thus adsorb better at low pH and basic species adsorb better at high pH.

C. Adsorption from solution

Adsorption from solution is much simpler than that of gas adsorption. A known mass of adsorbent is kept in touch with a known volume of solution at a given temperature until there is no further change in the concentration of the supernatant solution. This concentration can be determined by a variety of methods involving chemical or radiochemical analysis such as colorimetry, refraction index, *etc.* The experimental data are usually expressed in terms of an apparent absorption isotherm in which the amount of solute adsorbed at a given temperature per unit mass of adsorbents calculated from the decreases of solution concentration is plotted against the equilibrium concentration. By analogy with gas adsorption, one might hope to calculate the monolayer capacity, the application of an equation of the individual isotherm has a pattern of a sharp knee followed by a clear plateau; the monolayer capacity is then given by the height of the plateau.

1.23 Photochemistry

Photochemistry is concerned with the interaction of light quantum and a molecule and the subsequent chemical and physical changes which result from this

interaction. The study of photochemistry includes the entire phenomenon associated with the absorption and emission of radiation by chemical system. It includes phenomena such as fluorescence and phosphorescence, luminescence chemical reaction, photo-stimulated reactions such as photographic, photosynthetic and photolytic reactions of various kinds.

Absorption of light: A photochemical reaction takes place by the absorption of electromagnetic radiation by a molecule. According to Planck's quantum theory, absorption of energy is quantized and is given by $E=h\nu$ where, h is the Planck's constant and ν is the frequency of the absorbed radiation. Planck's equation can also be written as $E=hc/\lambda$ where, c is the velocity of light and λ is the wave length of the absorbed radiation.

Spectrum: A plot of absorbance or transmittance or reflectance as a measure of intensity of radiation against the wavelength or frequency or wave number of the radiation absorbed or transmitted or reflected by the substances.

Emission and absorption spectrum: The intensity of emission is directly proportional to the concentration of the analyte in the solution being aspirated. The absorption spectrum is dependent on the absorption capability of light by analyte species.

Consequences of the Absorption of Light: As light is a radiant energy, absorption of light means absorption of energy. The changes that might be produced by the absorbed energy may be as follows:

Excitation: The internal energy of the molecules or atoms may be raised in specific amounts i.e. are raised from ground state to excited states. (Quantum transition)

Dissociation: The molecule breaks down to form smaller molecules, atom or free radicals.

Luminescence: When the substance, absorbing the light does not undergo photochemical reaction. The substance is then said to show luminescence. The

emission of light in the visible region of the spectrum is attributed to the return of one or more outer electrons of the excited molecules or atoms to the normal position as result of collisions with other atoms or molecules.

Fluorescence: In the fluorescence process a molecule is first excited to higher singlet state and if the life time of the excited state is less than 10^{-6} second, it undergoes non radiative vibrational deactivation in the excited singlet state and finally turns back to the ground singlet sate with the emission of photon having longer wavelength than that absorbed in the initial photon absorption process. Fluorescence stops just after the removal of the exciting light source.

Phosphorescence: In the phosphorescence process a molecule is first excited to upper singlet state by the absorption of photon of a certain wavelength. The molecule then undergoes nonradiative vibrational deactivation in the upper singlet state as well as intersystem crossing to the comparatively stable excited triplet state from which it turns back to the ground singlet state with the emission of photon of longer wavelength. Since excited triplet state has considerable lifetime, the molecule may continue emission of light even after the removal of the exciting light source.

Chemiluminescence: This is the phenomenon of emission of light as a result of certain chemical reactions. The glow of fireflies due to the aerial oxidation of luciferon (a protein) in the presence of enzyme luciferase is an example of chemiluminescence.

1.24 Theoretical aspects of the experimental techniques

1.24.1 SEM Technique

The scanning electron microscope (SEM) uses a finely focused beam of electrons to scan over the area of interest. The beam-specimen interaction is a complex phenomenon. The electrons actually penetrate into the sample surface, ionizing the sample and cause the release of electrons from the sample. These electrons are detected and amplified into a SEM image that consists of Back Scattered Electrons and Secondary Electrons. Since the electron beam has a specific energy and the sample a specific atomic structure, different image will be collected from different samples, even if they have the same geometric appearance.

The specimen stage allows movement of the specimen along 5 axis as indicated in Fig.1.8 (a) & (b). The basic stage is controlled manually by micrometers and screw-type adjusters on the stage door. The motorized stage has motors driving the X, Y, Z and rotation controls, all with manual override.

The stage can be tilted over 90° . The tilt axis always intersects the electron optical axis of the column at the same height (10 mm). When the specimen positioned at this height, the specimen can be tilted in the eucentric plane. This means that during tilt, almost no image displacement occurs. The tilting mechanism can be locked for more stability at high magnification.

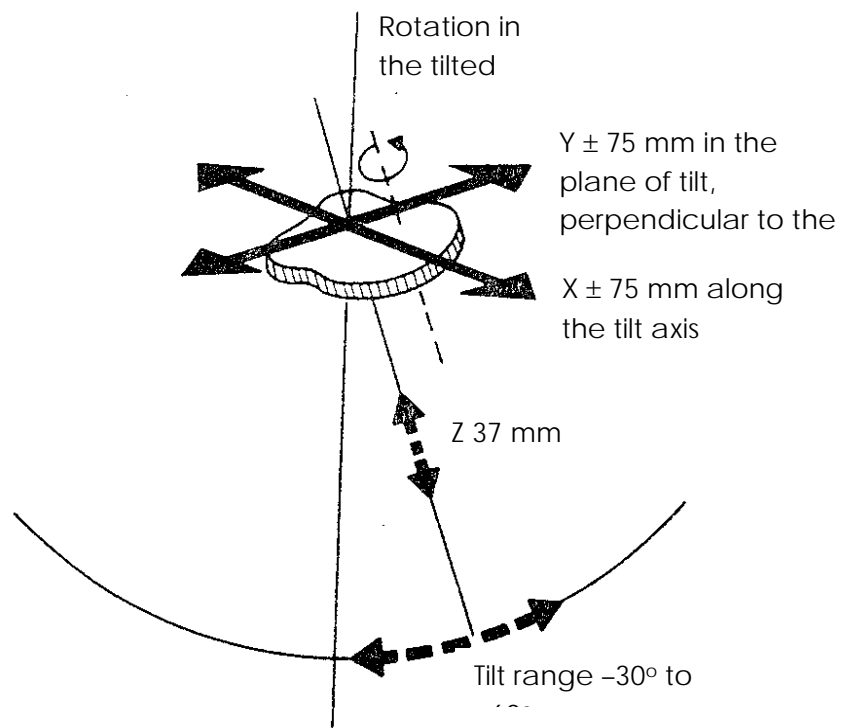
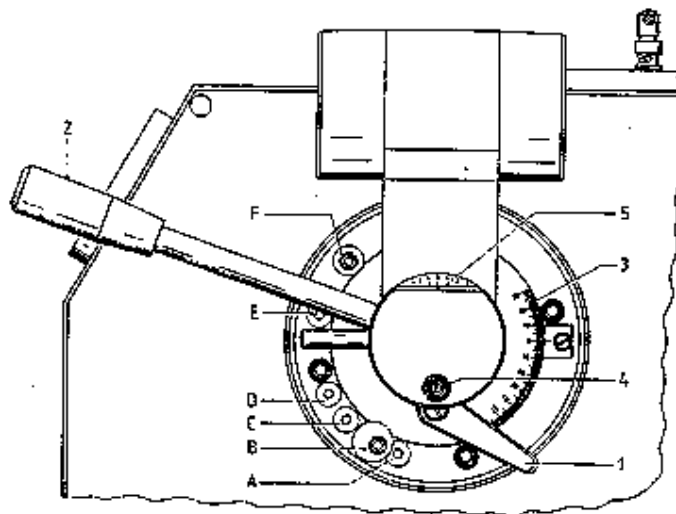


Fig. 1.8 (a): Illustration of specimen stage movement in SEM arrangements.



1.24.2 Elemental analysis: Energy dispersive X-ray micro analysis(EDX)

EDX is a micro analytical technique that uses the characteristic spectrum of X-ray emitted by the specimen after excitation by high-energy electrons to obtain information about its elemental composition. An electron beam strikes the surface of the sample. The energy of the beam is 120 keV. This causes X-rays to be emitted. The energy of the X-rays emitted depends on the material under examination. The X-rays are generated in the whole section. The detector used in EDX is the Lithium drifted Silicon detector. This detector must be operated at liquid nitrogen temperatures. When an X-ray strikes the detector, it will generate a photoelectron within the body of the Si. As this photoelectron travels through the Si, it generates electron-hole pairs. The electrons and holes are attracted to opposite ends of the detector with the aid of a strong electric field. The size of the current pulse thus generated depends on the number of electron-hole pairs created, which in turn depends on the energy of the incoming X-ray, which depends on the composition of the sample. Thus, an X-ray spectrum can be acquired giving information on the elemental composition of the material under examination. By moving the electron beam across the material an image of each element in the sample can be acquired.

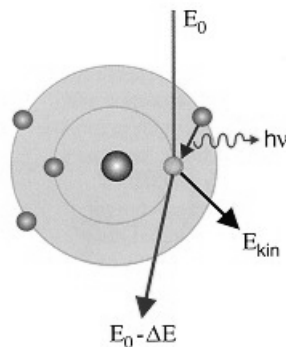


Fig. 1.9: Emission of X-ray due to the collision of electron beam with the surface of the solid.

If an electron beam strikes the surface X-rays ($h\nu$) were emitted, which energy depends on the elemental composition of the sample and Vice versa the energy of the electrons is reduced. Analysis of the X-rays is called EDX.

1.24.3 X-Ray diffraction

The X-ray diffraction (XRD) provides substantial information on the crystal structure. This method is applied for the investigation of orderly arrangements of atoms or molecules through the interaction of electromagnetic radiation to give interface effects with structures comparable in size to the wavelength of the radiation. Studies on the crystal structures developed based on methods using single crystals after the discovery of X-ray diffraction by crystals made by the Von Laue . Now a days XRD is used not only for the determination of crystal structure but also chemical analysis, such as chain conformations and packing for polymers, for stress measurements and for the measurement of phase equilibria and the measurement of particle size, for the determination of the orientation of the crystal and the ensemble of orientations in a polycrystalline material.

X-rays are the electromagnetic radiation whose wavelength is in the neighborhood of 1° A. The wave length of an X-ray is thus of the same order of magnitude as the lattice constant of crystals, and it is this which makes X-rays so useful in structures analysis of crystals whenever X-ray are incident on a crystal surface they are reflected. The reflection abides by the celebrated Bragg's law as given below:

$$2d \sin\theta = n\lambda$$

Where, d is distance between crystal planes, θ is the incident angle, λ is the wave length of X-ray and n is a positive integer. The diffracted X-ray may be detected by their action on photographic films or plates or by means of a radiation counter or electronic equipment feeding data to a computer.

The main purpose of using this technique for the analysis of the studied polymeric is to observe, from the X-ray diffraction pattern, the change in crystallinity in the series upon same condition.

1.24.4 Infra-red (IR) spectroscopy

Emission or absorption spectra arise when molecules undergo transition between quantum states corresponding to two different internal energies. The energy difference ΔE between the states is related to the frequency of the radiation emitted or absorption by the quantum relation

$$\Delta E = h\nu \quad (1.4.2)$$

where $h \rightarrow$ Planck's constant $\nu \rightarrow$ frequency. Infrared frequencies have the wave length range from 1 μm to 50 μm are associated with molecular vibration and vibration-rotation spectra. Detection of chemical groups and bonding are done by the typical spectra.

In oxides surface, the IR absorption spectrum is often surprisingly simple, if one considers the number of atoms involved. This simplicity results first from the fact that many of the normal vibrations have almost the same frequency and therefore appear in the spectrum as one absorption band and second, from the strict selection rules that prevent many of the vibrations from causing absorptions. In our experiment, we tried to observe the change in frequency of different samples Iron oxide, silicon oxide, Iron-silicon mixed oxide and detection of Iron oxide, silicon oxide, mixed oxide by following the Fe-O or Si-O frequencies. IR spectrums of all the compounds were recorded on IR spectrophotometer in the region of 4000-400 cm^{-1} . Samples were introduced as KBr pellets. A block diagram of an IR spectrophotometer is shown in Fig. 1.10.

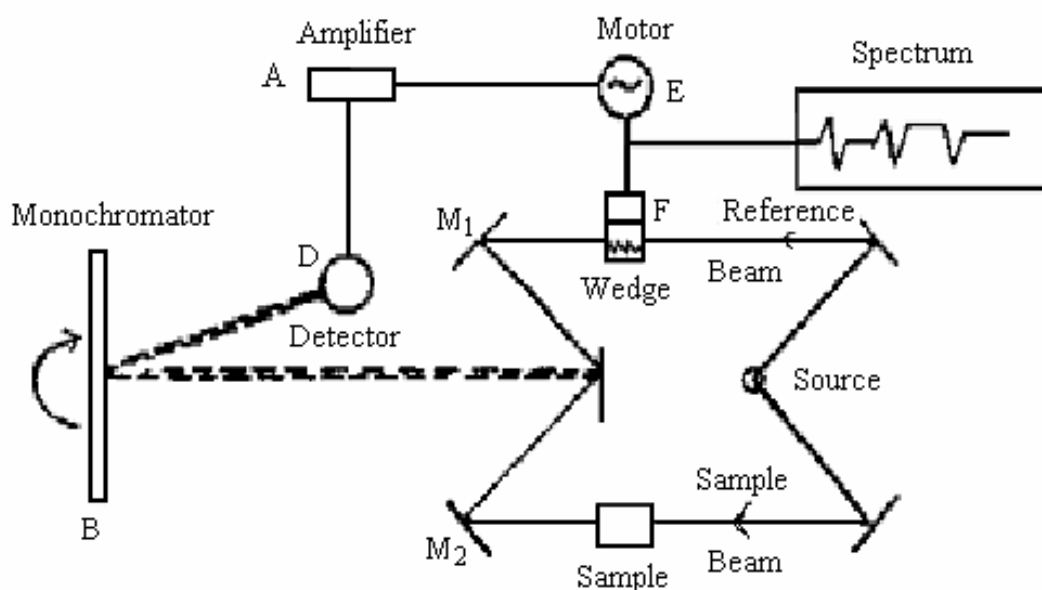


Fig.1.10: A block diagram of an IR spectrophotometer.

1.24.5 Principle of absorption spectroscopy

The greater the number of molecules capable of absorbing light of a given wavelength; the greater will be the extent of light absorption. Furthermore, the more effective a molecule is in absorbing light of a given wavelength, the greater will be the extent of light absorption. From these guiding ideas, the following empirical expression, known as the Beer-Lambert law, which is the basis of spectrometric methods of chemical analysis, may be formulated:

$$A = \log (I_0/I) = \epsilon cl \text{ (for a given wavelength)} \quad (1)$$

where, I_0 = Intensity of the light incident upon the sample cell.

I = Intensity of the light having the sample cell.

c = Molar concentration of solute.

l = Thickness of sample cell (cm).

ϵ = Molar absorption coefficient.

A = Absorbance.

The Molar absorption coefficient (ϵ) is a property of the molecule undergoing an electronic transition and related to transition probability and is not a function of the variable parameters involved in preparing a solution. The value of ϵ indicates how intense a given transition is and totally an intrinsic property of the molecule, i.e.

$\epsilon > 10^4$ is high intensity absorption.

$\epsilon < 10^3$ is low intensity absorption.

$\epsilon = 100$ to 1000 is forbidden transition.

1.25 Characterization of surface properties by adsorption methods

Adsorption methods may be used to provide information about the total surface area of a catalyst, the surface area of the phase carrying the active sites, or possibly even the type and number of active sites. The interaction between the adsorbate and the adsorbent may be chemical (chemisorption) or physical (physisorption) in nature and ideally should be a surface-specific interaction. It is necessary to be aware, however, that in some cases the interaction between the adsorbate and the adsorbent can lead to a chemical reaction in which more than just the surface layer of the adsorbent is involved. For example, when using oxidizing compounds as adsorbates (O_2 or N_2O) with metals such as copper or nickel or sulfides, sub-surface oxidation may occur.

Physical adsorption is used in the BET method to determine total surface areas [46]. Many catalysts comprise an active component deposited on a support. In order to investigate relationships between catalytic properties and the amount of active surface it is necessary to have a means of determining the surface area of the phase carrying the active sites (active phase) in the presence of the support. One has to resort to phenomena specific to the active phase. Chemisorption on the active phase is commonly used for this purpose.

Because of its intrinsically specific nature, chemisorption has an irreplaceable role. It should be recognized, however, that well defined thermodynamic equilibrium physisorption is much more difficult to achieve by chemisorption than with physisorption. Moreover, it does not obey simple kinetics. Empiricism permits the derivation of procedures which give reproducible results, and yield values which are proportional to the true surface area within certain limits. But the real coefficient of proportionality is actually unknown. Different procedures are used, according to UIC nature of the active phase/support system to be characterized, and depending on the choice of adsorbate. Provided standard, reproducible procedures are used, invaluable information can be obtained.

A wide variety of adsorbates has been used, the choice depending on the nature of the surface to be examined and the type of information being pursued; e.g. for metals, H_2 , CO , O_2 and N_2O ; for sulfides, NO , CO , O_2 , H_2S and organo-sulfur compounds; for oxides, NH_3 , CO_2 and various organic compounds.

With simple probe molecules, such as H_2 , information about the number of surface metal atoms is readily obtained by using adsorption measurements. However, even with such simple probe molecules further information about the heterogeneity of a surface may be obtained by performing temperature-programmed desorption measurements. With probe molecules which are chemically more specific (e.g. NH_3 and organic amines, H_2S and organic sulfides) it may be possible to obtain information about the number and nature of specific types of surface sites, for example, the number and strength of Lewis or Bronsted acid sites on oxides, zeolites or sulfides.

The use of more than one technique can provide important additional information about the nature of sites on a particular solid surface. For example, infrared spectroscopy may be used in conjunction with quantitative chemisorption measurements of CO to determine the type of binding of CO and hence the nature and number of the active sites. The combination of chemisorption and ESR spectroscopy permits the characterization of the electronic properties of the surface. Care should be taken when using adsorption with microporous solids, as new effects may arise. Specific literature should be consulted in this case.

1.26 Determination of specific surface area by adsorption measurements

Adsorption measurements have a variety of uses and applications, but perhaps the most important from our point of view is in determining the surface areas of catalysts. Provided the rate of transport of reactants to the surface, and product away from the surface, is faster than the catalyzed reaction, then the observed rate should be proportional to the surface area of the active phase of the catalyst.

Adsorption measurement can be performed by two ways,

- (1) Gas adsorption measurement.
- (2) Dye adsorption measurement.

The surface area of a catalyst could then be determined by either BET or Langmuir adsorption equation depending on which is appropriate for given data.

1.26.1 Gas adsorption measurements

Gas adsorption is accompanied by adsorption of a gas or vapour onto a bare solid surface. The total surface area of the catalyst can be determined by adsorption of relatively inert gases like Ar, N₂ etc. at near their condensation temperature, as at such condition adsorption is non specific and physical in nature. If the catalysts are not susceptible to poisoning by H₂, O₂, CO, NO gases, the specific surface area, i.e. the surface area due to active metal component can be determined by chemisorption of these gases.

1.26.2 Dye adsorption measurements

Dye adsorption technique involves the adsorption of dye molecules from solution onto a solid surface, in particular, dyes such as methylene blue. The method of adsorption of methylene blue in liquid phase for specific surface area

determination has been adopted widely for various natural solids: activated carbon, charcoal, silica.

1.27 Point of zero charge

The pH_{PZC} of solid surface naturally depends on the relative number of each type of grouping and on their respective dissociation constants. It has been found that the zero point charge is usually not obtained at equal concentration of the positive and negative ions but at a slight excess of one of the ions. The zero point does not necessary occur at neutral pH, but it known to vary with the crystal structure of the solid. For example, alumina is not neutral at pH.

The pH where the net total surface charge is zero is called the point of zero charge (PZC), which is one of the most important parameters used to describe variable-charge surfaces. The PZC of the oxide may be the most important parameter since it is the pH around which strong buffering effect is observed [47]. The buffering effect is seen through the plateau on a pH final (pH after oxide addition) vs. pH initial graph.

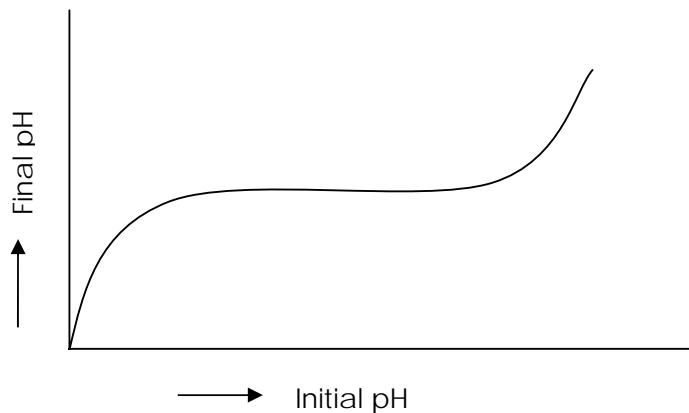


Fig. 1.11: Plot of a pH final (pH after oxide addition) vs pH initial.

The oxide surface becomes protonated (deprotonated) when the initial pH is below (above) the afore-mentioned plateau region [47]. Oxide ions are strong bases. Thus, in aqueous solutions, they become neutralized by water to form hydroxyl groups. The hydroxyl groups on the surface of an amphoteric oxide then become protonated or deprotonated, which leads the solution pH increasing or decreasing. In other words, as oxides in an acidic (basic) pH become protonated (deprotonated) the solution, which supplies (consumes) protons, becomes more basic (acidic). Adsorption is largely depends on the pH of the bulk. If the pH of the bulk higher than pH_{PZC} surface become negative and the lowering of the pH of the bulk than pH_{PZC} surface become positive.

This general concept is shown in the diagram (Figure 1.10).

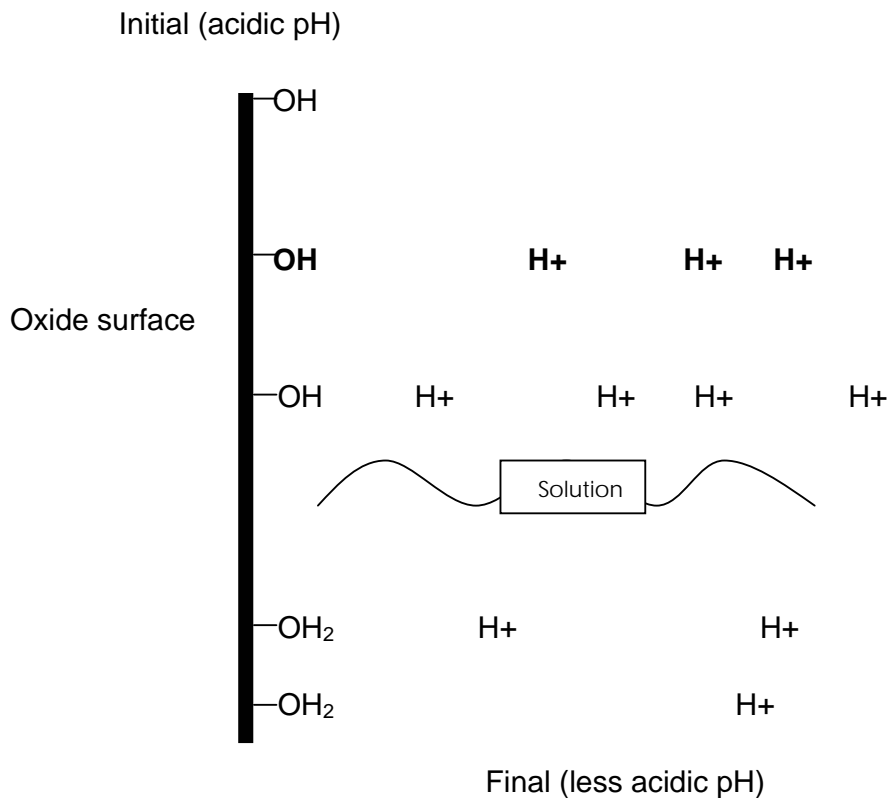


Fig. 1.12: A visual representation of a pH shift.

In solution, when the pH is greater than the PZC, the surface of the oxide is negatively charged and deprotonated. When the pH is less than the PZC, the surface of the oxide is positively charged and protonated. So oxides that are placed in solutions with a pH greater than its PZC will absorb cations and oxides contacted with a solution with a pH less than its PZC will absorb anions. Two important points are to be noted here,

1. The surface charge is equal to the fraction of positively charged sites minus the fraction of negatively charged sites.
2. The electrical double layer consists of a layer of charge on the oxide's particle surface and another layer of opposite charge in the surrounding solution.

1.28 Methods for the determination of point of zero charge (PZC)

There are several methods namely:

- (1) Potentiometric titration.
- (2) Mass titration.
- (3) Ion adsorption.
- (4) Electrophoretic mobility.

1.28.1 Mass titration

Mass titration was originally developed for pure metal oxides [48-50] and later extended so that it can be used also for contaminated samples [43/50m]. The principle of the method is simple; one needs to be added subsequent portions of metal oxide powder to the water or aqueous electrolyte solution, which might be acidified or may contain a base. The pH of the system is changed gradually and approaches a constant value, which is the PZC in the case of pure oxide. If the sample is contaminated, i.e. if it contains a certain portion of acid or base, the final pH is higher or lower than PZC, depending on the type and amount of the acid or base in the powder.

1.29 Literature survey and aim of the present work

Mixed metal oxide (MMO) should be an interesting technology of materials since the overall properties of the MMO are superior to those of the individual oxide, as can be seen from the following survey:

Preparation of new mixed metal oxides of both industrial and synthetic importance has become a routine work in advanced material laboratories. Much work has been directed in the synthesis and characterization of metal oxide and mixed metal oxides type semiconductor photo catalyst and adsorbent as they have effective capability to destroy toxic and hazardous organic substances.

Nano scale oxide particles of transition metals are gaining continues importance for various applications such as catalysis, passive electronic components and ceramic materials [51]. Due to their small size, nano particles exhibit novel material properties that are significantly different from those of their bulk counterparts. Nickel oxide nano particles with a uniform size and well dispersions are desirable for many application in designing ceramic, magnetic, electrochromic and heterogeneous catalytic materials [52].

Hudson, M. J. *et al* have performed an excellent piece of work [53] on the preparation and characterization of mesoporous, high-surface-area zirconium(IV) oxide. They prepared high-surface-area zirconium(IV) oxide by incorporation of cationic quaternary ammonium surfactants in the hydrous oxide and subsequent calcinations of the inorganic/organic intermediate. The surfactants are

incorporated by cation exchange at a pH above the isoelectric point of the hydrous oxide. After calcinations to 723 K and above, the ordering is a linear function of the chain length. Scaffolding, rather than a templating, mechanism is invoked to explain this ordering. Calcination of the materials to 723–973 K results in the formation of a mesoporous zirconium(IV) oxide.

An ingenious piece of research was conducted by Stephanopoulos, M. F. *et al* [54] on nano structured cerium oxide “ecocatalysts”. Various techniques can be used to prepare nanocrystalline cerium oxide. For large scale production, several precipitation and gelation techniques are suitable. Ceria doped with rare-earth oxides or zirconia can be easily prepared by a coprecipitation (CP) method using ammonium carbonate as the precipitant. This involves mixing an aqueous solution of cerium(III) nitrate and other metal nitrates in desired proportions with $(\text{NH}_4)_2\text{CO}_3$ at 60–70°C, keeping a constant pH value of 8, and aging the precipitate at 60–70°C for 1 h. After aging, the precipitate is filtered and washed with distilled water several times, then it is dried at 100–120°C and calcined in air at several hundred degrees Celsius for 10 h at a heating rate of 2°C/min. This method typically produces a well-crystallized material with needlelike crystals.

Point of zero charge (PZC) of metal oxide catalyst is an important parameter in preparation of the catalyst, since most of the metal oxide catalysts are amphoteric in nature. Park, J. and coworkers [55] determined surface charging parameters in aqueous solution by the method of equilibrium pH at high oxide loading. They determined PZC of alpha-alumina, gamma-alumina, theta- alumina and silica by this method. 500 ml pH solutions ranging from 0 to 13 with increments of approximately 0.5 were prepared. The ionic strength of all the solutions was kept constant. After the oxide addition the solutions were placed on a shaker. Final pH increasing was recorded. The initial pH versus the final pH was plotted to show the PZC.

Appel, C. and coworkers [56] determined the PZC in soil and, minerals (kaolinite and synthetic goethite) collected from Puerto Rico an oxisol and ultisol using three methods:

- (1) Potentiometric titration measuring the adsorption of H^+ and OH^- on amphoteric surfaces in solutions of varying ionic strength,
- (2) Direct assessment of surface charges via non-specific ion adsorption as a function of pH and ionic strength and
- (3) Electroacoustic mobility of reversible particles as it varies with pH and ionic strength.

Their studies reveal that the PZC values, determined by first two methods, for Kaolinite are 2.7-3.2 and that of synthetic goethite is 7.4-8.2. The PZC for soil range from 3.9 to 4.4 for oxisol and 2.3-3.7 for the ultisol The PZC, determined by electroacoustic mobility, of Kaolinite is 3.8-4.1 and that of synthetic goethite is 8.1-8.2, furthermore the values found for oxisol is 3.4-3.5 and that of ultisol 2.6-2.7. Parker, J. C. *et al* [57] have proposed several methods for the determination of the PZC in soils and other materials dominated by variable surface-charge colloids. In soils researchers have generally relied on potentiometric titration, which masses changes in surface potential with changes in activities of H^+ and OH^- , to determine the point of zero salt effect (PZSE) or point of zero net proton charge (PZNPC). They have also used non-specific ion adsorption, which measures changes in the electrostatic adsorption of a cation and anion with changes in the activities of H^+ and OH^- , to find the point of zero net charge (PZNC)

Another method for determining of the PZC is Mass Titration method, originally developed for pure metal oxides by Noh, J. S. *et al* [58] and later extended by Zalac, S. [59] for contaminated samples. The principle of this method is simple; one needs to add subsequent portions of metal oxide powder to the water or an aqueous electrolyte solution, which might be acidified or may contain a base. The pH of the system changes gradually and approaches a constant value, which is the point of zero charge in the case of pure oxide. If the sample is contaminated, i.e. if it contains a certain portion of acid or base, the final pH is higher or lower than PZC, depending on the type and amount of the acid or base in the powder. In

the case of contamination, one needs to perform an acid-base titration of the concentrated suspension and the inflexion point provides the information on the PZC, and on the fraction of impurities in the powder. The advantage of mass titration is that one does not need to perform blank titration; instead one simply adds metal oxide powder to the electrolyte aqueous solution of known pH [60].

Kosmulski, M. determined the PZC of TiO_2 by means of potentiometric titration of by means of electrokinetic methods [61]. He used a set of 138 PZC of titanium dioxide to explore the effect of the crystalline structure on the PZC. The average and median PZC at pH 5.6 and 5.8, respectively, was found when the entire data set was taken into account. The PZC of anatase (31 entries, average and median 5.9 and 6, respectively) is slightly higher than that of rutile (49 entries, average and median 5.4 and 5.5, respectively), and the difference between the polymorphs corresponds to half of a standard deviation in each set of PZC.

From the early days of using bone charcoal for decolorization of sugar solution and other foods, to today's thousand of applications, the adsorption phenomenon has become a useful tool for purification and separation technologies. Adsorption phenomena are operative in most natural, physical, biological and chemical systems and adsorption operations employing solids such as activated carbon, alumina, silica gel and zeolite are so far used widely in industrial applications and for purification of waters and wastewater [62-65].

A large specific surface area is preferable for providing large adsorption capacity. As a result, presently, a great deal of attention has been focused on the search for new materials with better adsorption capacity [66-68]. In catalysis, alloys or multicomponent system often perform better than its pure or single component [69-70]. Like catalysis, adsorption is also a surface property. Thus, employment of a binary or multicomponent surface for adsorption seems to be interesting to be investigated.

Cobalt oxide like other transition metal oxides has attracted much attention due to its potential application in many fields and its distinctive structure and properties

[71-72]. Nano-size substances were found to be superior to bulk ones in battery applications improving the toughness of ceramics, increasing the density of magnetic recording and improving performance as a catalyst. There are the preparation of pure nano-sized substances is very important not only for the study of their properties but also for their application.

Materials based on cobalt oxides have attracted a great interest in view of their technological and fundamental scientific importance [73-75]. Kobayashi, T. *et al.*, [73] have reported that in the presence of CO and H₂ thin film of Co₃O₄ shows reversible change in the Vis-near IR absorption band. This phenomenon can be applied in the fabrication of solid-state gas sensors. Thin films of Co₃O₄ have been reported to change color from brown to light yellow when Li⁺ ions are inserted [74]. The reversible change of optical properties of Co₃O₄ under an external stimulus can be used to fabricate electrochromic devices [75]. Such a broad perspective of utilization has increased the importance of synthesizing cobalt oxide nanocomposites.

Ting, Y. U. and Zexaing, S., [76] successfully fabricated Metal oxide nanostructures (CuO, Co₃O₄, ZnO and α -Fe₂O₃) by a simple and efficient method: heating the appropriate metals in air at low temperatures ranging from 200 to 400°C. The chemical composition, morphology and crystallinity of the nanostructures have been characterized by micro-Raman spectroscopy, X-ray diffraction, scanning electron microscopy and transmission electron microscopy.

Systematic synthesis of mixed-metal oxides in NiO-Co₃O₄, NiO-MoO₃, and NiO-CuO systems via liquid-feed flame spray pyrolysis (LF-FSP) was studied by Azurdia, J. A., Mccrum, A. and Laine, R. M. [77]. The LF-FSP process is a general aerosol combustion synthesis route to a wide range of lightly agglomerated oxide nanopowders. The materials reported here were produced by aerosolizing ethanol solutions of propionate and ammonium molybdate precursors synthesized by reacting the metal nitrate with propionic acid.

Mixed metal oxide system produced via the sol-gel method are of particular interest also because the opportunity exists for generating materials intermixed at atomic level. Such systems have the potential for exhibiting chemical properties that differ notably from those of the corresponding single component oxides. Synthesis and characterization of several mixed metal oxides with unique properties has been reported [78-79].

The present study is aimed to examine the process characteristics in terms of the mode of the adsorbent preparation, its surface behaviour and viable application in removing toxics from water. The possible outcome of this study may include:

- 1) Optimization of the experimental technique for the control of the particle size by varying metal/metal molar ratio.
- 2) The study of aging time, drying temperature and process pH effects on the adsorbent's behaviours and physico-chemical properties.
- 3) Establishment of an adsorbent for column adsorption with high physical strength, regeneration and low cost as well.
- 4) Information about the surface morphology and surface charge of the mixed oxide adsorbent.
- 5) Removal of the dye toxics from water.
- 6) To compare the adsorption capacity of the mixed oxide surface by removing the using both the multi-component and single oxide surfaces.
- 7) Batch experiments to remove organic dyes from water under various parameters such as pH, concentration etc.
- 8) The evaluation of the parameters for the adsorption of dyes on the MMO surface.

Chapter - 2

EXPERIMENTAL

2.2 Materials and Probes

2.1.1 Chemicals

The chemicals and reagents used in this work are listed below. These are analytical grade and used without further purification. Doubly distilled water was used as solvent to prepare most of the solution of this work.

- (i) Iron (III) nitrate [Uni-chem, China]
- (ii) Sodium carbonate [Merck, India]
- (iii) Sodium silicate [Merck, India]
- (iv) Hydrochloric acid (32%) [E. Merck, Germany]
- (v) Sodium hydroxide [E. Merck, Germany]
- (vi) Sodium chloride [Uni-chem, China]
- (vii) Methylene blue [E. Merck, Germany]
- (viii) Orange green [E. Merck, Germany]

2.1.2 Instruments

Analysis of the samples performed in this work employed the following instruments:

- (i) UV-visible spectrophotometer [UV-1601 PC, Shimadzu, Japan]
- (ii) Scanning electron microscope [Philips XL30, Holland]
- (iii) X-ray diffractometer [Philips, Expert Pro, Holland]
- (iv) pH meter [Hanna, pH 209, India]
- (v) Centrifuge machine [Hermle, 2200 A, Germany]

- (vi) Shaker machine [Heidolph Unimex 1010]
- (vii) 100 mesh sieve [Endecotls test sieves limited, England]
- (viii) Digital balance, [FR-200, Japan]
- (ix) Furnace [DK, Chino, England]
- (x) Microburette [China]

2.2 Preparation of metal oxide and mixed oxide material

Iron (III) - based binary oxide adsorbent was prepared in a reactor which involve the simultaneous generation of hydrous ferric oxide (FeOOH) and silica sol. A mixture containing sodium silicate (Na_2SiO_3) and sodium carbonate (Na_2CO_3) was kept under stirring. After that, the iron (III) nitrate solution, $\text{Fe}(\text{NO}_3)_3$ was added in the former mixture also under stirred condition to yield a gel of Fe-Si components at an appropriate pH. The Fe-Si slurry was then allowed to age for a few hours. The slurry was then washed and separated by filtration. Finally, it was dried at a temperature of 200 °C for 3 hours in an oven. The iron(III), and silicon single oxides were prepared following the method described above.

Fe-Si mixed oxide were also prepared as above procedure but maintaining the following conditions:

1. kept the concentration of both Fe (III) salt and Na_2SiO_3 constant but varying concentration of Na_2CO_3 .
2. kept the concentration of both Na_2CO_3 and Na_2SiO_3 constant but varying concentration of Fe (III) salt.

2.3 Characterization of synthesized materials

2.3.1 IR spectra

IR spectra of all the dried samples iron oxides, silicon oxides and iron-silicon mixed oxide, were recorded on an IR spectrometer in the region of 4000 - 400 cm^{-1} . IR spectra of the solid samples were frequently obtained by mixing and grinding a small amount of materials with dry and pure KBr crystals. Thorough mixing and grinding were done in a mortar by a pestle. The powdered mixture was then compressed in a metal holder under a pressure of 8-10 tons to make a pellet. The pellet was then placed in the path of IR beam for measurements.

2.3.2 X-ray Diffraction

Iron oxides, silicon oxides and iron-silicon mixed oxide materials were analyzed for their X-ray diffraction pattern in the powder state. For this purpose, the samples were prepared as the procedure described in section 1.24.3. The powder samples were pressed in a square aluminum sample holder (40 mm \times 40 mm) with a 1 mm deep rectangular hole (20 mm \times 15 mm) and pressed against an optical smooth glass plate. The upper surface of the sample was labeled in the plane with its sample holder. The sample holder was then placed in the diffractometer.

2.3.3 Surface Morphology

Iron oxides, silicon oxides and iron-silicon mixed oxide samples were dispersed on a conducting steel plate. Iron oxides, silicon oxides and iron-silicon mixed oxide, thus prepared following the methods described in section 1.11 were examined for their surface morphology. For this purpose, scanning electron microscopy technique was adopted. The dried powder iron oxides, silicon oxides and iron-silicon mixed oxide samples were dispersed on a conducting carbon glued strip. The sample-loaded strip was then mounted to a chamber that evacuated to $\sim 10^{-3}$ to 10^{-4} torr and then a very thin gold layer (\sim few nanometers thick) were sputtered on the sample to ensure the conductivity of the sample surface. The sample was then placed in the main SEM chamber to view its surface. The system was

computer interfaced and thus provides recording of the surface images in the computer file for its use as hard copy.

2.3.4 Electron Diffraction X-ray (EDX) Spectra

Elemental analysis of the synthesized iron oxides, silicon oxides and iron-silicon mixed oxide materials was performed by EDX spectra. The dried powders of iron oxide, silicon oxide and iron-silicon mixed oxide were dispersed on a 1cm × 1cm conducting steel plate. The still plates were then placed on a conducting carbon glued strip and a very thin gold layer was sputtered on the sample to ensure the conductivity of the sample surface. The sample was then placed in the main SEM chamber integrated with the EDX machine.

2.4. Removal of MB and OG dye using the (Fe-Si) mixed oxide

2.4.1 Preparation of dye solution

A. Stock MB Solution

It was prepared by dissolving 0.036 g of solid MB in 500 mL double distilled water. In this way, 2.02×10^{-4} M MB solution was prepared which was used as stock MB solution.

B. Dilution of MB stock solution

Some solution having concentration 5×10^{-5} M, 1×10^{-5} M were prepared simply by diluting the stock MB solution.

C. Stock OG Solution

It was prepared by dissolving 0.046g of solid OG in 500 mL double distilled water. In this way, 2.03×10^{-4} M OG solution was prepared which was used as stock OG solution.

D. Dilution of OG stock solution

Using the stock OG, some solution having concentration 5×10^{-5} M, 1×10^{-5} M were prepared as before just by dilution method.

2.4.2 Determination of the concentration of dye solutions

Concentration of the dye solution was measured spectroscopically by a UV-Vis spectrophotometer in the visible region.

The UV-Vis spectral analysis of the sample solutions was employed a double beam spectrophotometer. Adsorption and degradation of the dye were also studied spectroscopically by following the spectral change. For this purpose dye solution were prepared at different pH in the aqueous media. The references in these cases were the corresponding aqueous solutions at that pH.

2.4.3 Adsorption (batch) process

In this process, first initial concentration of the dye solution was determined spectroscopically. Then required amount of the adsorbent (Fe-Si) oxide was added in a 50 mL dye solution having a known concentration. This solution was shaken for a required period at different temperatures. During this period, adsorption of the dye took place on the mixed oxide surface. The mixture was then centrifuged. Finally the supernatant dye solution after adsorption was then analyzed for its concentration using the spectrophotometer as before. The difference between the initial and final spectra gave the amount adsorbed by the Fe-Si mixed oxide adsorbent.

2.4.4 Spectrum of MB

The following figure shows the absorption spectrum of a 1×10^{-6} M MB solution of pH = 6.99. The spectrum shows an absorption maxima at 664 nm which indicates the λ_{\max} of MB.

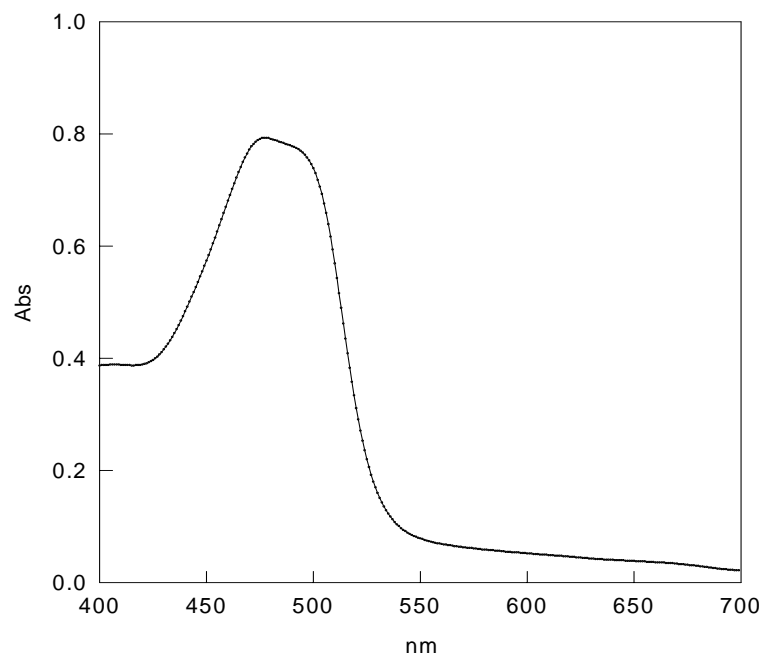


Fig. 2.1: Spectrum of an aqueous solution of MB.

2.4.5 Spectrum of OG

The following figure shows the absorption spectrum of a 1×10^{-5} M OG solution of pH = 6.92. The spectrum shows an absorption maxima at 477 nm which indicates the λ_{max} of OG.

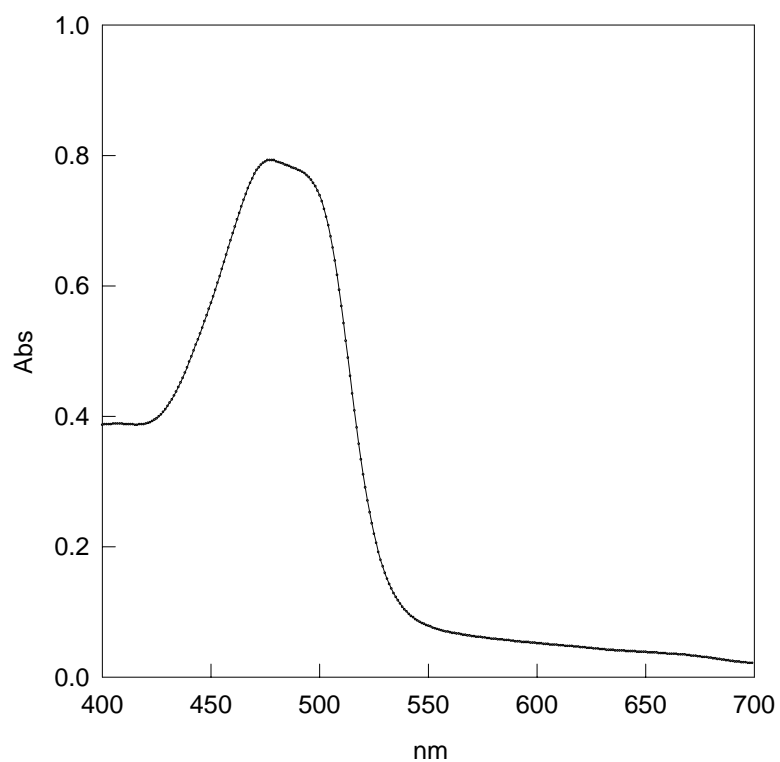


Fig. 2.2: Spectrum of an aqueous solution of OG.

2.4.6 Determination of molar absorption co-efficient (ϵ) of MB

For this purpose different concentration of MB solutions were prepared as given in the table 2.1. The corresponding absorbance of the MB solutions were then determined by the spectrophotometer. The absorbance values are depicted in the

table too. A plot absorbance vs MB concentration are presented in the fig. 2.3. The result yielded a straight line passing through the origin which has well verified the Beer-Lambert law. For the slope of the line, the molar absorption co-efficient ϵ was calculated as below

$$A = \epsilon Cl.$$

The molar absorption co-efficient (ϵ) was found to be under the experimental condition employed $74246 \text{ L mol}^{-1}\text{cm}^{-1}$.

Table 2.1: Absorbance of MB solution at different concentrations

Reference: Water

λ_{max} for MB Solution: 664 nm

Temperature: 34°C

pH: 6.92

Run No	Concentration of MB (M)	Absorbance
1	1.00×10^{-6}	0.07
2	2.00×10^{-6}	0.14
3	4.00×10^{-6}	0.28
4	6.00×10^{-6}	0.43
5	8.00×10^{-6}	0.58
6	10.00×10^{-6}	0.74

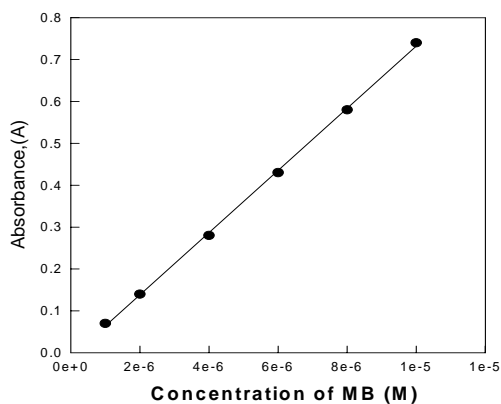


Fig. 2.3: Beer-Lambert plot for the determination of molar absorption co-efficient of MB.

2.4.7 Determination of molar absorption co-efficient (ϵ) of OG

For this purpose different concentration of OG solutions were prepared as given in the table 2.2. The corresponding absorbance of the OG solutions were then

determined by the spectrophotometer. The absorbance values are depicted in the table too. A plot absorbance vs OG concentration are presented in the Fig. 2.4. The result yielded a straight line passing through the origin which has well verified the Beer-Lambert law. For the slope of the line, the molar absorption co-efficient ϵ was calculated as below.

$$A = \epsilon Cl.$$

The molar absorption co-efficient (ϵ) was found to be $13920 \text{ L mol}^{-1}\text{cm}^{-1}$ under the experimental condition employed.

Table 2.2: Absorbance of OG solution at different concentrations

Reference: Water
Temperature: 29°C

λ_{max} for OG Solution: 477 nm
pH: 6.55

Run No	Concentration of OG (M)	Absorbance
1	1.00×10^{-5}	0.14
2	2.00×10^{-5}	0.28
3	4.00×10^{-5}	0.57
4	6.00×10^{-5}	0.68
5	8.00×10^{-5}	1.14
6	10.00×10^{-5}	1.42

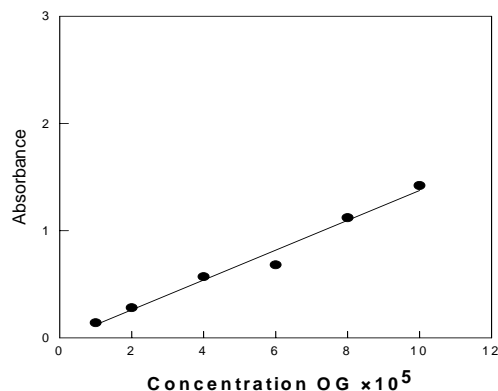


Fig. 2.4: Beer-Lambert plot for the determination of molar absorption co-efficient of OG.

2.4.8 Effect of pH on the spectral behavior of MB

The stability of the MB solutions at different pH was investigated. For this studies, absorbance of a freshly prepared solution was first taken (instant absorbance). The solution was then allows to stand for 24 hours. After this duration, absorbance of the solution was again taken (absorbance after 24 hours). The results are presented in the table 2.3 and Fig. 2.5. The results show that MB solution is stable for 24 hours.

Table 2.3: Absorbance of MB solutions at different pH of the media

Reference: Water

Temperature: 33°C

λ_{\max} for MB Solution: 664 nm

Run No	Conc. Of MB (M) $\times 10^5$	pH	Instant Abs.	Abs. after 24 hours
1	1.00	5.35	0.694	0.694
2	1.00	6.92	0.694	0.694
3	1.00	9.24	0.694	0.694

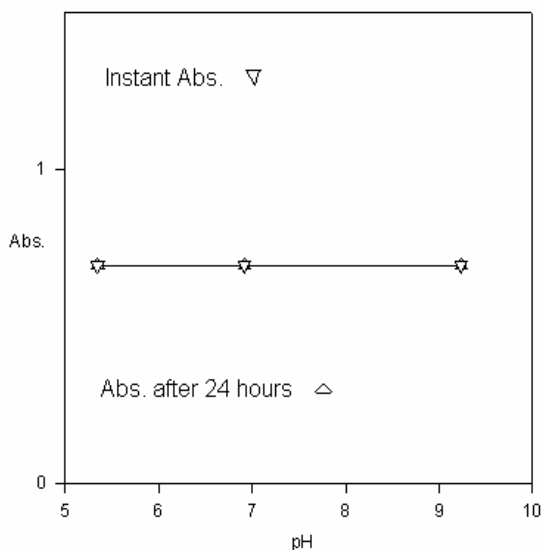


Fig. 2.5: A plot of absorbance versus pH for determination of stability of MB solution.

2.4.9 Effect of pH on the spectral behavior of OG

The stability of the OG solutions at different pH was investigated. For this studies, absorbance of a freshly prepared solution was first taken (instant absorbance). The solution was then allows to stand for 24 hours. After this duration, absorbance of the solution was again taken (absorbance after 24 hours). The results are presented in the table 2.4 and Fig. 2.6. The results show that OG solution is stable for 24 hours.

Table 2.4: Absorbance of OG solutions at different pH of the media

Reference: Water

Temperature: 33°C

λ_{\max} for OG Solution: 477 nm

Run No	Conc. of OG (M) $\times 10^5$	pH	Instant Abs.	Abs. after 24 hours
1	1.00	4.95	0.71	0.71
2	1.00	6.55	0.71	0.71
3	1.00	8.75	0.71	0.71

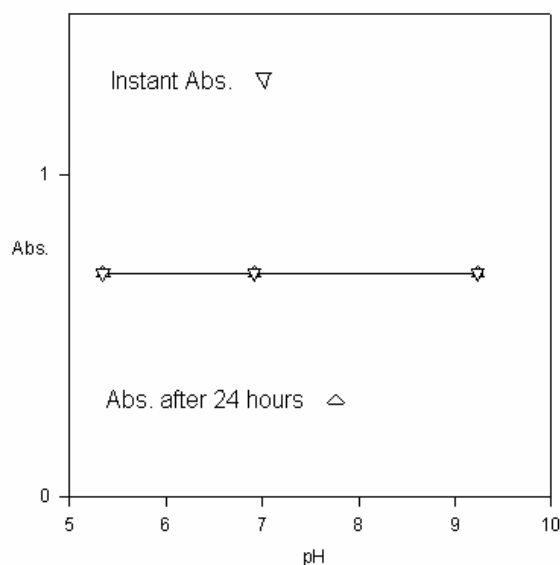


Fig. 2.6: A plot of absorbance versus pH for determination of stability of MB solution.

2.5 Determination of specific surface area of the mixed oxide

Dye adsorption technique involves the adsorption of dye molecules from solution onto a solid surface. The method of adsorption of MB dye in liquid phase for specific surface area determination has been adopted widely for various natural solids: activated carbon, charcoal, silica. In aqueous solution MB is a cationic dye which adsorbs to negatively charged surface. The MB molecule has a rectangular shape with dimensions of approximately ($17\text{\AA} \times 7.6\text{\AA} \times 3.25\text{\AA}$). This molecule may attach to the surface in various orientations, so the area covered by one MB molecule may vary; if (1) molecule lies on its largest face on the surface under study, the covered area is about $130 (\text{\AA})^2$ per molecule, (2) molecule is tilted ($65\text{-}70^\circ$) with respect to the surface under study, the covered area is about $66 (\text{\AA})^2$ per molecule and (3) if the longest is oriented perpendicular to the surface, the covered area is about $24.7 (\text{\AA})^2$ per molecule. MB is chosen in this study because of its strong adsorption onto solid and recognized usefulness in characterization of catalyst. Also in aqueous solution it shows distinct absorption band near UV-visible region (400-800 nm) of the electromagnetic radiation with absorption maxima at 664 nm. The following subsections describes the procedure for the determination of the specific surface area of the Fe-Si mixed oxide.

i) Calculation of amount adsorbed on per gram of adsorbent (X/m):

$$X/m = (C_0 - C_{eq}) \times V \times M / (1000 \times 0.01) \text{ mol g}^{-1}$$

Where, C_0 = Conc. of dye solution before adsorption

C_{eq} = Conc. of dye solution at equilibrium (after adsorption)

V = Volume of the dye solution

M = Molecular weight of dye

m = amount of adsorbent (Fe-Si mixed oxide)

ii) Calculation of surface area

The adsorption technique is characterized by high bonding energy (ionic coulombian attraction - chemisorption) and it is generally limited to a monolayer formation. Thus, the Langmuir adsorption isotherm can be applicable in determining the specific surface area of the mixed oxide.

The linear form of the Langmuir adsorption equation is given by:

$$[C_e]/(X/m) = [C_e]/K' + 1/K K'$$

Where,

C_e = Concentration of the MB dye solution at equilibrium (after adsorption)

X = Amount of the dye (MB) adsorbed on per gram of adsorbent
(Fe-Si mixed oxide)

m = Amount of adsorbent

K' = Monolayer capacity

K = Adsorption coefficient

A Plot of $[C_e]/(X/m)$ vs $[C_e]$ yields a straight line; from the slope one can get the amount of dye adsorbed requires to form a monolayer of adsorbate on the adsorbent.

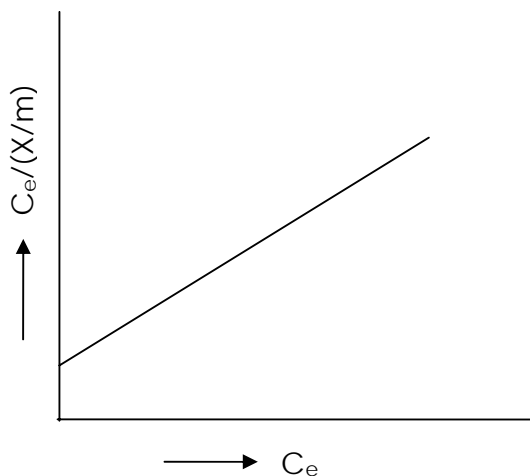


Fig. 2.7: Langmuir-Hinshelwood plot of $C_e/(X/m)$ vs C_e .

The surface area (A_s) of the catalysts then can be calculated from the equation

$$A_s = K' \times N_a \times A \times 10^{-20} \text{ m}^2 \text{ g}^{-1}$$

Where,

N_a = Avogadro number,

A = Cross sectional area of the adsorbate.

2.6 Determination of (pH_{PZC}) of iron-silicon mixed oxide

The point of zero charge, pH_{PZC} , of solid substance means the pH at which the positive and negative charge in the surface is equal. To determine the point of zero charge of Fe-Si mixed oxide, the experiment was done in the following way:

Exactly 1.0 g of Fe-Si mixed oxide was taken in four different reagent bottles. Then 1×10^{-1} M 50 mL NaCl solution was added to each bottle. The sample solution was agitated for 24.0 hours at low speed in a shaker. Then the suspensions were observed in each bottle. Two bottles of them were titrated directly with 0.065 M HCl and 0.065 M NaOH using microburette (± 0.01 mL). The pH values were noted carefully after addition of each drop of titrant (acid and alkali). Contents of other two bottles were filtered with sintered crucible and the supernatant thus obtained were titrated with 0.065 M HCl acid and 0.065 M NaOH. The experiments were carried out in the same way for the 1×10^{-2} M and 1×10^{-3} M NaCl solutions.

Chapter - 3

RESULT & DISCUSSION

3.1 Characterization of synthesized oxide materials

Iron oxide, silicon oxide and iron- silicon mixed oxides were prepared by sol-gel method. The above three oxides were characterized by Energy-dispersive X-ray spectroscopy (EDX), Scanning Electron Microscopy (SEM), X-Ray Diffraction (XRD), Specific Surface area (SSA) and Point of Zero Charge (pH_{PZC}). EDX provided the information about chemical composition. The oxides were characterized in terms of their particle size and morphology by SEM. In XRD analysis, the information about crystalline structure and particle size were found [83]. The overall surface charge pH_{PZC} of materials and the specific surface area were obtained by acid-base titration and dye adsorption method, respectively [55].

3.1.1 EDX spectral analysis

Energy-dispersive X-ray spectroscopy is an analytical technique [84] used for the elemental analysis or chemical characterization of a sample. It is one of the variants of X-ray fluorescence spectroscopy which relies on the investigation of a sample through interactions between electromagnetic radiation and matter, analyzing X-rays emitted by the matter in response to being hit with charged particles. Its characterization capabilities are due in large part to the fundamental principle that each element has a unique atomic structure allowing X-rays that are characteristic of an element's atomic structure to be identified uniquely from one another.

To stimulate the emission of characteristic X-rays from a specimen, a high-energy beam of charged particles such as electrons or protons, or a beam of X-rays, is focused into the sample being studied. At rest, an atom within the sample contains ground state (or unexcited) electrons in discrete energy levels or electron shells bound to the nucleus. The incident beam may excite an electron in an inner shell, ejecting it from the shell while creating an electron hole where the electron was. An electron from an outer, higher-energy shell then fills the hole, and the difference in energy between the higher-energy shell and the lower energy shell may be released in the form of an X-ray. The number and energy of the X-rays emitted from a specimen can be measured by an energy-dispersive spectrometer. As the energy of the X-rays is characteristic of the difference in energy between

the two shells, and of the atomic structure of the element from which they were emitted, this allows the elemental composition of the specimen to be measured.

Mixed (Fe-Si) oxide

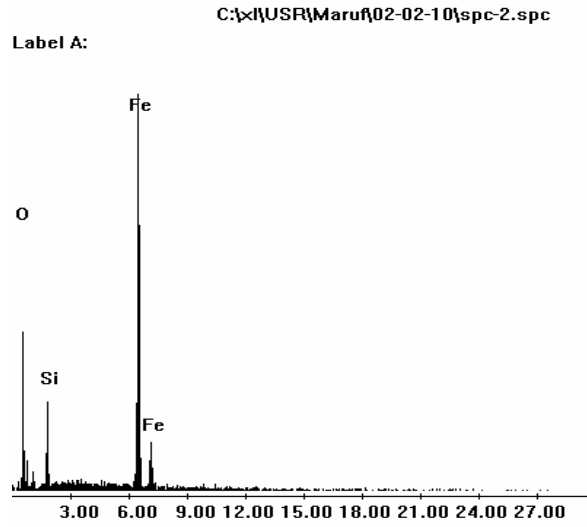


Fig. 3.1.1(a): Elemental analysis of iron-silicon mixed oxide at sample location 1.

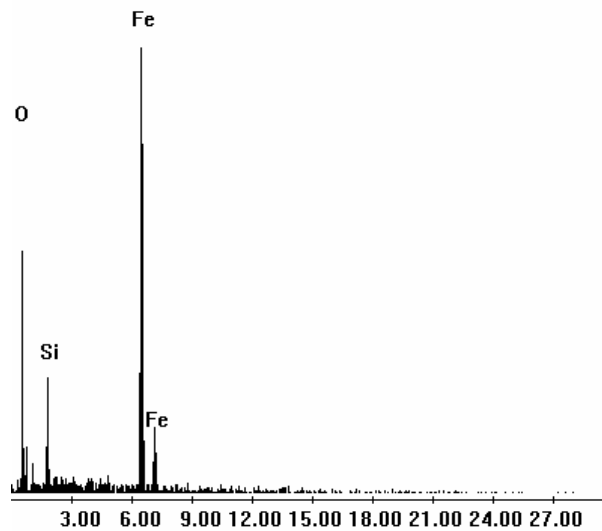


Fig. 3.1.1(b): Elemental analysis of iron-silicon mixed oxide at sample location 2

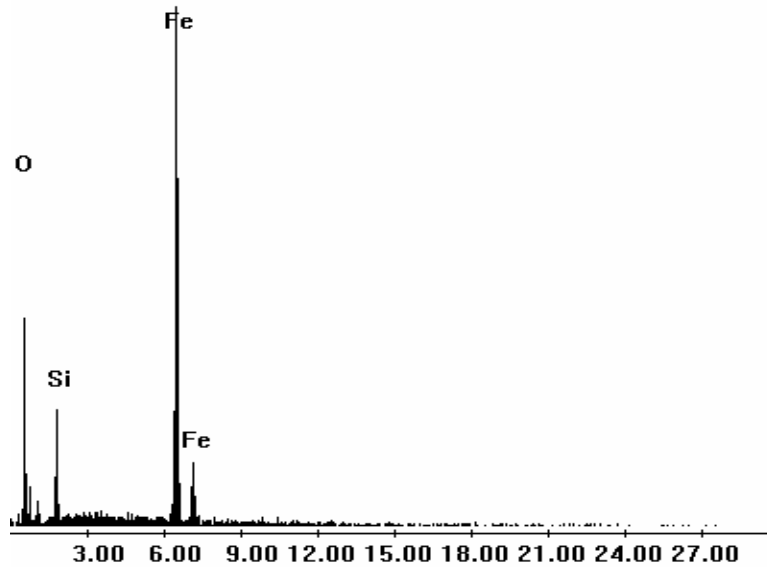


Fig. 3.1.1(c): Elemental analysis of iron-silicon mixed oxide at sample location 3.

Elemental analysis of the prepared mixed (Fe-Si) oxide was performed by employing EDX method. For this purpose, the sample was used which was also employed in the SEM analysis as described in section 2.3.4. The pattern of the EDX spectrums are presented in Figs. 3.1.1(a), 3.1.1(b), and 3.1.1(c). The peaks observed at 6.34, 6.35 and 6.34 keV for K of the iron element in the figure 3.1.1(a), 3.1.1(b) and 3.1.1 (c) respectively; and for the silicon we observed in the Figs. 3.1.1(a), 3.1.1(b), and 3.1.1(c), the peaks at 1.8, 1.9 and 1.8 keV for K series respectively and 0.52 keV for K lines of the oxygen element. The percentage of Fe, Si and O were determined from the intensity of the lines and the results are summarized further in Table 3.1.1.1.

Table 3.1.1.1: Elemental composition of Iron- Silicon mixed oxide.

Name of elements	Sample location 1	Sample location 2	Sample location 3	Average composition elements (%)	Average composition formula
Iron (%)	56.12	55.06	53.40	54.86	
Silicon (%)	10.58	10.79	10.55	10.64	$\text{Fe}_{1.47} \text{Si}_{0.53} \text{O}_3$
Oxygen (%)	33.29	34.15	36.05	34.50	

Iron oxide and silicon oxide:

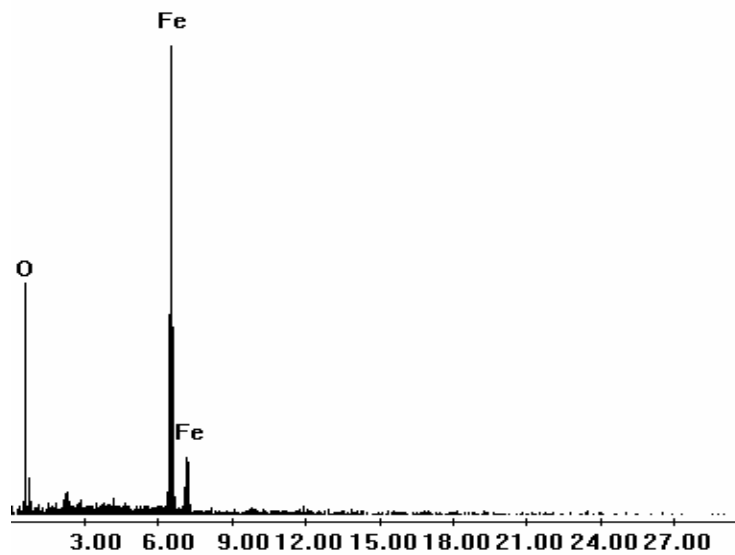


Fig. 3.1.1(d): Elemental analysis of iron oxide at sample location 4.

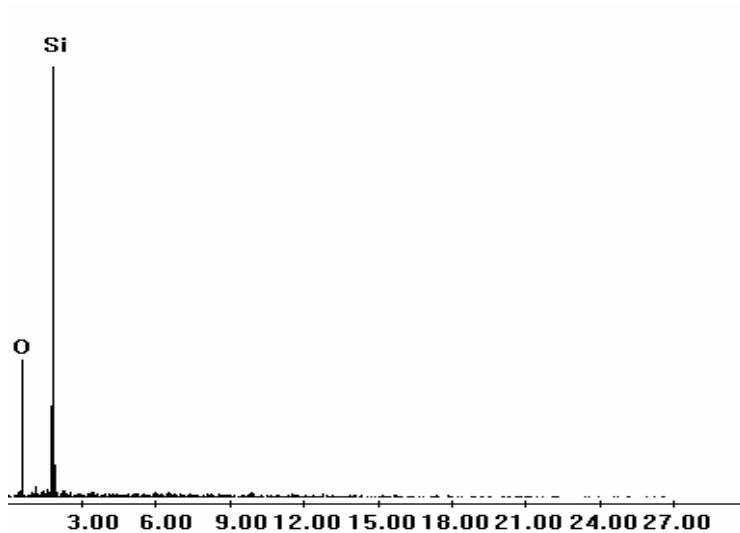


Fig. 3.1.1(e): Elemental analysis of silicon oxide at sample location 3.

The patterns of the EDX spectrum of iron and silicon single oxide peaks are presented in Figs. 3.1.1(d) and 3.1.1(e). The iron peak observed at 6.34 and in the silicon peak observed at 1.34 keV for K and 0.52 keV for k lines of the oxygen element. The percentage of Fe, Si and O were determined from the intensity of the lines and the results are summarized further in Table 3.1.1.2 and 3.1.1.3

Table 3.1.1.2: Elemental composition of iron oxide.

Iron (%)	Oxygen (%)	Tentative Chemical formula
71.96	28.04	$\text{Fe}_{2.24}\text{O}_3$

Table 3.1.1.3: Elemental composition of silicon oxide

Silicon (%)	Oxygen (%)	Tentative Chemical formula
49.59	50.41	Si _{1.1} O ₂

Thus, from the chemical composition obtained from the EDX spectrum, it can be calculated that the composition of the prepared iron oxide and silicon oxide are Fe_{2.24}O₃ and Si_{1.1}O₂, respectively.

3.1.2 X-ray diffraction

X-ray scattering technique is a non-destructive analytical techniques which reveal information about the crystallographic structure, chemical composition, and physical properties of materials. This technique are based on observing the scattered intensity of an X-ray beam hitting a sample as a function of incident and scattered angle, polarization, and wavelength or energy [83].

X-ray diffraction yields the atomic structure of materials and is based on the elastic scattering of X-rays from the electron clouds of the individual atoms in the system. The most comprehensive description of scattering from crystals is given by the dynamical theory of diffraction. Single-crystal X-ray diffraction is a technique used to solve the complete structure of crystalline materials, ranging from simple inorganic solids to complex macromolecules, such as proteins. Powder diffraction (XRD) is a technique used to characterize the crystallographic structure, crystallite size (grain size), and preferred orientation in polycrystalline or powdered solid samples. Powder diffraction is commonly used to identify unknown substances, by comparing diffraction data against a database maintained by the International Centre for Diffraction Data. It may also be used to characterize heterogeneous solid mixtures to determine relative abundance of crystalline compounds and, when coupled with lattice refinement techniques, such as Rietveld refinement, can provide structural information on unknown materials. Powder diffraction is also a common method for determining strains in crystalline materials. An effect of the finite crystallite sizes is seen as a broadening of the peaks in an X-ray diffraction as is explained by the Scherrer Equation.

The XRD pattern of iron oxide, silicon oxide and iron-silicon mixed oxide are given in the Figs. 3.1.2.1 to 3.1.2.3. The scattering pattern as a function of Bragg angle, 2θ at $\lambda=0.154$ nm for the studied samples powder are present in those figures.

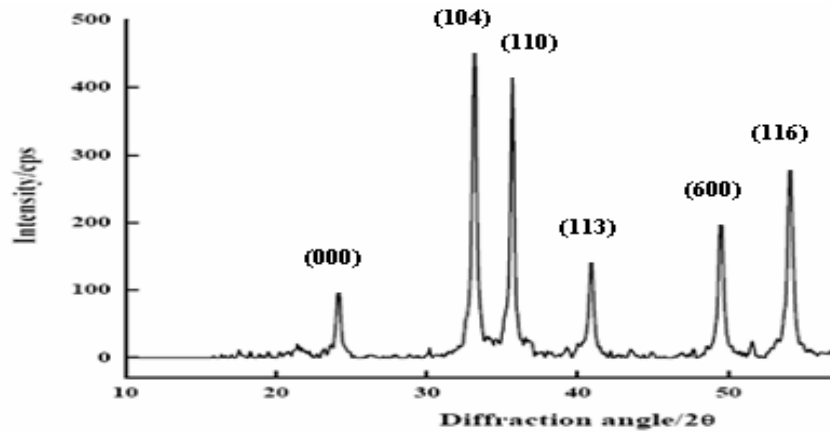


Fig. 3.1.2.1: XRD pattern of Iron oxide.

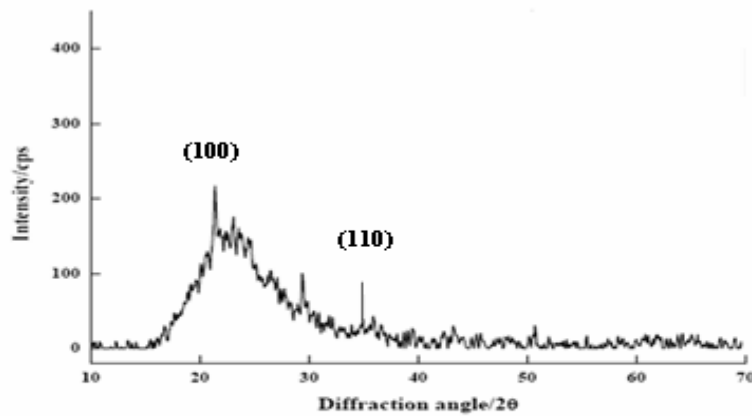


Fig. 3.1.2.2: XRD pattern of silicon oxide.

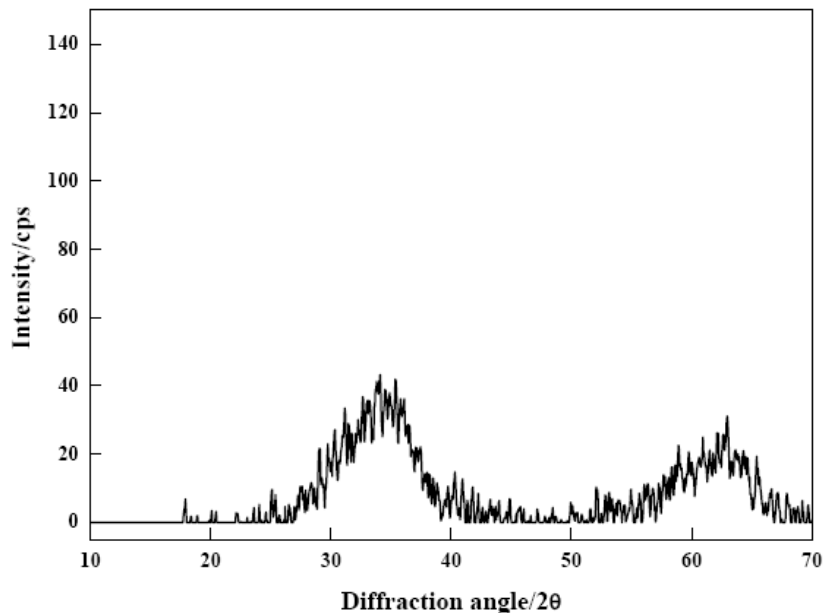


Fig. 3.1.2.3: XRD pattern of iron-silica mixed oxide.

Fig. 3.1.2.1 shows the XRD results of the reference sample. The content of our results matches with JCPDS (Joint Committee on Powder Diffraction Standard) card 730603 on Annes A indentifying the sample to be α -Fe₂O₃.

Fig. 3.1.2.2, the XRD pattern of Silica Oxide displays the characteristic peaks 100 (20.4°) and 110 (35.8°) which are similar to the JCPDS card 110252.

The XRD pattern of Iron- Silicon Mixed oxide is illustrated in Fig. 3.1.2.3. The distinguishing lattice plane peaks are present in 100 (23.7°), 104(34.8°), 110(35.8°), 448 (36.8°), 600(49.5°) and 440 (59.4°). The peaks 100 and 110 are counterpart of JCPDS card 110252; 600, 440 and 448 are match with JCPDS card 361216; 104 is match with JCPDS card 730603. The Miller Indices (h, k, l) lattice planes of Iron and Silicon single oxide are present in the mixed (Fe-Si) oxide with partial deviation of 2θ angle of the plane. The XRD pattern shows the evidence that the mixed (Fe-Si) oxide was perfectly synthesized in this work.

Crystallite size of single and multi-component oxide

The finite crystallite sizes is found as a broadening of the peaks in an X-ray diffraction as is explained by the Scherrer Equation. The Scherrer Equation is

$$D_p = \frac{0.94\lambda}{\beta_{1/2} \cos \theta}$$

Where, θ = Bragg angle,

$\lambda=0.154$ nm = wave length of X-ray

$\beta_{1/2}$ = Full Width Half- maxima (FWHM),

D_p = crystallite size of particle

For using Scherrer Equation the crystallite size of these materials are obtained. The particle size of, iron-silicon mixed oxide, iron oxide and silicon oxide is 18, 24 and 37 nanometer, respectively. Therefore, it can be conclude from this result that the oxides that are prepared in this study are in the nano state.

3.1.3 IR spectral analysis

IR spectral analysis provide some useful qualitative information on the identification of compounds. Both organic and inorganic substrates absorb IR light and thus IR active. In order to get some insight about the structure of the synthesized matrices, IR spectra of iron single oxide, silicon single oxide and iron-silicon mixed oxide are presented in Figs. - 3.1.3.1, 3.1.3.2 and 3.1.3.3.

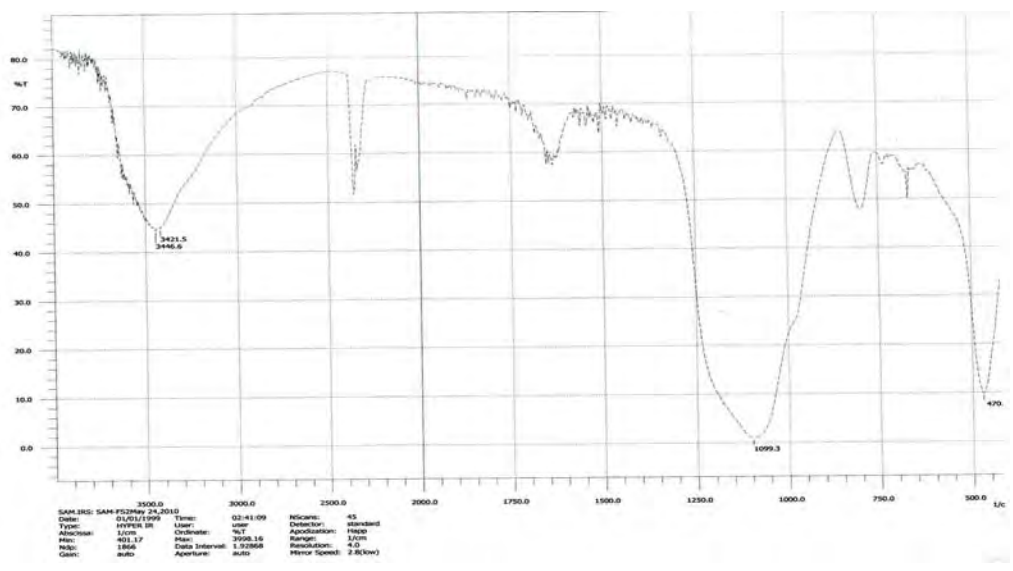


Fig. 3.1.3.1: IR spectra of silicon oxide.

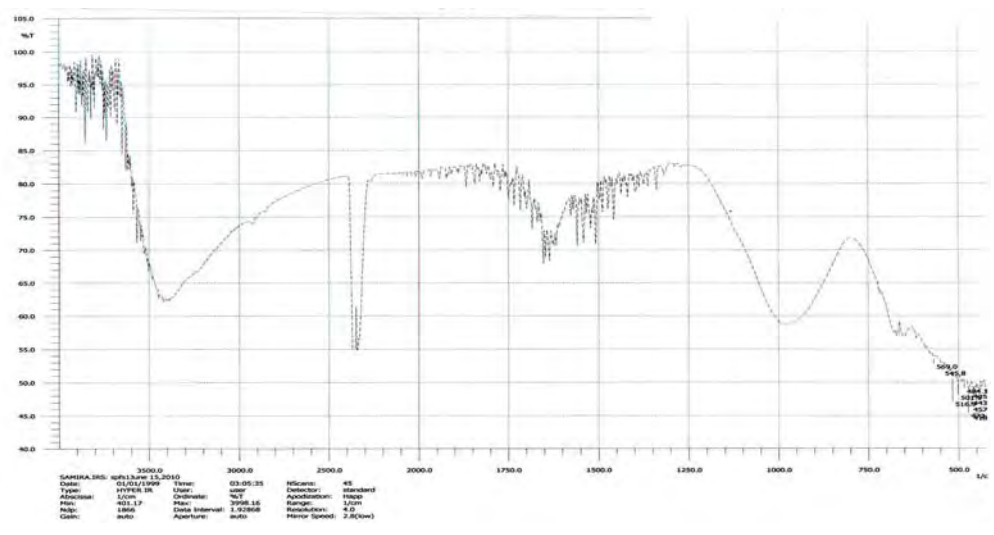


Fig. 3.1.3.2: IR spectra of iron oxide.

Fig. 3.1.3.1 shows the IR spectra of silicon single oxide. In the spectra of SiO_2 , bands corresponding to the symmetric stretch (470 cm^{-1}) of O–Si–O bond and asymmetric (1099 cm^{-1}) stretch of the Si–O–Si bond are observed, [87]. The peaks at about 3421 cm^{-1} are observed due to stretching and bending vibration of Si–OH and OH bonds in H_2O .

Fig. 3.1.3.2 shows the IR spectrum of iron single oxide. The infrared band in $620\text{--}450 \text{ cm}^{-1}$ range was reported for the stretching vibration of Fe–O [87]. On examining the IR-spectra of the iron single oxide, it can be seen that the characteristic signals at $457, 545$ and 569 cm^{-1} for stretching vibration of Fe–O bond are observed.

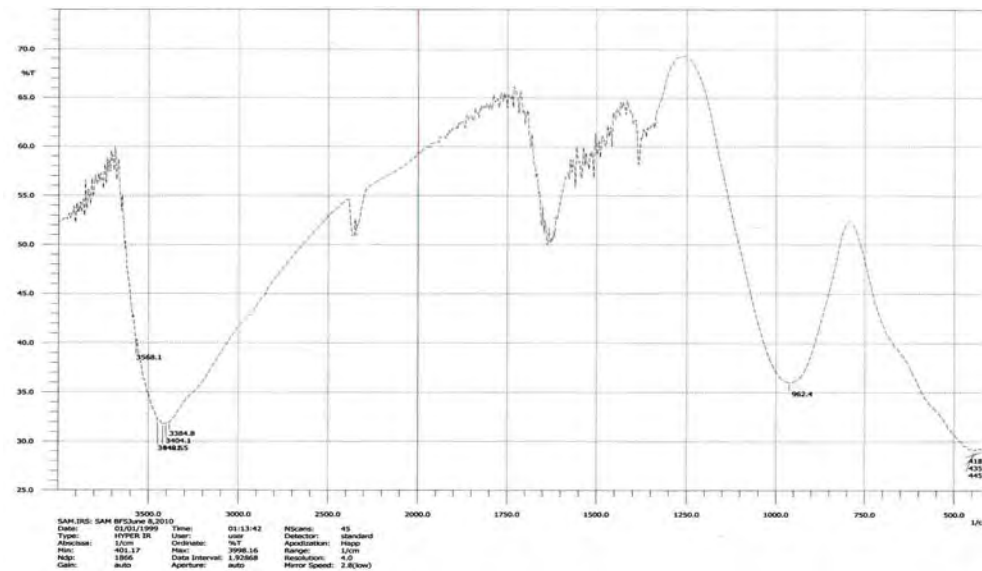
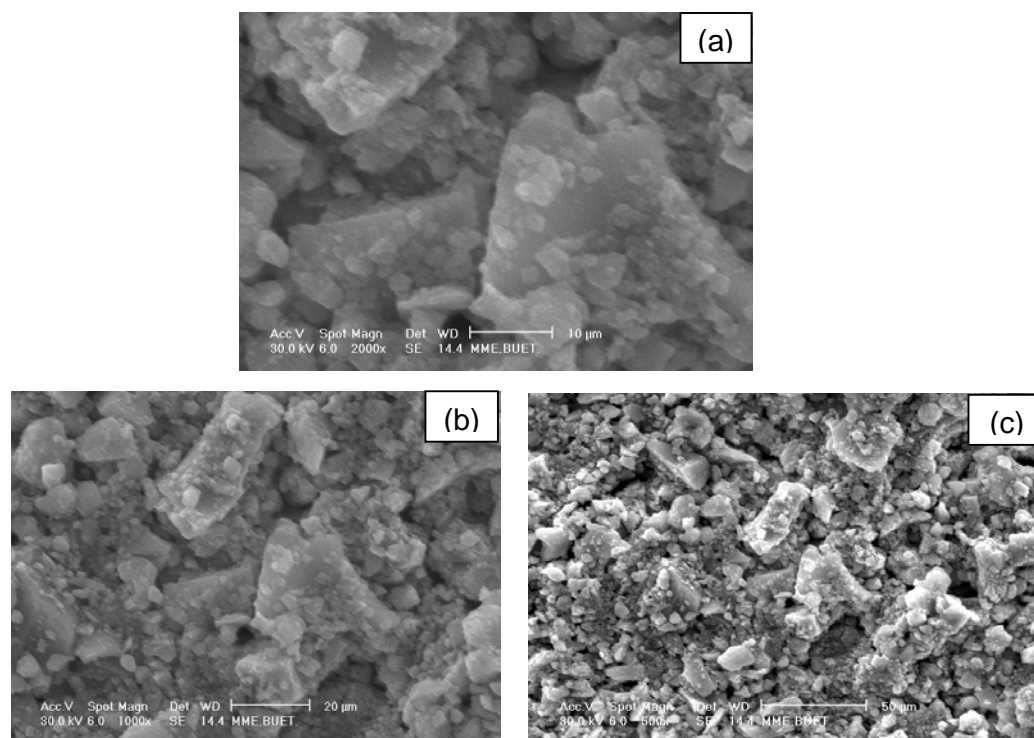


Fig. 3.1.3.3: IR spectra of iron silicon mixed oxide.

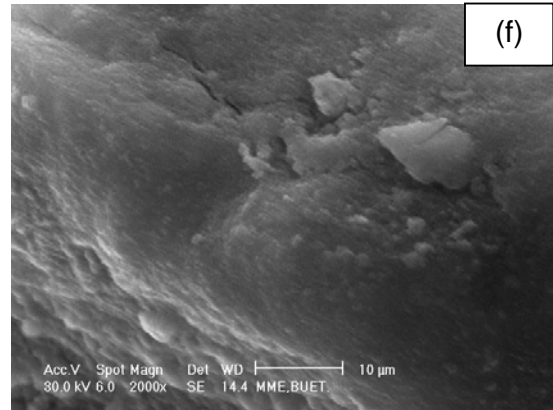
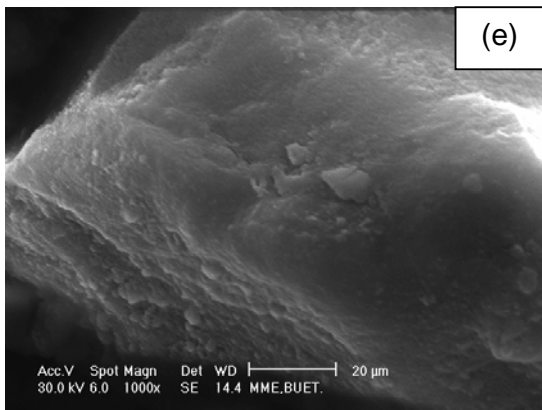
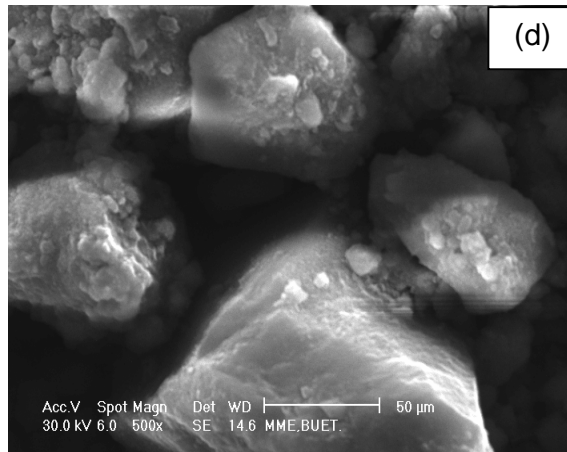
For iron silicon mixed oxide (Fig. 3.1.3.3), bands at $992\text{--}950 \text{ cm}^{-1}$ range has been reported for the characteristics of Si–O–Fe bond [88, 89]. On examining the IR spectra of the iron–silicon mixed oxide the characteristics signal at 962 cm^{-1} which is indicative of the presence of Si–O–Fe bond can be seen. A broad band in between 3000 and 3500 cm^{-1} is assigned to O–H bending and O–H stretching vibrations, respectively. In addition, the individual oxides peaks are also observed here as predicted in the spectra of Fe–O and Si–O presented in Figs. 3.1.3.1 and 3.1.3.2, respectively.

3.1.4 Scanning electron microscopy

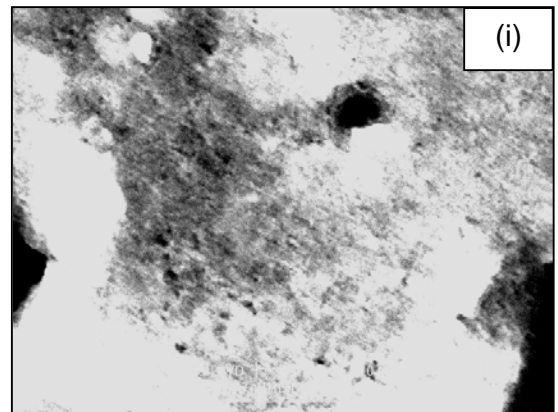
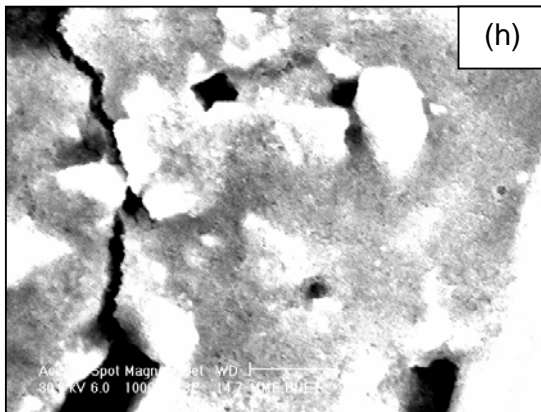
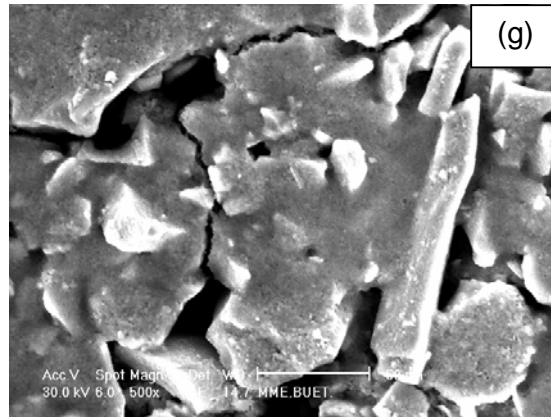
The scanning electron microscope (SEM) is a type of electron microscope that images the sample surface by scanning it with a high-energy beam of electrons in a raster scan pattern [6]. The electrons interact with the atoms that make up the sample producing signals that contain information about the sample's surface topography, composition and other properties such as electrical conductivity. A wide range of magnifications is possible, from about 10 times (about equivalent to that of a powerful hand-lens) to more than 500,000 times, about 250 times the magnification limit of the best light microscopes. The Iron single oxide (Figs. 3.1.4.1; a-c), silicon single oxide (Figs. 3.1.4.2: d-f), and mixed (Fe-Si) oxide (Figs. 3.1.4.3; g-j) samples obtained were layered over steel plate for its SEM analysis. From the SEM analysis of the mixed oxide Fig. 3.1.4.3(g-i), it can be seen that surface is consists of very small particles and the over all surface seems to be highly porous. The high porosity may result high adsorption on the surface. In fact, adsorption of MB and OG dyes was studied on the mixed oxide surface and has been described elsewhere in the later sections. All the images display well-dispersed particles, however, with different morphologies and varying uniformity [4].



Figs. 3.1.4.1(a-c): SEM micrograph of Iron oxide at different pixels.



Figs. 3.1.4.2 (d-f): SEM micrograph of silicon oxide at different pixels.



Figs. 3.1.4.3 (g-i): SEM micrograph of mixed (Fe-Si) oxide at different pixels.

The average particle size distribution measured from SEM may be in higher range (10 nm to 100 nm) than the crystallite size measured from XRD. This is expected as the XRD measurement is a mean of the actual crystallite size. Albeit, the particles were found to be highly crystallite according to the X-ray diffraction studies but from the SEM images a thick amorphous layer surrounding each particle was observed [80].

3.1.5 Determination of specific surface area of the mixed (Fe-Si) oxide by the (MB) dye adsorption method

Table 3.1.5.1: Data for the calculation of surface area

Amount of mixed oxide: 0.02g

pH of the solutions: 6.92

Shaking time: 120 min

Volume of each solution: 50 mL

Molar absorption co-efficient: 74246 L mol⁻¹cm⁻¹

Run No	Initial conc. of MB×10 ⁶ C ₀ (molL ⁻¹)	Final Abs	Equilibrium conc. of MB ×10 ⁶ C _e (molL ⁻¹)	Adsorbed conc of MB C ₀ -C _e ×10 ⁶ (X) (molL ⁻¹)	Amount adsorbed of MB×10 ⁶ (X/m) (molg ⁻¹)	C _e /(X/m)×10 ³
1	10.5	0.097	1.31	9.19	22.98	56.84
2	11.7	0.115	1.55	10.15	25.38	61.03
3	14.3	0.134	1.80	12.50	31.24	57.78
4	15.9	0.163	2.20	13.70	34.26	64.08
5	18.9	0.223	3.00	15.90	39.74	75.58
6	20.1	0.258	3.47	16.63	41.56	83.61
7	22.1	0.307	4.13	17.97	44.91	92.07
8	23.3	0.373	5.02	18.28	45.69	109.95
9	25.7	0.462	6.22	19.48	48.69	127.79
10	28.1	0.623	8.39	19.71	49.27	170.30
11	29.6	0.734	9.89	19.71	49.28	200.59

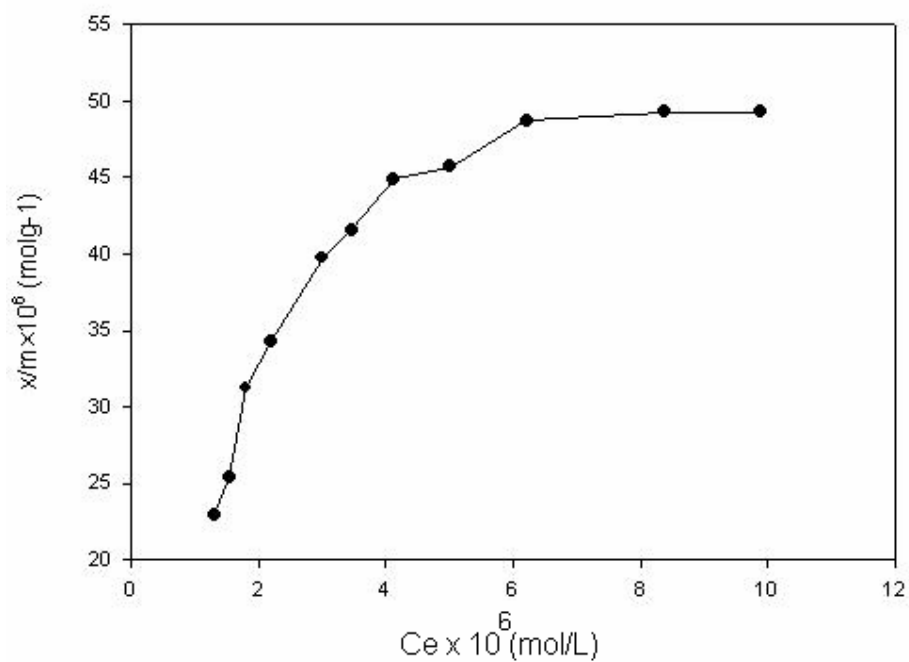


Fig. 3.1.5.1: A plot of X/m vs C_e for the adsorption of MB onto the mixed (Fe-Si) oxide surface.

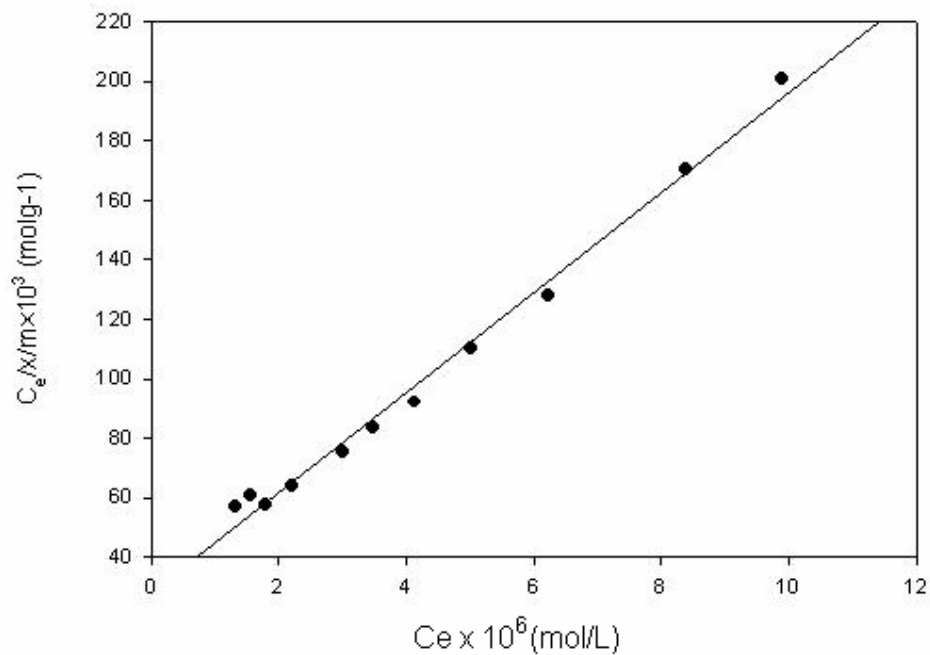


Fig. 3.1.5.2: Langmuir- Hinshelwood plot of $C_e / (X / m)$ vs C_e for the adsorption of MB onto the Fe-Si mixed oxide surface.

The adsorption of MB onto mixed (Fe-Si) oxide follows Langmuir–Hinshelwood isotherm at pH 6.92 at room temperature ($R^2= 0.99$). From the Langmuir-Hinshelwood plot of $C_e/(X/m)$ vs C_e , it has been found that monolayer capacity $K' = 5.97 \times 10^{-5} \text{ mol g}^{-1}$ that obtained from the slope and adsorption constant $K = 59.47 \times 10^{-2} \text{ L mol}^{-1}$ that obtained from the intercept. Then the specific surface area of the mixed (Fe-Si) oxide was calculated. The specific surface area of mixed iron (Fe-Si) oxide at pH 6.92 and room temperature is found to be $46.74 \text{ m}^2 \text{ g}^{-1}$.

3.1.6 Determination of point of zero charge (pH_{PZC}) of the mixed (Fe-Si) oxide

The point of zero charge of a solid substances (pH_{PZC}) means the pH at which the positive and negative charge in the surface are equal. pH_{PZC} has been determined by simple acid-base titration. It is described in section 2.6. The pH metric titration data and the curves for three different concentration of NaCl solution are shown in Table 3.1.6.1 - 3.1.6.3 and Figs. 3.1.6.1- 3.1.6.3. The data for the net titration is given in Table 3.1.6.4. The net titration curves corresponding to three different ionic strengths as shown in Figs. 3.1.6.4. If the pH of the bulk is higher than pH_{PZC} surface then becomes negative and the lowering of the pH of the bulk than pH_{PZC} make the surface positive. In the present study, pH_{PZC} of the Fe-Si mixed oxide surface was found to be 8.8.

Optimize data for pHpzc

Amount of mixed oxide: 1.0 g

Volume of NaCl solution taken: 50mL

Strength of NaCl: $1 \times 10^{-1}\text{M}$, $1 \times 10^{-2}\text{M}$ and $1 \times 10^{-3}\text{M}$

Rate of agitation: 215 rpm

Time of agitation: 24 hours

Strength of HCl and NaOH solution: 0.065M

Table 3.1.6.1: pH metric titration with $1 \times 10^{-1} \text{M}$ NaCl

Volume of HCl (mL)	pH of the solution		Volume of NaOH (mL)	pH of the solution	
	Suspension	Filtrate		Suspension	Filtrate
0.00	9.1	8.93	0.00	9.02	8.92
0.50	8.98	8.71	0.50	9.07	9.13
1.0	8.84	8.43	1.0	9.12	9.32
1.5	8.71	7.75	1.5	9.15	9.50
2.0	8.56	6.87	2.0	9.25	9.66
2.5	8.43	6.65	2.5	9.37	9.79
3.0	8.14	6.45	3.0	9.50	9.88
3.5	7.99	6.15	3.5	9.57	9.97
4.0	7.89	6.10	4.0	9.66	10.03
4.5	7.62	5.90	4.5	9.74	10.08
5.0	7.39	5.70	5.0	9.82	10.11
5.5	7.28	5.10	5.5	9.88	10.14
6.0	7.12	4.95	6.0	9.92	10.17
6.5	7.05	4.75	6.5	9.97	10.19
7.0	6.87	4.00	7.0	10.02	10.21
7.5	6.69	3.80	7.5	10.06	10.23
8.0	6.59	3.50	8.0	10.09	10.25
8.5	6.55	3.19	8.5	10.12	10.27
9.0	6.45	3.14	9.0	10.15	10.29
9.5	6.34	3.09	9.5	10.18	10.30
10.0	6.31	3.04	10.0	10.19	10.31
10.5	6.2	3.01	10.5	10.22	10.33
11.0	6.10	2.98	11.0	10.23	10.34
11.5	6	2.96	11.5	10.25	10.35
12.0	5.93	2.93	12.0	10.27	10.36
12.5	5.83	2.91	12.5	10.28	10.37
13.0	5.81	2.89	13.0	10.30	10.38
13.5	5.76	2.88	13.5	10.31	10.39
14.0	5.7	2.86	14.0	10.33	10.39
14.5	5.71	2.84	14.5	10.35	10.40
15.0	5.54	2.83	15.0	10.36	10.41
15.5	5.5	2.69	15.5	10.37	10.42
16.0	5.31	2.68	16.0	10.38	10.43
16.5	5.00	2.67	16.5	10.39	10.44

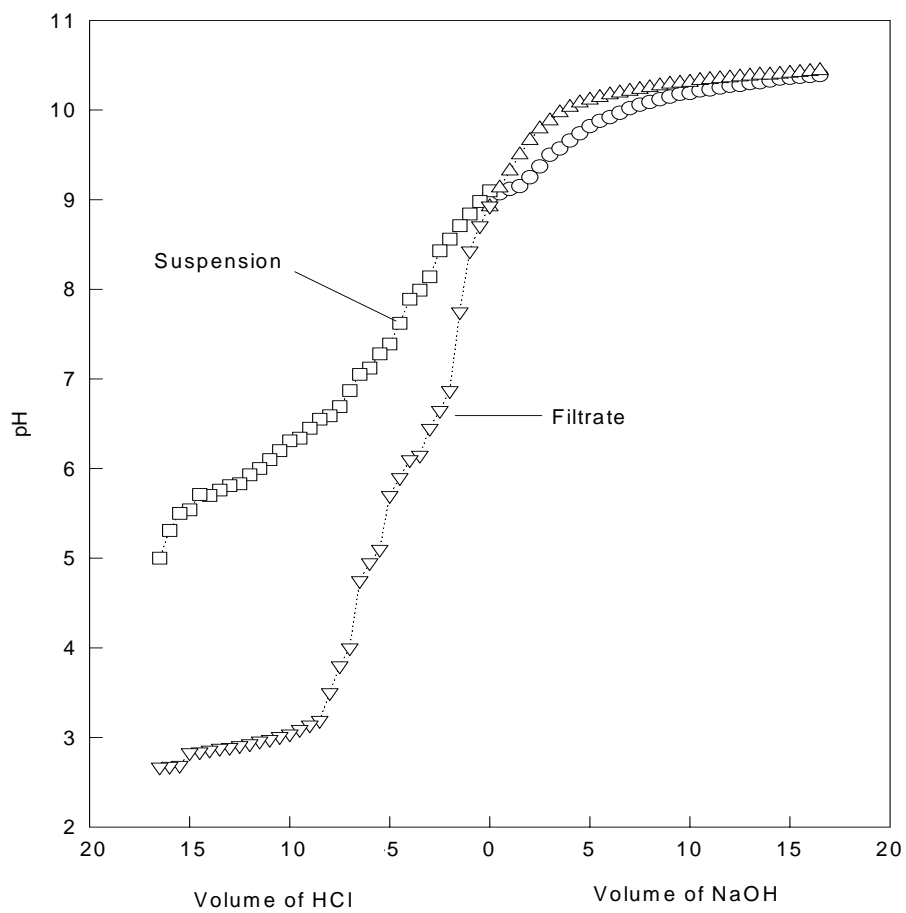


Fig. 3.1.6.1: pH metric titration curves for mixed (Fe-Si) oxide with $1 \times 10^{-1} \text{ M}$ NaCl.

Table 3.1.6.2: pH metric titration with $1 \times 10^{-2} \text{M}$ NaCl

Volume of HCl (mL)	pH of the solution		Volume of NaOH (mL)	pH of the solution	
	Suspension	Filtrate		Suspension	Filtrate
0.00	9.25	9.32	0.00	9.23	9.32
0.50	9.14	9.13	0.50	9.32	9.47
1.0	9.04	8.75	1.0	9.38	9.62
1.5	8.92	8.64	1.5	9.46	9.76
2.0	8.75	8.22	2.0	9.56	9.87
2.5	8.69	7.40	2.5	9.61	9.94
3.0	8.57	6.88	3.0	9.67	10.02
3.5	8.42	6.73	3.5	9.73	10.06
4.0	8.27	6.66	4.0	9.77	10.11
4.5	8.07	6.45	4.5	9.81	10.15
5.0	7.89	6.40	5.0	9.84	10.18
5.5	7.70	6.30	5.5	9.86	10.21
6.0	7.48	5.50	6.0	9.88	10.24
6.5	7.13	4.80	6.5	9.92	10.27
7.0	7.00	4.20	7.0	9.94	10.29
7.5	6.97	4.00	7.5	9.97	10.31
8.0	6.93	3.50	8.0	9.99	10.33
8.5	6.88	3.40	8.5	10.01	10.35
9.0	6.83	3.30	9.0	10.03	10.36
9.5	6.78	3.10	9.5	10.05	10.37
10.0	6.76	3.09	10.0	10.07	10.39
10.5	6.73	3.07	10.5	10.09	10.4
11.0	6.69	3.05	11.0	10.11	10.42
11.5	6.6	3.01	11.5	10.13	10.43
12.0	6.53	3.00	12.0	10.15	10.44
12.5	6.38	2.99	12.5	10.16	10.45
13.0	6.11	2.98	13.0	10.17	10.46
13.5	6.09	2.96	13.5	10.18	10.47
14.0	5.95	2.95	14.0	10.19	10.48
14.5	5.94	2.94	14.5	10.20	10.49
15.0	5.93	2.93	15.0	10.21	10.50
15.5	5.92	2.92	15.5	10.22	10.51
16.0	5.91	2.91	16.0	10.23	10.52
16.5	5.90	2.90	16.5	10.23	10.52

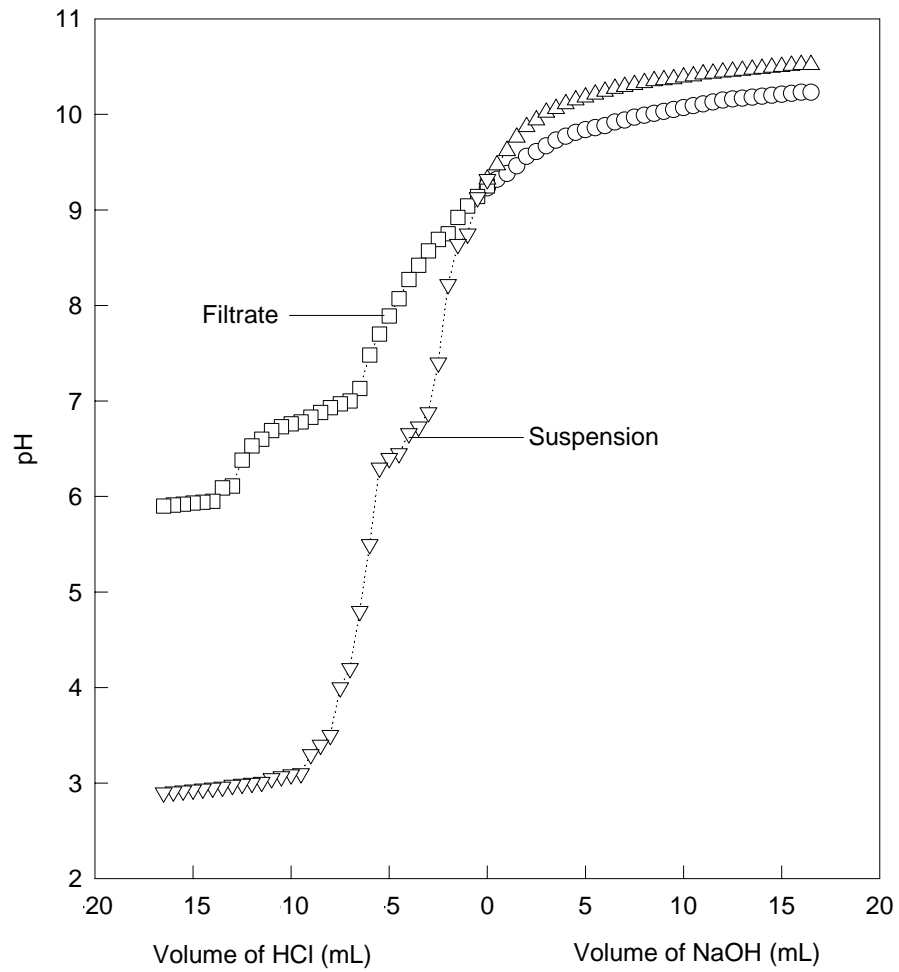


Fig. 3.1.6.2: pH metric titration curves for mixed (Fe-Si) oxide with $1 \times 10^{-2} \text{M}$ NaCl.

Table:3.1.6.3: pH metric titration with $1 \times 10^{-3} \text{M}$ NaCl.

Volume of HCl(mL)	pH of the solution		Volume of NaOH	pH of the solution	
	Suspension	Filtrate		Suspension	Filtrate
0.00	9.26	9.37	0.00	9.26	9.37
0.50	9.20	9.23	0.50	9.36	9.47
1.0	9.13	9.00	1.0	9.44	9.56
1.5	8.98	8.75	1.5	9.54	9.69
2.0	8.92	8.70	2.0	9.64	9.82
2.5	8.75	8.25	2.5	9.72	9.90
3.0	8.70	7.40	3.0	9.79	10.0
3.5	8.57	7.22	3.5	9.85	10.08
4.0	8.41	7.17	4.0	9.88	10.15
4.5	8.19	7.06	4.5	9.93	10.18
5.0	8.08	6.93	5.0	9.96	10.20
5.5	7.99	6.38	5.5	10.0	10.22
6.0	7.71	5.89	6.0	10.05	10.24
6.5	7.70	5.50	6.5	10.02	10.26
7.0	7.48	5.10	7.0	10.15	10.29
7.5	7.36	4.85	7.5	10.17	10.31
8.0	7.27	4.50	8.0	10.19	10.33
8.5	7.22	4.20	8.5	10.21	10.36
9.0	7.17	3.95	9.0	10.23	10.39
9.5	7.13	3.50	9.5	10.25	10.41
10.0	7.11	3.20	10.0	10.27	10.44
10.5	6.93	3.00	10.5	10.29	10.46
11.0	6.83	2.93	11.0	10.31	10.48
11.5	6.72	2.92	11.5	10.33	10.49
12.0	6.59	2.91	12.0	10.35	10.51
12.5	6.55	2.90	12.5	10.36	10.53
13.0	6.46	2.89	13.0	10.37	10.54
13.5	6.45	2.87	13.5	10.38	10.55
14.0	6.38	2.85	14.0	10.39	10.56
14.5	6.37	2.83	14.5	10.40	10.57
15.0	6.36	2.82	15.0	10.41	10.58
15.5	6.35	2.81	15.5	10.42	10.59
16.0	6.34	2.8	16.0	10.43	10.59
16.5	6.33	2.77	16.5	10.43	10.59

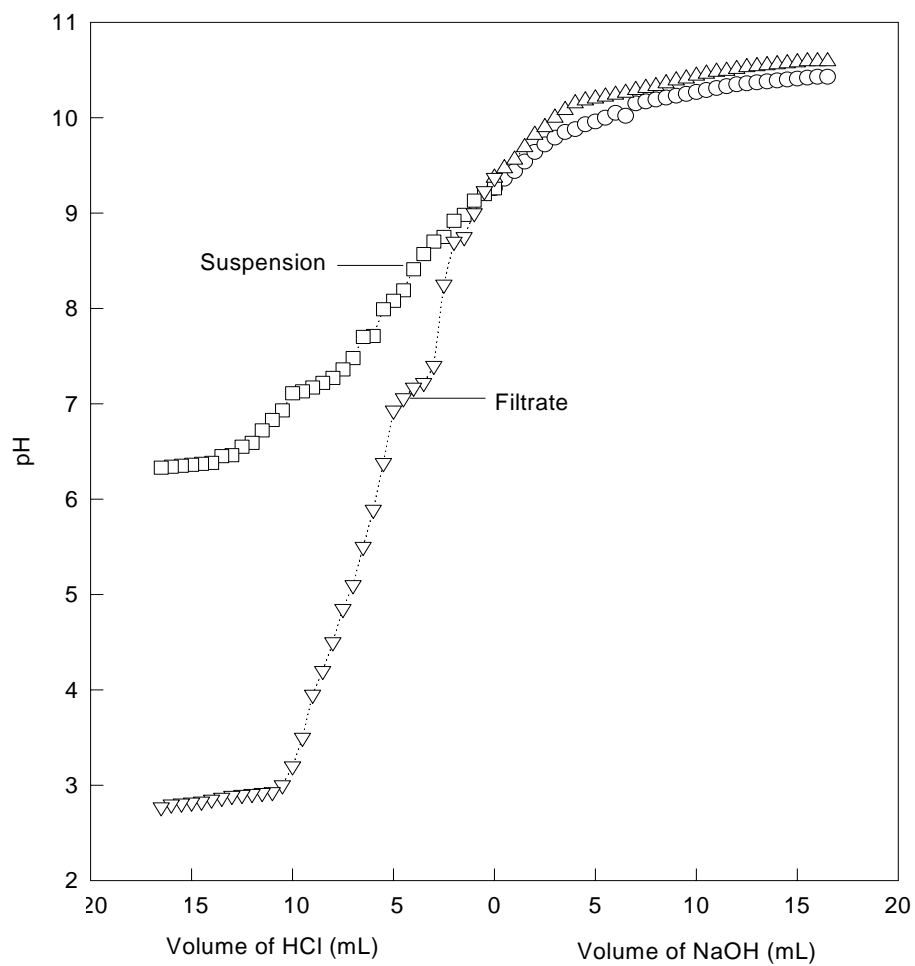


Fig. 3.1.6.3: pH metric titration curves for mixed (Fe-Si) oxide with $1 \times 10^{-3} \text{ M}$ NaCl.

Table 3.1.6.4: Data for net titration of mixed (Fe-Si) oxide.

Strength of NaCl	ΔV of HCl	pH	ΔV of NaOH	pH
1×10^{-1}	1	8.71	1.5	9.50
	5	6.87	2.5	9.88
	7	6.10	3.0	9.97
			3.5	10.19
			3.5	10.23
			3.5	10.25
			3.5	10.27
			3.5	10.30
			3.5	10.31
			3.5	10.33
			3.0	10.35
			3.0	10.38
			3.0	10.39
1×10^{-2}	1	8.75	0.5	9.32
	5.5	6.88	4.5	9.94
			7	10.11
			7.5	10.15
			8.5	10.18
1×10^{-3}	1.0	8.70	2.5	10.00
	4.5	6.93	3.0	10.15
	8.5	6.38	3.5	10.31
			3.5	10.33
			4.0	10.36
			5	10.39
			5.5	10.41

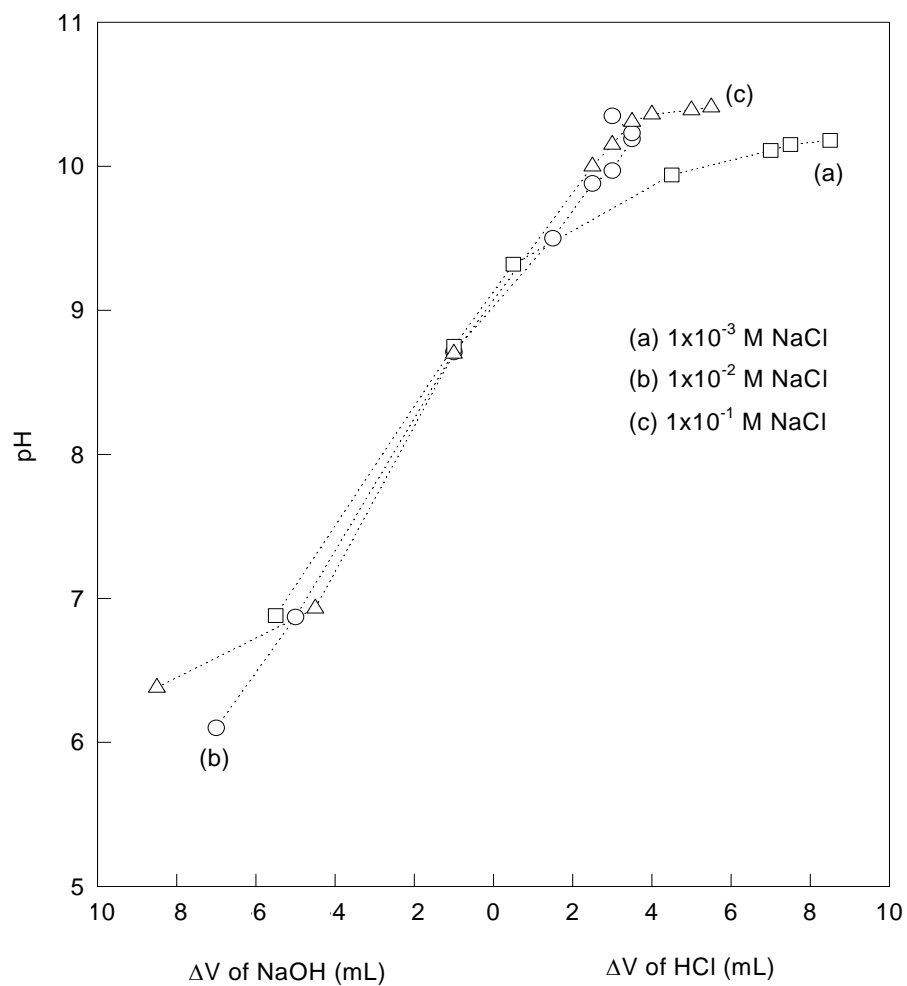


Fig. 3.1.6.4: Net titration curves for mixed (Fe-Si) oxide in the presence of different concentrations of NaCl. These curves intersect at pH_{pzc} .

Result: From Fig. 3.1.6.4, the point of zero charge of mixed (Fe-Si) oxide was found to be 8.8.

3.2 Removal of organic dyes (MB and OG) using batch experiment

The comparative studies of the removal capacity of the dyes between the multi-component (Fe-Si) and single oxide surface were employed by batch adsorption experiments and the effect of concentration of dye, pH, temperature, mixed oxide doses, contact time on the absorption processes were also conducted. The surface property of multi-component (Fe-Si) oxide was examined.

3.2.1 Comparative study of the removal of dyes between the multi-component (Fe-Si) and single oxide surface

Table 3.2.1.1: Comparative study of the removal capacity of MB dye between multi-component (Fe-Si) and single oxide surface

Temperature: 34°C

Shaking Time: 15 min

Shaking Speed: 4.5 rpm

Volume of the MB solution: 50mL

Amount of Adsorbent: 0.05g

Centrifuge Time: 10 min (2500 rpm)

Run No	Oxide Surface	Initial conc. of MB×10 ⁵ q ₀ (molL ⁻¹)	Abs.	Equilibrium conc. of MB×10 ⁵ q _e (molL ⁻¹)	Adsorbed conc. of MB×10 ⁵ q _m (molL ⁻¹)	Amount Adsorbed of MB×10 ⁵ q _m /m (molg ⁻¹)
1	Mixed (Fe-Si) oxide	5	0.116	0.15	4.85	4.85
2	Silicon oxide	5	1.936	2.61	2.39	2.39
3	Iron Oxide	5	2.228	3.00	2	2

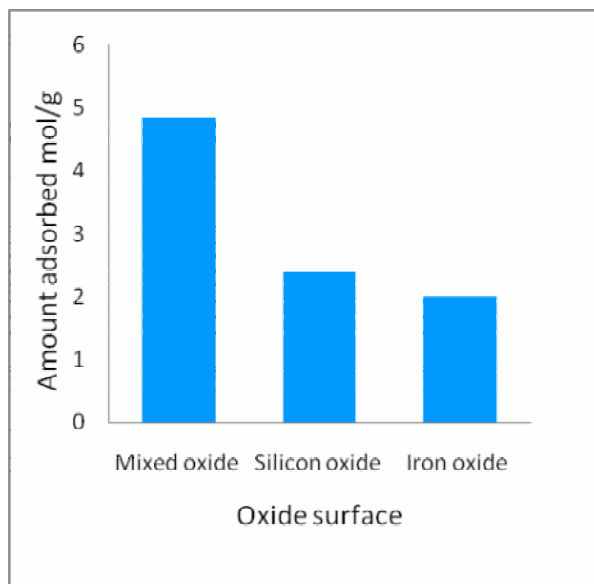


Fig. 3.2.1.1: Amount of MB adsorbed on the different oxides.

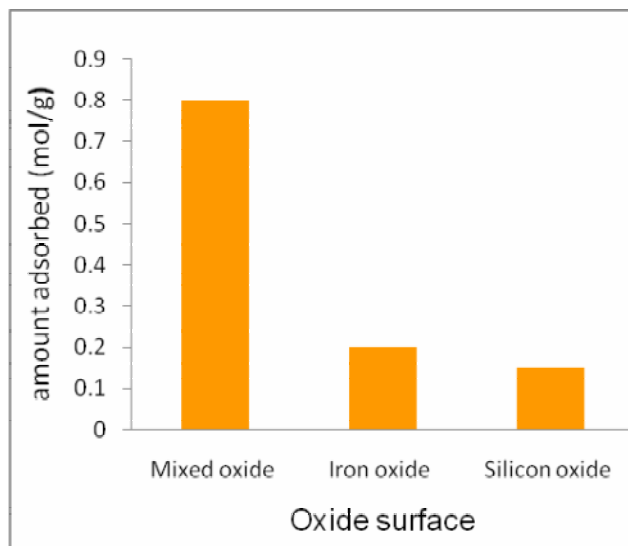


Fig. 3.2.1.2: Amount of OG adsorbed on the different oxides.

Table 3.2.1.2: Comparative study of the removal capacity of OG dye between multi-component (Fe-Si) and single oxide surface

Temperature: 34°C

Shaking Time: 15 min

Shaking Speed: 4.5 rpm

Amount of Adsorbent: 0.05g

Volume of the OG solution: 50mL

Centrifuge Time: 10 min (2500 rpm)

Run No	Oxide Surface	Initial conc. of OG×10 ⁵ q ₀ (molL ⁻¹)	Abs.	Equilibrium conc. of OG×10 ⁵ q _e (molL ⁻¹)	Adsorbed conc. of OG×10 ⁵ q _m (molL ⁻¹)	Amount Adsorbed of OG×10 ⁵ q _m /m (molg ⁻¹)
1	Mixed (Fe-Si) oxide	5.10	0.598	4.30	0.80	0.80
2	Iron Oxide	5.10	0.685	4.90	0.20	0.20
3	Silicon oxide	5.10	0.69	4.95	0.15	0.15

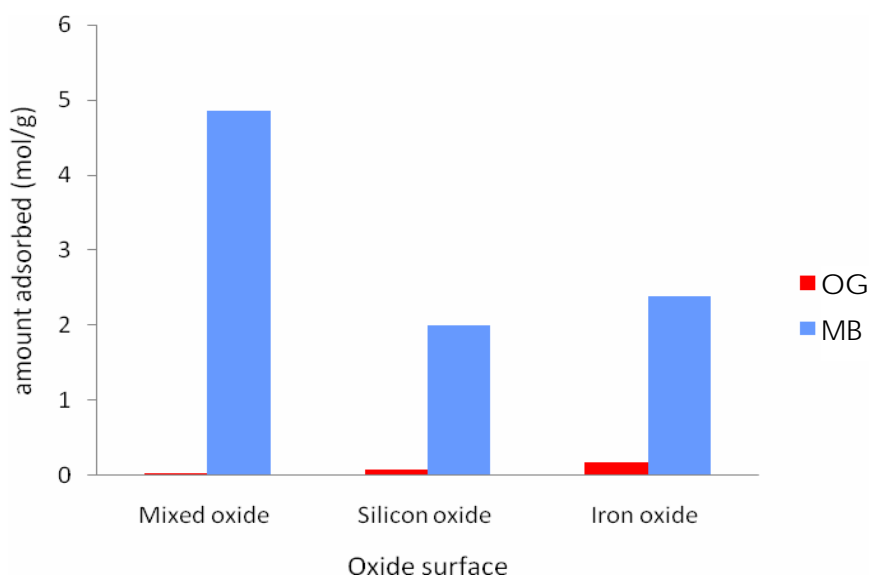


Fig: 3.2.1.3: Comparison of amount adsorbed on MB and OG dyes by different oxide.

In Figs. 3.2.1.1 and 3.2.1.2, it has been observed that multi-component (Fe-Si) mixed oxide was showed the highest removal capacity of cationic (MB) dye from its single oxide. It seems to be an effective adsorbent for cationic dye, but (Fe-Si) mixed oxide was showed the lowest removal capacity of anionic dye (OG) other than cataionic (MB) dye. So, because of the negligible adsorption, further experiments was not carried out by using of anionic dye (OG) onto (Fe-Si) mixed oxide surface. Thus details adsorption studies of the multi-component (Fe-Si) oxide were successfully carried out in this research work using the cationic (MB) dye only.

3.2.2 Effect of variation of Na₂CO₃ concentration on adsorbent preparation

Table 3.2.2.1: Data for adsorption of MB by mixed (Fe-Si) oxide prepared by varying Na₂CO₃ concentration.

Temperature: 34°C

Volume of the MB solution: 50mL

Shaking Time: 15 min

Centrifuge Time: 10 min (2500 rpm)

Shaking Speed: 4.5 rpm

Molar absorption co-efficient: 74246 L mol⁻¹cm⁻¹

Amount of Adsorbent: 0.05g

Sam	Conc. of Na ₂ CO ₃ (M)	Conc. of Fe (M)	Conc. of Si (M)	Molar ratio Fe:Si	Initial Conc. of MB×10 ⁵ (molL ⁻¹)	Abs.	Equilib. conc. of MB×10 ⁵ (molL ⁻¹)	Adsorb. conc. of MB×10 ⁵ (molL ⁻¹)	Amount of Adsor. of MB×10 ⁵ (molg ⁻¹)
1	0.5				5	0.2410	0.156	4.85	4.85
2	1.0				5	0.1160	0.394	4.60	4.60
3	2.0	0.15	0.05	3:1	5	0.2664	0.977	4.02	4.02
4	3.0				5	0.3268	0.156	4.85	4.85

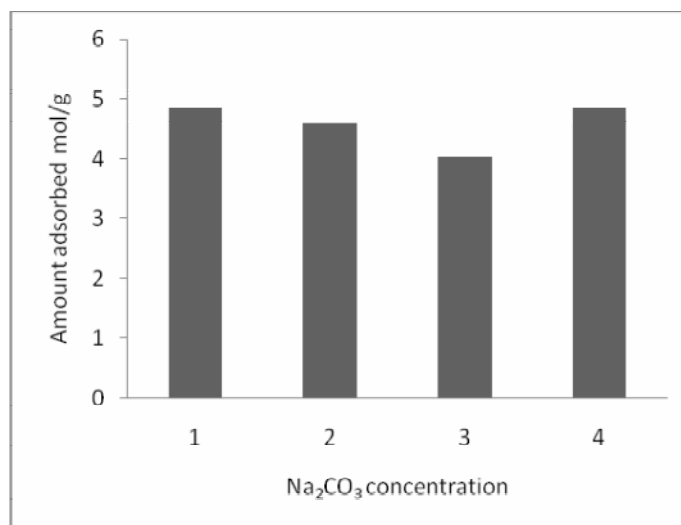


Fig. 3.2.2.1: Amount of MB adsorbed by the Fe-Si oxides prepared by variation of Na₂CO₃ concentrations.

To determine the effect of Na₂CO₃ concentration on adsorbent quality for the MB cationic dye, MB adsorption. Several adsorbents were prepared under similar conditions except with variation of Na₂CO₃ concentrations. The results of the cationic dye MB adsorption on these adsorbents are given in Table 3.2.2.1 and Fig. 3.2.2.1.

The result show that, no significant quality difference was observed for the adsorbents with the Na₂CO₃ concentration between 0.5 M and 3.0 M. However, the optimum concentration of 0.5 M Na₂CO₃ in this work was maintained.

3.2.3 Effect of Si/Fe molar ratio on adsorbent strength

Table 3.2.3.1: Data for the Si/Fe molar ratio on adsorption behaviour of MB by mixed (Fe-Si) oxide

Temperature: 34°C

Shaking speed: 4.5 rpm

Shaking time: 15 min

Amount of adsorbent: 0.05g

Centrifuge time: 10 min (2500 rpm)

Volume of the MB solution: 50mL

Molar absorption co-efficient: 74246 L mol⁻¹cm⁻¹

Samp	Conc. of Na ₂ CO ₃ (M)	Conc. of Fe (M)	Conc. of Si (M)	Molar ratio Si/Fe	Initial conc. of MB×10 ⁵ (molL ⁻¹)	Abs	Equilibrium conc. of MB×10 ⁵ (molL ⁻¹)	Adsor. conc. of MB×10 ⁵ (molL ⁻¹)	Amount Adsorbed of MB×10 ⁵ (molg ⁻¹)
1		0.05		1.0		0.1632	0.219	4.78	4.78
2		0.10		0.5		0.2410	0.324	4.67	4.67
3	0.5	0.15	0.05	0.33	5	0.1160	0.156	4.85	4.85
4		0.20		0.25		0.2664	0.358	4.64	4.64
5		0.25		0.2		0.3268	0.440	4.56	4.56

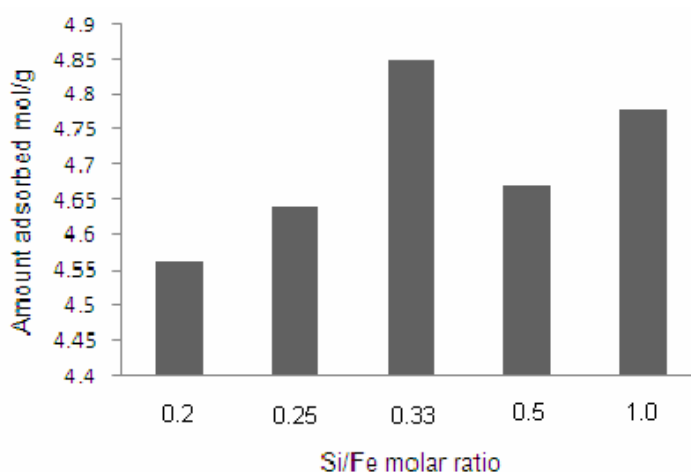


Fig. 3.2.3.1: Amount adsorbed of MB dye by Si/Fe molar ratio adsorbent.

The results of quality testing for several adsorbents with different Si/Fe molar ratios are given in Table 3.2.3.1 and Fig. 3.2.3.1. Significant strength difference was observed for the adsorbents with the Si/Fe molar ratio.

The optimum Si/Fe molar ratio in the adsorbent strength and cationic dye MB higher adsorption capacity was approximately 0.33 (i.e. Fe/Si = 3 mol/mol).

3.2.4 Effect of pH on MB uptake

Table 3.2.4.1: Data for the influence of pH on adsorption of MB by mixed (Fe-Si) oxide adsorbent.

Reference: Water

Amount of mixed oxide: 0.05g

λ_{\max} for MB solution: 664nm

Temperature: 32°C

Volume of the solution: 50mL

Shaking time: 15 min

Molar adsorption co-efficient: 74246 Lmol⁻¹cm⁻¹

Run No	Conc. Of MB (M) ×10 ⁵	pH	Instant Abs.	Equilibrium conc of MB×10 ⁶ q _e molL ⁻¹	Adsorbed conc of MB×10 ⁵ q _m molL ⁻¹	Amount Adsorbed of MB×10 ⁶ q _m /m molL ⁻¹
1	5	5.35	0.4775	6.43	4.35	4.35
2	5	6.92	0.355	4.78	4.52	4.52
3	5	9.24	0.4249	5.72	4.42	4.42

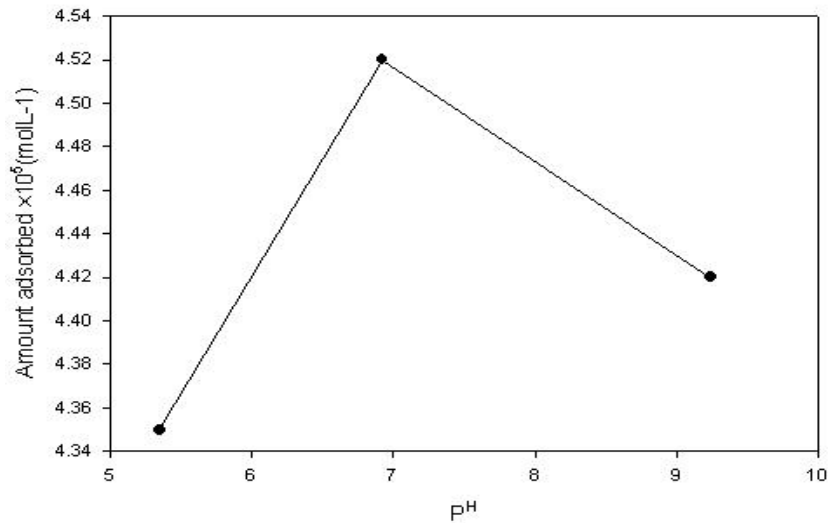


Fig. 3.2.4.1: Effect of pH of MB adsorption

The pH of the system exerts profound influence on the adsorptive uptake of adsorbate molecules presumably due to its influence on the surface properties of the adsorbent and ionization or dissociation on the adsorbate molecule. Despite of the importance of pH, pH control is not easily maintained. Fig. 3.2.4.1 shows the variations on the removal of dyes from synthetic solution at different pH. From the figure it is evident that the amount of adsorbed MB dye per gram adsorbent is the highest at neutral pH. The amount of adsorbed cationic dye (MB) per gram adsorbent is low in acidic condition. This indicates the strong force of attraction between the dyes and mixed (Fe-Si) oxide during the adsorption process.

3.2.5 Effect of contact time and kinetic study

Table 3.2.5.1: Data for the influence of contact time on the adsorption of MB by mixed (Fe-Si) oxide adsorbent.

Reference: Water
 λ_{\max} for MB solution: 664nm
 Volume of the solution: 50mL
 Amount of mixed oxide: 0.05g
 Temperature: 31°C
 pH: 6.92

Run No	Initial conc. of MB $\times 10^5$ $q_0(\text{molL}^{-1})$	Time t (min)	Abs.	Equilibrium conc. of MB $\times 10^5$ $q_e(\text{molL}^{-1})$	Adsorbed conc. of MB $\times 10^5$ $q_m(\text{molL}^{-1})$	Amount Adsorbed of MB $\times 10^5$ $q_m/m(\text{molg}^{-1})$
1	5	15	0.3949	0.531	4.469	4.469
2	5	30	0.3647	0.491	4.509	4.509
3	5	60	0.2534	0.341	4.659	4.659
4	5	90	0.1982	0.267	4.733	4.733
5	5	120	0.1972	0.266	4.734	4.734

Kinetic models applied to the adsorption of MB onto the mixed (Fe-Si) oxide

Several steps can be used to examine the controlling mechanism of adsorption process such as chemical reaction, diffusion control and mass transfer; kinetic data are used to test experimental data from the adsorption of MB onto mixed (Fe-Si) oxide is required for selecting optimum operating conditions for the full-scale batch process. The kinetic parameters, which are helpful for the prediction of adsorption rate, give information designing and modeling the adsorption process. Thus the kinetics of MB adsorption onto mixed (Fe-Si) oxide was analysis using pseudo-first order [31], pseudo-second order [33], intraparticle diffusion [46] kinetic models. The conformity between experimental data and model predicted values was expressed by the co-relation coefficients (r^2 , values closed to equal to 1). The relative higher values are the applicable model to the

kinetics of dye adsorption onto mixed (Fe-Si) oxide. The required derived data for these kinetics models is given below in Table 3.2.5.2.

Table 3.2.5.2: Derived data for various kinetic model of adsorption of MB onto Fe-Si mixed oxide.

Dye	Time (t) (min)	$t^{1/2}$	Adsorbed amount at time (t) q_t (molg ⁻¹) $\times 10^5$	Amount adsorbed at equilibrium at time (q_{et}) q_{et} (molg ⁻¹) $\times 10^5$	$\ln(q_{et} - q_t) \times 10^5$	$t/q_t \times 10^{-3}$
MB	15	3.87	4.469		-1.3	3.36
	30	5.48	4.509		-1.49	6.65
	60	7.75	4.659	4.734	-2.59	12.88
	90	9.49	4.733		-6.91	19.02
	120	10.45	4.734			25.35

Pseudo-first- Order equation

The adsorption kinetic data (Table 3.2.5.2) were described by the Lagergren pseudo-first-order model [9], which is the earliest known equation describing the adsorption rate based on the adsorption capacity. The first order rate equation is generally express as follows:

$$\ln(q_{et}-q_t) = \ln q_{et} - k_1 t \quad (1)$$

Where q_{et} and q_t are the adsorption capacity at equilibrium and at time t , respectively (molg⁻¹), k_1 is rate constant of pseudo-first- order adsorption (Lmol⁻¹).

In order to obtain the rate constants, the values of $\ln(q_{et}-q_t)$ were linearly correlated with t by plot of $\ln(q_{et}-q_t)$ versus t to give a linear relationship from k_1 and predicted q_{et} can be determined from the slope and intercept of the plot, respectively [Fig. 3.2.5.1]. The variation in rate should be proportional to the first power and concentration for strict surface adsorption. However, the relationship

between initial solute concentration and rate of adsorption will not be linear when pore diffusion limits the adsorption process.

Fig. 3.2.5.2 shows that the pseudo-first-order equation fits well for the first 30 min both MB adsorption process and thereafter the data deviate from theory. Thus, the model represents the initial stages where rapid adsorption occurs well but cannot be applied for the entire adsorption process. Furthermore, the correlation coefficient r^2 are relatively low (Table 3.2.5.3). This shows that the adsorption of MB onto mixed (Fe-Si) oxide cannot be applied and the reaction mechanism is not a first order reaction.

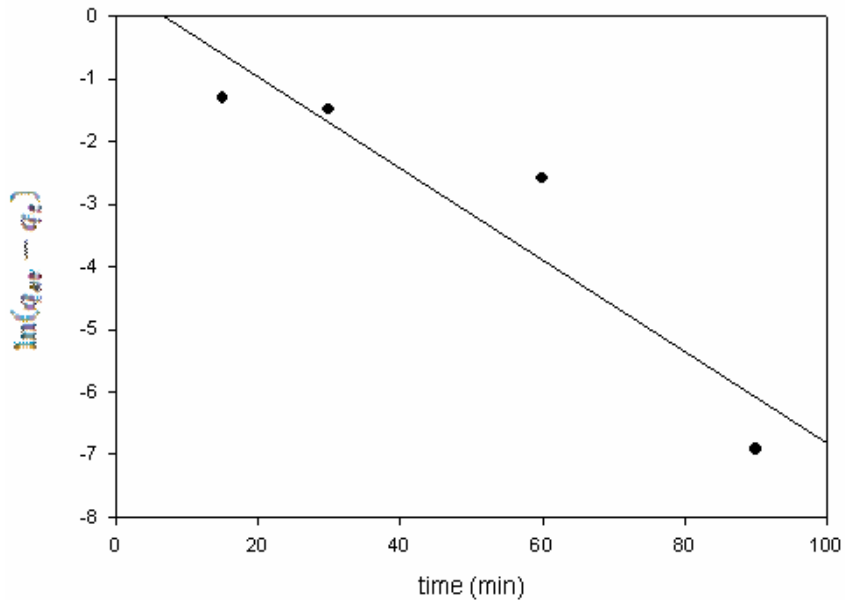


Fig. 3.2.5.1: Pseudo first order kinetics for MB adsorption onto mixed (Fe-Si) oxide for entire process.

Table 3.2.5.3: Comparison of the first and second order constants and calculated and experimental q_{et} values for MB adsorption process onto mixed (Fe- Si) oxide.

Parameter→ Dye ↓	Experimental $\times 10^5$ q_{et} (mol g ⁻¹)	Pseudo-first-order kinetic model (Calculated)			Pseudo-second-order kinetic model (Calculated)		
		k_1 $\times 10^2$	$q_{et} \times 10^5$ (mol g ⁻¹)	r^2	k_2 $\times 10^2$	$q_{et} \times 10^5$ (mol g ⁻¹)	r^2
MB	4.77	4.5	1.48	0.95	30.9	4.9	0.99

Pseudo-second-order equation

The adsorption kinetic may be described by the pseudo-second-order model. The equation is generally given as follows:

$$\frac{t}{q_t} = \frac{1}{kq_e^2} + \frac{1}{q_e}t \quad (2)$$

Where, k_2 [g (mol min)⁻¹] is the pseudo-second-order rate constant of adsorption.

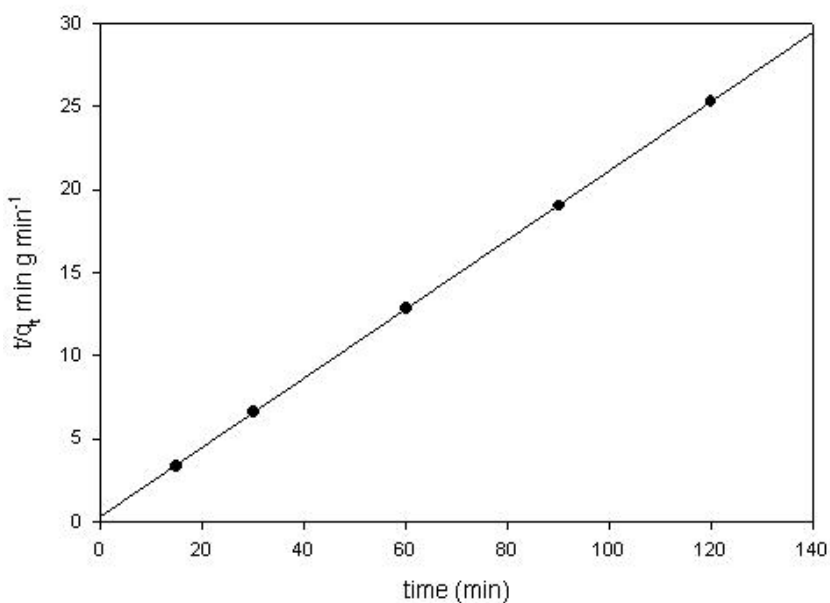


Fig. 3.2.5.2: A plot of pseudo-second- order- Kinetics of MB adsorption.

If the pseudo-second-order kinetics [33] is applicable, then the plot of t/q_t versus t should show a linear relationship values of k_2 and equilibrium adsorption capacity q_{et} were calculated from the intercept and slope of the plots of q_t versus t (Fig. 3.2.5.2). The linear plots of t/q_t versus t show good agreement between experimental and calculated q_{et} values at MB adsorption onto Mixed (Fe-Si) oxide. The correlation coefficient for the pseudo-second-order kinetic model are very close to 1 that is 0.999 which led to believe that the pseudo-second-order kinetic model provided good correlation for the adsorption of MB onto mixed (Fe-Si) oxide.

The Intra-particle diffusion model

The adsorbate species are most probably transported from the bulk of the solution into the solid phase through intraparticle diffusion or transport process [81], which is often the rate limiting step in many adsorption processes, especially in a rapidly stirred batch reactor. Since the dyes are probably transported from its aqueous solution to the mixed (Fe-Si) oxide by intraparticle diffusion, so the intraparticle diffusion is another kinetic model should be used to study the rate of dye adsorption onto mixed (Fe-Si) oxide. The possibility of intraparticle diffusion was explored by using the intraparticle diffusion model, which is commonly expressed by the following equation:

$$q_t = k_{id} t^{1/2} + C \quad (3)$$

Where, C (mol g^{-1}) is the intercept and k_{diff} rate constant ($\text{mol g}^{-1} \text{min}^{1/2}$).

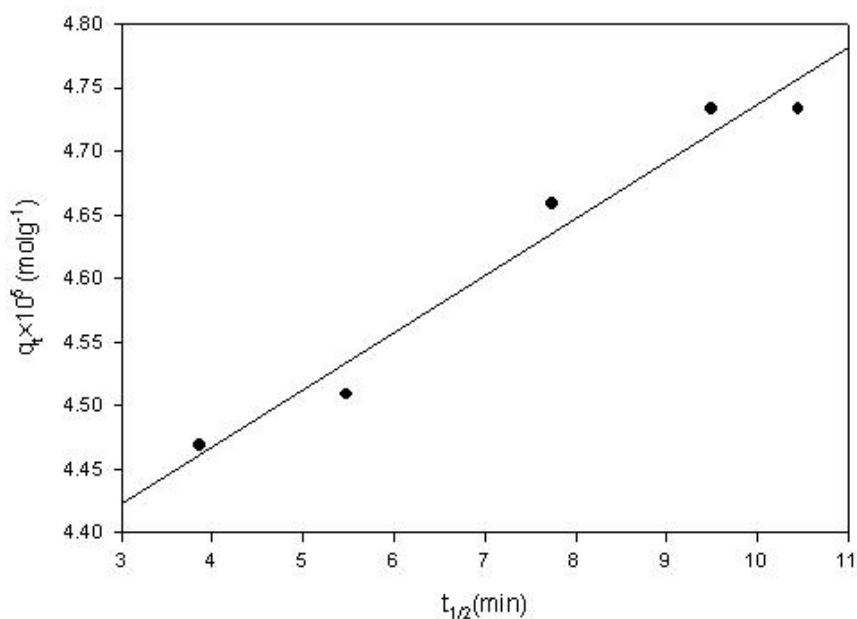


Fig. 3.2.5.3: A plot of intraparticle diffusion model for MB.

Table 3.2.5.4: The parameter obtained from intraparticle diffusion mode for MB

Dye	Parameter of intraparticle diffusion		
	k_{diff} (mol g ⁻¹ min ^{1/2})	C (mol g ⁻¹)	r^2
MB	0.03	4.29	0.96

The values of q_t were found to be linearly correlated with values of $t^{1/2}$ and rate constant k_{diff} directly evaluated from the slope of the regression line (Fig. 3.2.5.3). The values of intercept C (Fig. 3.2.5.3) provide information about thickness of the boundary layer, the resistance to the external mass transfer increase as the intercept increase. The r^2 values given in Table 3.2.5.4 is 0.96 indicating the application of this model. This may confirm that the rate limiting step may be intraparticle diffusion process [82]. The linearity of the plots demonstrated the intraparticle diffusion played a significant role in the uptake of the adsorbate by adsorbent.

3.2.6 Effect of concentration of dye and isotherm study

Table 3.2.6.1: Data for the influence of the concentration of dye on adsorption of MB by mixed (Fe-Si) oxide adsorbent.

Reference : Water

Amount of mixed oxide: 0.02g

pH of the solutions: 6.92

Contact time: 120 min

Volume of the solution: 50 mL

Molar absorption co-efficient: 74246 L mol⁻¹cm⁻¹

Run No	Initial Abs	Initial conc. of MB×10 ⁶ q ₀ (molL ⁻¹)	Final Abs	Equilibrium conc. of MB ×10 ⁶ q _e (molL ⁻¹)	Adsorbed conc. of MB×10 ⁶ q _m (molL ⁻¹)	Amount Adsorbed of MB×10 ⁵ <i>q_m/m</i> (molg ⁻¹)
1	0.78	10.5	0.097	1.31	9.19	22.98
2	0.87	11.7	0.115	1.55	10.15	25.38
3	1.06	14.3	0.134	1.80	12.50	31.24
4	1.18	15.9	0.163	2.20	13.70	34.26
5	1.36	18.9	0.223	3.00	15.90	39.74
6	1.49	20.1	0.258	3.47	16.63	41.56
7	1.64	22.1	0.307	4.13	17.97	44.91
8	1.73	23.3	0.373	5.02	18.28	45.69
9	1.91	25.7	0.462	6.22	19.48	48.69
10	2.09	28.1	0.623	8.39	19.71	49.27
11	2.2	29.6	0.734	9.89	19.71	49.28

Isotherm data analysis

The parameters obtained from the different models provide important information on the adsorption mechanism and the surface properties and affinities of the adsorbent. The most widely accepted surface adsorption models for single solute systems are the Langmuir and Freundlich models. The correlation with the amount of adsorption and the liquid-phase concentration was tested with the Langmuir, Freundlich isotherm equations. Linear regression is frequently used to determine the best-fitting isotherm, and the applicability of isotherm equations is compared by judging the correlation coefficients.

Langmuir isotherm

The theoretical Langmuir isotherm is valid for adsorption of a solute from a liquid solution as monolayer adsorption on a surface containing a finite number of identical sites. Langmuir isotherm model assumes uniform energies of adsorption onto the surface without transmigration of adsorbate in the plane of surface [85]. Therefore, the Langmuir isotherm model was chosen for estimation of the maximum adsorption capacity corresponding to complete monolayer coverage on the adsorbent surface. The linear form of Langmuir equation is commonly expressed as followed:

$$\frac{q_e}{q_m/m} = \frac{1}{k_a} \times \frac{1}{Q_m} + \frac{1}{Q_m} \times q_e \quad (1)$$

In equation (1), q_e is the equilibrium concentration (mol L^{-1}); q_m/m is the Amount adsorbed (mol g^{-1}); Q_m is a constant and reflects a complete monolayer (mol g^{-1}), k_a is a adsorption equilibrium constant (L mol^{-1}) that is related to the apparent energy of adsorption. A plot of $\frac{q_e}{q_m}$ versus q_e should indicate a straight line slope of $\frac{1}{Q_m}$ and intercept $\frac{1}{k_a} \times \frac{1}{Q_m}$.

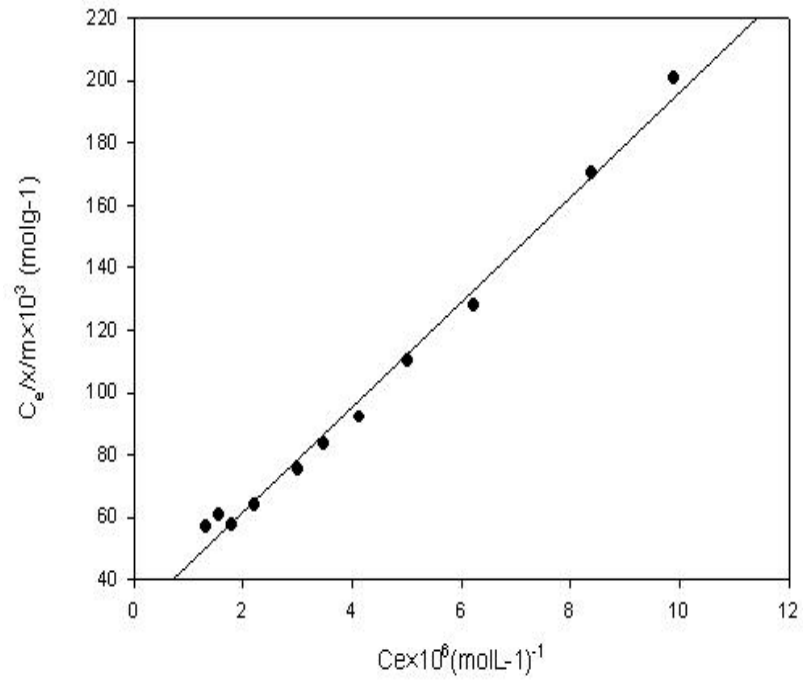


Fig. 3.2.6.1: Langmuir plot of $C_e/(X/m)$ vs C_e for the adsorption of MB by mixed (Fe-Si) oxide. $\frac{1}{2}$

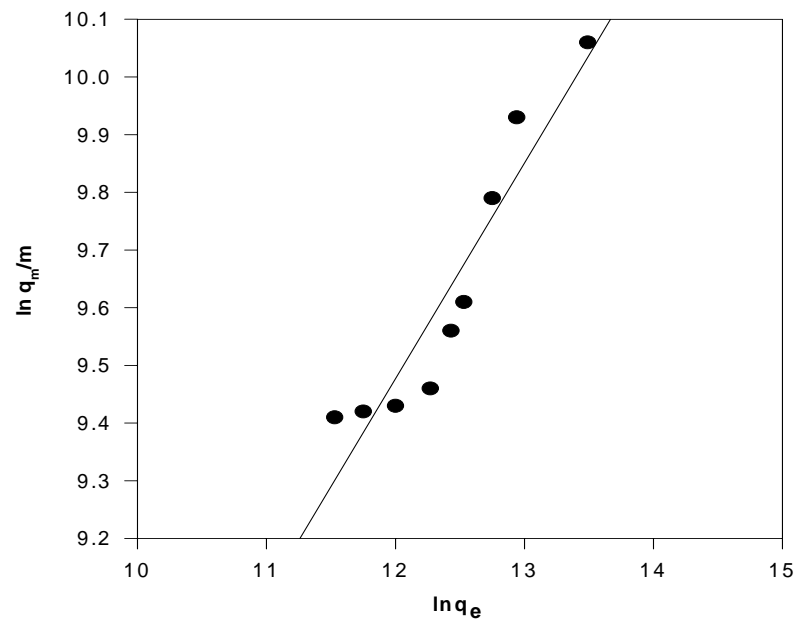


Fig. 3.2.6.2: Freundlich isotherm for the adsorption MB by mixed (Fe-Si) oxide.

The results obtained from the Langmuir model for the removal of MB onto nano mixed (Fe-Si) oxide are shown in Table 3.2.6.3. The correlation coefficients reported in Table 3.2.6.3 showed strong positive evidence on the adsorption of dyes onto nano mixed (Fe-Si) oxide follows the Langmuir isotherm. The applicability of the linear form of Langmuir model to nano mixed (Fe-Si) oxide was proved by the high correlation coefficients $r^2 = 0.99$. This suggests that the Langmuir isotherm provides a good model of the adsorption system. The maximum monolayer capacity Q_m obtained from the Langmuir isotherm is $5.97 \times 10^{-5} \text{ mol g}^{-1}$ for MB.

Table 3.2.6.3: Comparison of the coefficients of isotherm parameters for MB adsorption onto mixed (Fe-Si) oxide

Langmuir isotherm model			Freundlich isotherm model		
Q_m	k_a	r^2	n	k_F	r^2
(mol g^{-1})	(Lmol^{-1})			(mol g^{-1})	
5.97×10^{-5}	4.8×10^5	0.99	0.375	1.60	0.87

The Freundlich isotherm

The Freundlich isotherm model [86] is the earliest known equation describing the adsorption process. It is an empirical equation and can be used for non-ideal sorption that involves heterogeneous adsorption. The Freundlich isotherm can be derived assuming a logarithmic decrease in the enthalpy of adsorption with the increase in the fraction of occupied sites and is commonly given by the following linear equation:

$$\ln \frac{Q_m}{m} = \ln k_F + \frac{1}{n} \ln q_e \quad (2)$$

where, K_F is a constant for the system, related to the bonding energy. K_F can be defined as the adsorption or distribution coefficient and represents the quantity of dye adsorbed onto adsorbent for unit equilibrium concentration. $1/n$ is indicating the adsorption intensity of dye onto the adsorbent or surface heterogeneity,

becoming more heterogeneous as its value gets closer to zero. A value for $1/n$ below 1 indicates a normal Langmuir isotherm while $1/n$ above 1 is indicative of cooperative adsorption.

The applicability of the Freundlich adsorption isotherm was also analyzed, using the same set of experimental data, by plotting $\ln(q_m/m)$ versus $\log(q_e)$. The data obtained from linear Freundlich isotherm plot for the adsorption of the MB, onto mixed (Fe-Si) oxide is presented in Table 3.2.6.3. The correlation coefficients ($r^2=0.87$) showed that the Freundlich model is comparable to the Langmuir model. The $1/n$ is lower than 1.0, indicating that MB is favorably adsorbed by mixed (Fe-Si) oxide.

3.2.7 Effect of adsorption dose

Table 3.2.7.1: Data for the effect of adsorbent dose on adsorption behavior of MB by mixed (Fe-Si) oxide adsorbent.

Reference: Water

Time: 15 min

λ_{\max} for MB solution: 664nm

Temperature: 31°C

Volume of the solution: 50mL

pH: 6.92

Run No	Initial conc. of MB $\times 10^5$ q_0 (molL ⁻¹)	Dose (g)	Abs.	Equilibrium conc. of MB $\times 10^5$ q_m (molL ⁻¹)	Adsorbed conc. of MB $\times 10^5$ (q ₀ - q _m) (molL ⁻¹)	Amount Adsorbed of MB $\times 10^5$ q_m / m (molg ⁻¹)	% of MB removal
1	5	0.05	0.395	0.531	4.469	4.469	89.38
2	5	0.10	0.365	0.491	4.509	2.254	90.18
3	5	0.15	0.253	0.341	4.659	1.553	93.18

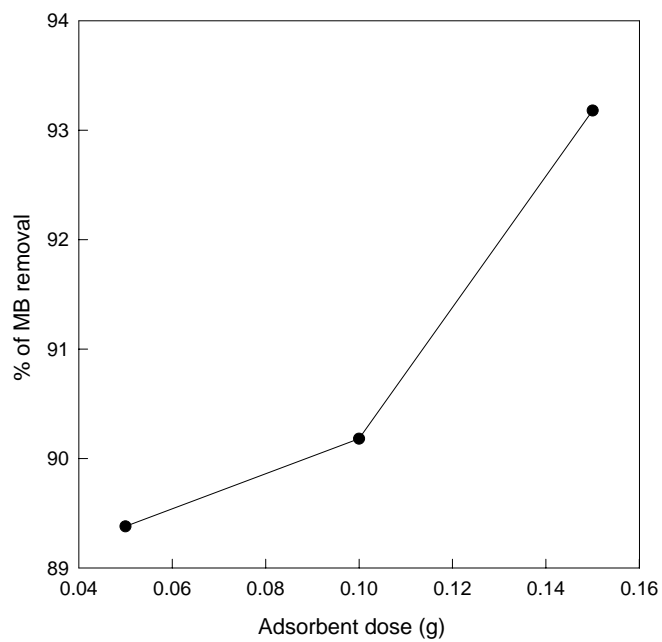


Fig. 3.2.7.1: Effect of adsorbent dose on % of MB removal.

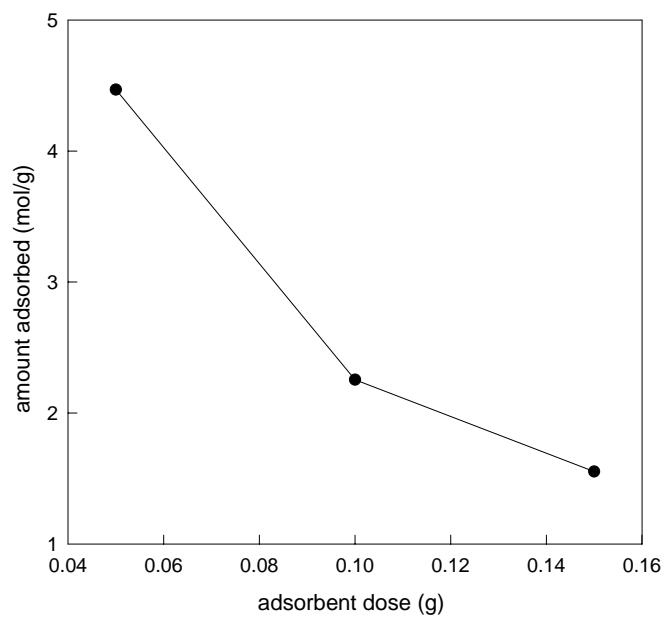


Fig. 3.2.7.2: A plot of amount adsorbed per gram vs adsorbent dose.

The dependence of MB adsorption on adsorbent dose with varying amounts of mixed (Fe-Si) oxide has been examined and the detail results are presented in Table 3.2.7.1. It is found that MB removal by adsorbents depends strongly on the adsorbent dose, indicating that adsorption is dependent on the availability of the bonding sites [90]. When the adsorbent dose of adsorbents was increased from 0.05 to 0.15 g/50mL the MB binding capacity was increased dramatically. The capacity was further increased, but the magnitude of the increase is proportionally less significant with each successive increase. It is postulated that at low adsorbent doses, all types of sites are entirely exposed for adsorption, and the surface may become saturated faster; whereas at higher adsorbent dosages the availability of higher energy sites may decrease [91]. However, when increase the amount of dose percent of removal of MB increased but amount adsorbed per gram dye onto mixed (Fe-Si) oxide is decreased (Figs. 3.2.7.1 and 3.2.7.2) which indicate optimization of adsorbent dose is necessary before adsorption because of effective use of synthesized particles.

CONCLUSION

4.0 Conclusion

Synthesis of metal oxide materials become very attractive because of their wide potential applications in various technologically important fields. Sol-gel process provides a facile route of preparing mixed metal oxides in which the mixing of two or more metal oxide phases can be controlled on both a molecular and nanometer scale. In the present study, iron-silicon mixed oxide surface was synthesized by sol-gel method. This method was found to be very effective to incorporate iron oxide into a silica gel network. EDX, XRD, SEM images, UV visible and IR spectroscopy were used to determine the phases present and the arrangement of species in the particles. The chemical composition, obtained by EDX analysis, of the prepared mixed (Fe–Si) oxide is calculated to $\text{Fe}_{1.47}\text{Si}_{0.53}\text{O}_3$. The IR spectra shows the characteristics signals of silicon oxide, iron oxide and iron–silicon mixed oxide and confirmed the presence of the components in each substrates. In XRD analysis, information about the crystallite structure and particle size were found. The Miller Indices (h, k, l) lattice planes of iron and silicon oxide are present in mixed oxide with partial deviation of 2θ angle of the plane. The obtained average crystallite size of iron-silicon mixed oxide is 18 nanometers which mean that the synthesized (Fe-Si) mixed oxide is in the nano state. Besides this, the mixed oxide surface is also highly porous that indicates a large amount of sites for higher adsorption. The particles were observed to be highly crystalline as ascertained from the XRD analysis. The SEM images of the oxide samples shows aggregating the particulate on the substrate.

This synthesized multi-component (Fe-Si) oxides prepared via a sol-gel method gave attractive surface areas ($46.79 \text{ m}^2\text{g}^{-1}$) and hence should have a potential application as adsorbent. The present result also indicated that the pH_{PZC} of the Fe-Si mixed oxide matrix is 8.8 and thus its surface is negatively charged. Consequently adsorption of a cationic MB dye on the Fe-Si mixed oxide matrix was found to be significantly high than that of OG an anionic dye. Iron-Silicon mixed oxide seems to be a specific adsorbent for the removal of cationic MB dye from water. A detail adsorption characteristics of the (Fe-Si) mixed oxide was successfully characterized in this work. Batch experiments was employed to remove the cationic MB dye from aqueous solution under the various parameters

such as effect of pH, contact time, initial dye concentration and adsorbent dose. Batch experiment study showed that adsorption of MB was highly pH dependent. pH 7 was found to be suitable for the maximum adsorption of the cationic MB dye onto the (Fe-Si) mixed oxide. Kinetic studies were also performed to investigate the rate of adsorption process. Experimental data fitted well the pseudo-second-order kinetic model while the first order kinetic model was not found valid for the whole range of adsorption process. Other than that, intraparticle diffusion was found to be prominent at a certain stage of adsorption but it would not be the only limiting step that controlled the adsorption dynamic.

Batch equilibrium (MB) data also found to have a good agreement with the Langmuir and Freundlich isotherm models. Overall, the Langmuir isotherm showed the best fit for all the adsorbents studied for all the systems. The analysis of isotherm showed that adsorption is favorable on the oxide matrices synthesized in this work. With the increase of adsorbent dose the percentage of dye removal was increased but the amount adsorbed per gram of adsorbent was decreased.

Finally the present study demonstrates well that (Fe-Si) mixed oxide is an effective adsorbent for the removal of cationic dye MB from water. In the real field, there are many dye effluents that are discharging everyday from the industries. These effluents then possibly be removed by using the (Fe-Si) mixed oxide. Therefore, further application of the (Fe-Si) mixed oxide in removing MB dye from the industrial effluent seems to be an interesting study for future work.

REFERENCE

References

1. Clapsaddle B.J, David W. Sprehn, Alexander E. Gash, Joe H. Satcher Jr., Randall L. Simpson " A versatile sol-gel synthesis route to metal-silicon mixed oxide nanocomposites that contain metal oxides as the major phase", *Non-crystalline Solids*, 2004, **350** ,173-181.
2. Nakamura, M. Saitoh, H. Maejima, M. Yamagiwa, S. and Kaneko, S. *Fresenius Z Anal Chem*, 1989, **335**, 573 – 575.
3. Fahlman, B. D., *J. Materials Chemistry*, 2000, **1**, 282-283.
4. Chowdhury, A.-N., Rahim A., Ferdousi, Y.J., Azam, M.S. and Hossain, M.M., "Cobalt-Nickel Mixed Oxide Surface: A Promising Adsorbent for the Removal of PR Dye from Water", *Appl. Surf. Sci.*, 2010, **256**, 3718-3724.
5. Greedon, J.E., *Magnetic oxides in Encyclopedia of Inorganic chemistry*, Ed. R. Bruce King, John Wiley & Sons, 1994, ISBN 0471936200
6. [http://en.wikipedia.org/wiki/Iron\(III\)_oxide](http://en.wikipedia.org/wiki/Iron(III)_oxide)
7. Iler, R.K., *The Chemistry of Silica*, Plenum Press. 1979, ISBN 047102404X.
8. Anderson, R. B., Dawson, P.T., *Experimental Methods in Catalytic Research*, Academic Press, New York, 1976, **2**, 215-219.
9. King, D. S., Nix, R. M., "Thermal Stability and Reducibility of ZnO and Cu/ZnO Catalysts", *J., Catal.*, 1996, **76**, 160.
10. Toshio, O., & Makato M., *Oxide catalyst in Solid state Chemistry*, 1987, 2889.
11. David, K., Ward and Edmond, I. K. "Preparing Catalytic Materials by the Sol-Gel Method", *Ind. Eng. Chem. Res.*, 1995, **34(2)**, 421-432.
12. Pollard, A. M., Spencer, M. S., Thomas, R. G., Williams, P. A. Holt, J. Jennings, J. R., *Appl. Catal. A*, 1992, **85**, 1–11.
13. Pavasupree, S. Ngamsinlapasathian, S. Pivsa-art, S. Suzuki, Y. and Yoshikawa, S. *Proceedings of The Joint International Conference on "Sustainable Energy and Environment (SEE)*, 1-3 December (2004), Hua Hin, Thailand, page: 58-62.
14. Tarafdar, A. Pramanik, P., *Microporous and mesoporous materials*, 2006, **91**, 221-224.

15. Biswas, K. Gupta, K. and Ghosh, U. C., *Adsorption of fluoride by hydrous iron(III)–tin(IV) bimetal mixed oxide from the aqueous solutions*, *Chemical Engineering Journal*, In Press, Corrected Proof, Available online 28 October 2008.
16. Nora, D. Nidola, V. Spaziante, A. Placido M. Giuseppe, B., US 4267025, 1981.
17. Koichi, T. and Akifusa, H., *Denki Kagaku oyobi Kogyo Butsuri Kagaku*, 2001, **69(9)**, 692-698.
18. Taylor et al., *Chem. Commun.*, 1999, 1373-1374.
19. Ishihara, T., Kometani, K., Hashida, M. and Takita, Y., *J. Electrochem. Soc.*, 1991, **138(1)**, 173-176.
20. Gill, E., Arshak, K., Arshak, A. and Korostynska, O., *Microsystem Technologies archive* 2008, **14(4)**, 499-507.
21. Rodney, S. D. (Edmond, OK), *Method for making a rutile mixed metal oxide pigment*, United States Patent 5759256, 1998.
22. Balko, E. N. and Nguyen, P. H., *Journal of Applied Electrochemistry*, 1572-8838 (Online), Issue: 1991, **21(8)**, 678-682.
23. Grätzel, M., (2001) Photoelectrochemical cells, *Nature*, **414**, pp. 338-344.
24. Zhang, F., Yang, S., Chen, H. and Yu, X. (2004), Preparation of discrete nanosize ceria powder, *Ceramics International*, **30**, pp. 997-1002.
25. Bouvy, C. and Su, B. L., *Journal of Materials Sciences & Technology*, 2008, **24** (04), 495-511.
26. Azam, M. S., "Synthesis of Catalytically Important Manganese Oxide Nanoparticles and Their Dispersion into a Polymeric Matrix" Department of Chemistry, BUET, Dhaka, Bangladesh, 2008, 4.
27. Agam, M. A. and Q. Guo, "Electron Beam Modification of Polymer nanospheres" *J. Nanosci. Nanotech.* 2007, **7**, 3615-3619.
28. Choy, J. H., Jang, E. S., Won, J. H., Chung, J. H., Jang, D.J. and Kim, Y.W., "Hydrothermal Route to ZnO nanocoral reefs and nanofibers" *Appl. Phys. Lett.*, 2004, **84**, 287.
29. Yugang, S. and Youman, *Xia Science*, 2002, **298**, 2176.
30. Aziz, M. A., "A Text Book of Water Supply Engineering", Hafij book centre, Dhaka, 1994, 178-182.

31. Mohan, N., Balasubramanian, N., Ahmed Basha, C. "Electrochemical Oxidation of Textile Wastewater and Its Reuse", *J. of Hazardous Materials.*, 2007, **147**, 644.
32. Cameselle, C., Pazos, M., Sanroman, M.A. "Selection of an Electrolyte to Enhance the Electrochemical Decolourization of Indigo Optimization and Scale-up", *Chemosphere.*, 2005, **60**, 1080.
33. Caner, N., Kiran, I., Ilhan, S. and Iscen, C.F. "Isotherm and Kinetic Studies of Burazol Blue ED Dye Biosorption by Dried Anaerobic Sludge", *Journal of Hazardous Materials.*, 2009, **165**, 279.
34. Zhao, W., Chen, C., Li, X., Jhao, J., Hidaka, H. and Serpone, N. "Photodegradation of Sulforhodamine-B Dye in Platinized Titania Dispersions under Visible Light Irradiation: Influence of Platinum as a Functional Co-catalyst", *J. Phys. Chem. B.*, 2002, **106**, 5022.
35. Tao, X., Su, J. and Chen, J.F. "Photooxidative Degradation of Dye Pollutants Accumulated in Self-Assembled Natural Polyelectrolyte Microshells under Visible Radiation" *J. Chem. Eur.*, 2006, **12**, 4164.
36. Akbal, F., "Photocatalytic Degradation of Organic Dyes in the Presence of Titanium Dioxide under UV and Solar Light: Effect of Operational Parameters", *Environmental Progress*, 2005, **24(3)**, 317-322.
37. Ranghu, S. and Ahmed, B. C., "Dye Destruction and Simultaneous Generation of Sodium Hydroxide Using a Divided Electrochemical Reactor" *Ind. Eng. Chem. Res.*, 2008, **47**, 5277.
38. Wellington, S., Pereira, S., Renato, S. and Freire, S., "Azo Dye Degradation by Recycled Waste Zero-Valent Iron Powder" *J. Braz. Chem. Soc.* 2006, **17**, 832.
39. Chen, C. C., Chaudhary, A. J. and Grimes, S. M., "Photodegradation of Acid Blue 29 and Ethyl Violet in the Presence/Absence of Sodium Hydroxide and Aluminium Ions" *Environmental Information Archives.*, 2005, **3**, 111.
40. Sanjay, S., Vaghel, A., Ashok, D., Jethv, A., Bhavesh, B., Meth, A., Sunil, P., Dave, Adimurthy, S. and Ramachandraiah, G., "Laboratory Studies of Electrochemical Treatment of Industrial Azo Dye Effluent", *Environ. Sci. Technol.*, 2005, **39**, 2848.

41. Malpass, G. R. P., Miwa, D. W., Machado, S.A.S. and Motheo, A.J., "Decolourization of Real Textile Waste Using Electrochemical Techniques: Effect of Electrode Composition" *J. of Hazardous Materials*, 2008, **156**, 170.
42. Wellington, S., Pereira, S., Renato, S. and Freire, S., "Azo Dye Degradation by Recycled Waste Zero-Valent Iron Powder", *J. Braz. Chem. Soc.*, 2006, **17**, 834.
43. Findenegg, G. H., *Fundamentals of Adsorption*; Engineering Foundation: New York, 1984, pp. 207-218.
44. Nolan, J. T., McKeehan T. W., Danner, R. P., *J. Chem. Eng. Data* 1981, **26**, 112.
45. Atkins, P. W., *Physical Chemistry*, Oxford University Press, sixth edition, 1998, 857.
46. Chang, R., *Chemistry*, McGraw-Hill Inc., fifth edition, International edition, 1994, 817-819.
47. Schreier, M., "A Theoretical Study on CO₂ Solubility in Water as a function of pH", *J. Can. Goetech.*, 2006, **12**, 14-17.
48. Marguev, D., *J. Phys. Chem*, 1998, **102**, 10778-10791.
49. Scott, A. B., "Catalyst Manufacture", Ellis Horwood, Chichester, 1993, 254.
50. Singal, R. L., "*Solid State Physics*", Kedar Nath Ram Nath & Co., Meerut, sixth edition, 1998, 304.
51. Feldman, C. and Jungk, H. O. *Angew. Chem. Int. Ed.* 2001, **40**, 359.
52. Wei, O. F. *Mater. Lett.* 2004, **58**, 3226.
53. Hudson, M. J. and James A., J, *Materials Chemistry*, 1996, **6**, 89-95.
54. Stephanopoulos, M. F., *MRS Bulletin*, November 2001.
55. Park, J., and John, R., "A Simple Accurate determination of Oxide PZC and the Strong Buffering Effect of Oxide Surfaces at Incipient Wetness", *J. Colloid and Interface Science*, 1995.
56. Appel, C., Ma, L., Rhue, D., Elizabeth, K., and Geoderma, *Elsevier.com*, 2003, **113**, 77-93.

57. Parker, J. C., Zelazny, L. W., Samprath, S. and Harris, W. G., "A critical Evolution of the Extension of Zero Point of Charge (ZPC) Theory to Soil System", *Soil Sci. Soc. Am*, 1991, **43**, 668-674.
58. Noh, J. S., and Schwarz, J. A., *J. Colloid Interface Sci.*, 2003, **140**, 157-164.
59. Zalac, S. and Kallay N., *J. Colloid Interface Sci.*, 2002, **149**, 233-240.
60. Preocanin, T., and Kally, N., *Crawatica Chemica Acta*, 1998, **71(4)**, 117-1125.
61. Kosmulski, M., *Advance in Colloid and Interface Science*, 2002, **99**, 255-264.
62. Suzuki, M., "Adsorption Engineering", Elsevier, Amsterdam, 1990, 135-137.
63. Ismail, A. A., El-Midany A. A., Ibrahim, I. A. and Matsunaga H., "Heavy Metal Removal Using SiO₂ -TiO₂ Binary Oxide", *Adsorption*, 2008, **14**, 21-29.
64. Raghavacharya, C., "Colour Removal from Industrial Effluent", *Chem. Engg. World*, 1997, **32**, 53-58.
65. Khan, A. R., Al-Bahri, T. A. and Al-Haddad, A., "Adsorption of Phenol Based Organic Pollutants On Activated Carbon From Multicomponent Dilute Aqueous Solutions", *Wat. Res.*, 1997, **31**, 2102-2112.
66. Crittenden, J. C. and Weber, W. J., "Model for Design of Multicomponent Adsorption System", *J. Environm. Engg. Div.*, 1978, **104**, 1175-1193.
67. Khenifi, A., Boubarka, Z., Kameche, M. and Derriche, Z., "Adsorption Study of an Industrial Dye by an Organic Clay", *Adsorption*, 2007, **13**, 149-158.
68. Oke, I. A., Olarinoye, N. O. and Adewusi, S. R. A., "Adsorption Kinetics for Arsenic Removal from Aqueous Solutions by Untreated Powdered Eggshell", *Adsorption*, 2008, **14**, 73-83.
69. El-Shobaky, H.G., "Surface and Calalytic Properties of Co, Ni and Cu Binary Oxide System", *Appl. Catal., A.*, 2004, **278(1)**, 1.
70. Babu, K. S. Singh, D. and Srivastava, O. N., "Investigatios on the Mixed Oxide Material TiO₂-In₂O₃ in Regard to Photocatalytic Hydrogen Production", *Semicond. Sci. Technol*, 1990, **5**, 364.
71. Roth, L., *Phys. Rev*, 1956, **110**, 1333.

72. M. Tachiki, *J. Phys. Soc. Japan*, 1964, **19**, 454.
73. Kobayashi, T., Haruta, M., Sano, H. and Delmon, B., *Proceeding of the third International Meeting on Chemical sensors*, Cleveland, 1990, 318.
74. Maruyama, S. T. and Arai, S., *J. Electrochem. Soc.*, 1996, **143**, 1383.
75. Svegl, F., Orel, B., Hutchins, M. G. and Kalcher, K., *J. Electrochem*, 1996, **143**, 1532.
76. Ting, Y. U. and Zexiang, S., *J. Mater. Sci. Technol.*, 2008, **24(4)**, 597-602.
77. Azurdia, J. A., Mccrum, A. and Laine, R. M., *J. of material chemistry*, 2008, **18**, 3249-3258.
78. Perry, C. C., Li, X. and Waters, D. N., *Spectrochem. Acta*, 1991, **47A**, 1874.
79. Harrison, P. G., Perry, C. C., Creaser, D. A., Li, X., *In Vilminol, Nass, Schmidt (Eds.), Eurogel*, 1992, **91**, 175.
80. Senthikumar, S., Varatharajan, P. R., Porkodi, K. and Subburaam, C. V., "Adsorption of Methylene Blue Carbon onto Jute Fibre Carbon", *Colloid. Interface Sci.*, 2005, **284**, 79.
81. Uddin, M. T., Islam, M. A., Mahmud, S. and Rukanuzzaman, M., "Adsorptive removal of methylene blue by tea waste" *J. of Hazardous Materials.*, 2009, **164**, 58.
82. Catherine, M., *Science*, 2002, **298**, 2176.
83. Atkins, P. W., "Physical Chemistry", Oxford University Press, sixth edition, 1998, 619-633.
84. Brinker, C. J. and Scherer, G. W., "Sol-Gel Science: The Physics and Chemistry of Sol-Gel Processing", Academic, San Diego, 1990.
85. Renmin, G., Yingzhi, S., Jian, C., Huijun, L., and Chao, Y "Effect of Chemical Modification on Dye Adsorption Capacity of Peanut Hull", *Dyes and Pigments.*, 2005, **67**, 179.
86. Catena, G.C., Bright, F.V., "Effect of Temperature on the Adsorption of Dyes" *Anal. Chem.*, 1999, **61**, 905.
87. Savii, C., Popovici, M., Enache, C., Subrt, J., Niznansky, D., Bakardzieva, S. Caizer, C., Hrianca, I., "Fe₂O₃-SiO₂ composites obtained by sol-gel synthesis", *Solid State Ionics*, 2002, **151**, 219-127.

88. Mustafa, S., Dilara, B., Nargis, K., Naeem, A., Shahida, P., "Surface properties of the mixed oxides of iron and silica", *Colloids and Surface*, 2002, **205**, 273-282.
89. Ehrmam, S. H. and Friedlander, S. K., "Phase segregation in binary $\text{SiO}_2/\text{TiO}_2$ and $\text{SiO}_2/\text{Fe}_2\text{O}_3$ nanoparticle aerosols formed in a premixed flame", *J. Mater. Res.*, 1999, **14**, 4551-4561.
90. Krishna, D.G., and Bhattacharyyya, G., "Adsorption of Methylene Blue on Kaolinite, *Appl. Clay Sci.*, 2002, **20**, 295.
91. Namasivayam, C. and Yamuna, R. T., "Adsorption of Direct Red by Biogas Residual Slurry", *Environ. Pollut*, 1995, **89**, 1.